INSTYTUT FIZYKI JĄDROWEJ
IM. HENRYKA NIEWODNICZAŃSKIEGO
POLSKIEJ AKADEMII NAUK

THE HENRYK NIEWODNICZAŃSKI INSTITUTE OF NUCLEAR PHYSICS

POLISH ACADEMY OF SCIENCES

Fractional Calculus and Material Clock Applied to Relaxation in Complex Systems

---

Author:
Ambra Lattanzi

Supervisor
dr. hab. Katarzyna Górska

Thesis submitted for the degree of Doctor of Philosophy

Kraków

2021

Ambra Lattanzi: Fractional Calculus and Material Clock Applied to Relaxation in Complex Systems ©: A.A. 2021

Abstract

The Debye model presents an elegant description for the relaxation and dispersion phenomena based on statistical mechanics. However, it describes systems, characterized by a single relaxation time, as perfect liquids and crystals, quite far from the complexity which affects almost all materials. In the last decades, many phenomenological models were developed to consider the anomalous deviations from the Debye model. Among these anomalous models, the Havriliak-Negami dispersion model in the frequency domain and the Kohlrausch-Williams-Watts relaxation in the time domain are cornerstones that successfully fit experimental data in their respective domains despite not being the relevant Fourier counterparts.

This thesis deals with a novel approach, involving nonlinear time and frequency variables, inspired by the idea to restore this *broken symmetry* between dispersion and relaxation models in order to tune the Debye's idea with the anomalous behaviours observed in experiments. Firstly, we introduce a phenomenological model based on a second order differential equation with time-dependent coefficients to describe the anomalous relaxation dynamics in photoluminescence highlighting the role of the complete monotonicity and the physical meaning of the Kohlrausch-Williams-Watts function with its singularity. Secondly, we introduce a general evolution equation for anomalous relaxation processes in terms of a commutator based on the Reynolds-Leibnitz theorem and a *material transform* that bridges the Havriliak-Negami dispersion model and the Kohlrausch-Williams-Watts relaxation. Collecting all the results was possible to find two different origins for the anomalous behaviour. To conclude, our attention focused on a more mathematical issue: the conditions for complete monotonicity of special functions used in the description of relaxation processes as the Mittag-Leffler function and the Meijer G-function.

Streszczenie

Model Debye'a przedstawia elegancki opis zjawisk relaksacji i dyspersji w oparciu o mechanikę statystyczną. Jednak układy charakteryzujące się pojedynczym czasem relaksacji opisuje jako doskonałe ciecze i kryształy, dość dalekie od złożoności, która dotyczy prawie wszystkich materiałów. W ostatnich dziesięcioleciach opracowano wiele modeli fenomenologicznych, aby uwzględnić anomalne odchylenia od modelu Debye'a. Wśród tych anomalnych modeli, model dyspersji Havriliaka-Negami w domenie częstotliwości i relaksacja Kohlrauscha-Williamsa-Wattsa w domenie czasu są kamieniami węgielnymi, które z powodzeniem dopasowują dane eksperymentalne w swoich domenach, mimo że nie są one odpowiednimi odpowiednikami Fouriera. Ta teza dotyczy nowatorskiego podejścia obejmującego nieliniowe zmienne czasu i częstotliwości, inspirowane ideą przywrócenia *złamanej symetrii* między modelami dyspersyjnymi i relaksacyjnymi w celu dostrojenia pomysłów Debye'a do anomalii obserwowanych w eksperymentach. Najpierw wprowadzamy model fenomenologiczny oparty na równaniu różniczkowym drugiego rzędu ze współczynnikami zależnymi od czasu w celu opisania anomalnej dynamiki relaksacji w fotoluminescencji, podkreślając rolę całkowitej monotoniczności i fizyczne znaczenie funkcji Kohlrauscha-Williamsa-Wattsa z jej osobliwość. Po drugie, wprowadzamy ogólne równanie ewolucji anomalnych procesów relaksacji w kategoriach komutatora oparte na twierdzeniu Reynoldsa-Leibnitza i transformacji materiałowej, która łączy model dyspersji Havriliaka-Negami i relaksację Kohlrauscha-Williamsa-Wattsa. Zebranie wszystkich wyników umożliwiło znalezienie dwóch różnych źródeł anomalnego zachowania. Podsumowując, nasza uwaga skupiła się na bardziej matematycznym zagadnieniu: warunkach pełnej monotonii funkcji specjalnych stosowanych w opisie procesów relaksacyjnych, takich jak funkcja Mittaga-Lefflera i funkcja G Meijera.

Acknowledgment

Before expressing my gratitude to all the people who have been instrumental in the successful completion of this thesis, I would start to acknowledge all the sources of funding that I received during the PhD.
I am grateful to the Institute of Nuclear Physics Polish Academy of Science (IFJ-PAN) that provided the PhD fellowship and the grants that support my research throughout all these years. I am also grateful to the funding received through the National Science Center (NCN) with the OPUS-12 grant no. UMO-2016/23/B/ST3/01714 that supported my PhD studies. I am deeply grateful to the funding received as a first investigator from the National Agency for Academic Exchange (NAWA) with the grant Program im. Iwanowskiej PPN/IWA/2018/1/00098.
Last but not least I would like to extend my sincere thanks to the committee of the Grant COST Action CA15225 "Fractional System": computational methods for fractional order-problems, which funds my stage at the summer school held in Bari in July 2019.

It is rather difficult to list all the names of those who helped me, but several people deserve my sincere and special thanks.
First of all I would like to thank my supervisor prof. Katarzyna Górska and prof. Andrzej Horzela for their continuous support of my PhD studies and related research. I want to thank them for forging me during these years, and I am extremely grateful to them for introducing me to this field of research. They have certainly spurred my academic growth with their invaluable suggestions and comments. Under their guidance, I learnt what type of researcher I want to be, and I had the possibility to collaborate with prof. Tibor Pogány of the University of Rijeka that I thank so much for the useful discussions on our common interests concerning special functions. Special functions have always had a *special place* in my heart, and I dedicated Chapter 4 of this thesis to them.
A further thank goes to the chief of PhD studies prof. Anna Kaczmarska that always supported me not only about studies matter but also helped me get through this difficult times of global pandemic with her advice.

My sincere thanks also goes to Prof. Giuseppe Dattoli, who provided me with an opportunity to join his team during the NAWA grant Program im. Iwanowskiej allowing me to access the ENEA research center and the National Laboratories in Frascati, he has also overseen my research and the thesis during the time I spent in Rome for the grant. In that period, I had the opportunity to perfect the mathematical techniques as the operator methods that I had learnt when I was his student and

therefore I deepen the understanding of the generalized transforms that turned out to be very useful for introducing the *material* transform in Chapter 3. He introduced me firstly to prof. Nicholas Behr of the University de Paris (CNRS-IRIF) and then to prof. Giuseppe Baldacchini, a world-class expert on relaxation in photonics and formerly head of Laser & Accelerator Section in the ENEA laboratory. I would like to express to them my sincere gratitude for their insightful comments and encouragement, in particular I am extremely grateful for the hard question proposed by prof. Baldacchini which prompted me to broaden my research from different perspectives, inspiring the second Chapter of this thesis. The importance of the results has been acknowledged in his book *Organometallic Luminescence: A Case Study on Alq3, an OLED Reference Material* published by Elsevier in 2021.

I would like to also express my sincere gratitude to prof. Decio Levi of the University of Rome3 for his unwavering support and belief in me that has been with me for years since I completed the second thesis under his supervision. I am deeply grateful to him for the enlightening discussions, precious advice that I received when I had doubts about the new physical interpretations that I introduced in this thesis as the composition rule introduced in Chapter 3. I thank him so much also for the warm welcome that I received in Montreal during the conference *Quantum Theory and Symmetry* in July 2019. Thanks to him, I had the possibility to forge exceptional relationships with Prof. Orlando Ragnisco, Prof. Zora Thomova and Dr. Giorgio Gubbiotti. Prof. Levi and Prof. Ragnisco introduced me to the chief of the Physics department of the University of Rome3 prof. Paola Gallo that suggested me references and useful books for the development of the thesis. I had also fruitful discussions with her on relevant and interesting open problems that inspired further developments of my research.

A very special thank is to Dr. Roberto Garra and Dr. Giampietro Casasanta with whom I could apply the model that I presented in this thesis to another situation with amazing applications and insights in physics of superconductors and in phosphorescent materials inspiring further developments of the research.

I am grateful also to prof. Čestmír Burdík who offered me the opportunity to be chairman of two sections in the conference *The 32nd International Colloquium on Group Theoretical Methods in Physics* that he organized in Prague in 2018. I also thank Prof. Jean Pierre Gazeau of the Université de Paris for his questions during that conference and for the courage he gave me.

Additionally, I would like to express gratitude to prof. Francesco Mainardi of the University of Bologna and prof. Roberto Garrappa of the University of Bari for giving me the possibility to attend the summer school in Bari where I had the pleasure of knowing and exchanging views with Prof. Kai Dielthem, Prof. Luciano Mescia, Prof. Tiziano Politi, and Dr. Alessandro Palmisano. My appreciation also goes out to Prof. Vincenzo Guidi and Prof. Federico Montoncello who invited me as a lecturer to the University of Ferrara where I presented part of the results discussed in this thesis and I received useful suggestions.

I am fully pleased and thankful to my dear friend Prof. Sladja Nicolic and Prof. Sasa Ivkovic of the University of Belgrade for inviting me as lecturer and for introducing me to Prof. Todor Mishonov of the University of Sophia that I thank for his valuable comments.

I would like to express my sincere gratitude to Prof. Irina Petreska and Prof. Trifce

Sandev of the Macedonian Academy of Science and Prof. Susana Topuzoski of the University of Skopje for their consideration, interesting discussions and a warm welcome in Macedonia.
I would like also thank Prof. Luca Giannessi for giving me the opportunity to participate to the conference *INTERLAB2021 meeting ENEA-INFN LNF-ELETTRA* and for giving me valuable advice. Last and not least my thanks goes also to Prof. Marek Bozejko of the Wroclaw University that always cheered me up during these years.

I would like to thank all my friends, lab mates, colleagues and research team for a cherished time spent together in the Institute, in laboratories, and in social settings. I want to especially thank Izabela Babiarz, Krzysztof Tyrała, Krzysztof Cieśla, Tomasz Stanisz and Dr. Vardan Baghmanyan and Dr. Dominika Kuzma for their availability and kindness throughout these years but also to Dr. Gregorio Vlad, Dr. Federico Nguyen, Dr. Alberto Petralia, Dr. Ivan Spassovsky, Dr. Emanuele Di Palma and Dr. Silvia Licciardi and Dr. Sarah Bollanti for their warm welcome when I was in ENEA. I had also the pleasure to spend my free time in Kraków together with prof. Ludovico Minati and I thank him so much for being an exceptional guide and friend. In conclusion I would like to acknowledge Piotr Serafin of the National Agency for the Academic Exchange (NAWA) for his extraordinary availability and his patience to answer to all my questions and doubts.

Beside these scientific and academic acknowledgments I would like to thank my family: my parents, my best friend Mariachiara, Tiziana and Coco for supporting me spiritually throughout writing this thesis. I'm grateful to my grandmother, the rock of stability throughout my life, for all her efforts I am here today. Last but not the least, I have to thank my beloved Matteo. *I adore you, sweetheart.* It is the love that I fell for you that whispers to me that the world is still beautiful and makes me look at these landscapes around us always with new eyes and perspectives.

Abbreviations

Alq_3	Tris(8-hydroxyquinoline)aluminum(III)
CC	Cole-Cole (dispersion model)
CD	Cole-Davidson (dispersion model)
D	Debye (relaxation or dispersion model)
KWW	Kohlrausch-Williams- Watt (function)
HN	Havriliak-Negami (dispersion model)
OLED	Organic Light Emitting Diode
PL	Photoluminescence (or Photoluminescent)
SSR	Sum of the squared of residuals

Nomenclature

A	Surface of conducting plates in a parallel-plate capacitor (m^2)
$\hat{A}$	Generator of the semigroup
$\mathbf{B}$	Magnetic induction (T)
c	Speed of light (2.997 924 588 ms^{-1})
$\mathbb{C}$	Set of Complex numbers
C	Capacitance (F)
C_0	Capacitance in the vacuum (F)
d	Separation between conducting plates in a parallel-plate capacitor (m)
δ	Loss angle
$\mathbf{D}$	Dielectric displacement (Cm^{-2})
$\mathcal{D}$	Dispersion factor
$\nabla\cdot$	Divergence
$\nabla\times$	Rotor
D^{-1}	Inverse derivative operator (or anti-derivative operator)
$\Delta\varepsilon$	Dielectric increment of dielectric relaxation strength
ΔV	Electric potential difference (kg m2 $s3A1$)
$\partial\mathcal{V}$	Surface of incompressible volume
e	Elementary charge (1.6020^{-19}C)
ε	Dielectric permittivity
$\tilde{\varepsilon}$	Normalized dielectric permittivity
ε_0	Vacuum electric permittivity (8.854187812810^{-12} $C^2m^{-2}N^{-1}$)
ε_r	Relative dielectric permittivity
ε'	Real part dielectric permittivity
ε''	Imaginary part dielectric permittivity
ε_∞	Optical (high frequency limit of) dielectric permittivity
ε_s	Static (low frequency limit of) permittivity
$\mathbf{E}$	Electric field (NC^{-1} or Vm^{-1})
$\mathbf{F}$	Force (N)
$\Gamma(\cdot)$	Gamma function
$\hbar$	Planck constant (1.054 572 66 10^{-34} Js)
$\mathbf{H}$	Magnetic field (Am^{-1})
$\mathcal{H}$	Hamiltonian of the system
i	Imaginary unit
$\Im$	Imaginary part
$I(t)$	Photoluminescence intensity decay (relaxation function for luminophores)
$\mathbf{J}$	Ohmic current density (Am^{-2})

K_D	Total detrapping rate (s^{-1})
K_{ISC}	Intersystem crossing rate (s^{-1})
K_O	Triplet trap decay rate (s^{-1})
K_P	Total trapping rate (s^{-1})
K_{rISC}	Reverse intersystem crossing rate (s^{-1})
K_S	Total singlet (state) decay rate (s^{-1})
$K_{\mathrm{rad}S}$	Radiative singlet (state) decay rate or fluorescence decay rate (s^{-1})
$K_{\text{non-rad}S}$	Non-Radiative singlet (state) decay rate (s^{-1})
K_T	Total triplet (state) decay rate (s^{-1})
$K_{\mathrm{rad}T}$	Radiative triplet (state) decay rate (s^{-1})
$K_{\text{non-rad}T}$	Non-radiative triplet (state) decay rate (s^{-1})
$\mathscr{L}$	Lagrangian of the system
$\mathcal{L}$	Laplace transform
ℓ	Integration path, Bromwich contour
μ	Magnetic permeability (kg m $\mathrm{s}^{-2}\mathrm{A}^{-2}$)
μ_0	Permeability of free-space ($4\pi\ 10^{-7}$ kg m $\mathrm{s}^{-2}\mathrm{A}^{-2}$)
μ_r	Relative magnetic permeability
m_e	Mass of the electron ($9.11\ 10^{-31}$Kg)
$\mathscr{m}$	Reduced mass
n_e	Electronic density per unit volume (electrons m^{-3})
n_0	Initial number of relaxing centers
n_S	Number of relaxing centers in singlet excited state
n_T	Number of relaxing centers in triplet state
$\mathbb{N}$	Set of Natural number without zero
$\mathbb{N}_0$	Set of Natural numbers with zero
ω	Frequency (s^{-1})
ω_0	Natural resonant frequency (s^{-1})
ω^*	Material frequency
ω_p	Plasma frequency (s^{-1})
$\mathbf{P}$	Polarization vector (C m^{-2})
ϕ	Pulse response function
Ψ	Relaxation function
q	Charge of a particle (C)
$\mathcal{Q}$	Quality factor
ρ	Electric charge density (C m^{-3})
$\mathbb{R}$	Set of Real Numbers
$\Re$	Real part
σ	Specific conductivity (S m^{-1})
S_0	Ground state
S	Singlet excited state
$\mathcal{T}$	Temperature
T	Triplet state
t	Time
t^*	Material time
$\hat{T}$	Semigroup operator
τ	Characteristic relaxation time (s)

τ^*	Material characteristic relaxation time
$\tan(\delta)$	Loss tangent
$\mathbf{v}$	Velocity of a particle (m s^{-1})
$\mathcal{V}$	Impressible volume
$\mathbf{x}$	Electron displacement
χ	Susceptibility
$\tilde{\chi}$	Normalized susceptibility
$\mathfrak{X}$	Banach space
ζ	Damping ratio (s^{-1})

In memory of my grandmother

Contents

Abstract iii

Acknowledgment vii

Abbreviations xi

Nomenclature xiii

Contents xix

List of Figures xxi

List of Tables xxv

Introduction 1

1 Introduction 5
- 1.1 The zoo of permittivities: ε, ε_0 and ε_r 7
- 1.2 Relaxation and dispersion: complementary concepts 11
- 1.3 Dispersion models and Debye relaxation 13
- 1.4 Non-Debye or anomalous relaxation and dispersion models 18

2 Photoluminescence for shining a light on anomalous relaxation processes 25
- 2.1 Basic concepts and mechanisms in photoluminescence 25
- 2.2 Time-resolved photoluminescence 28
  - 2.2.1 Part I: the material clock frame 28
  - 2.2.2 Part II: the KWW function as a sum of PL decays 36
  - 2.2.3 Part III: complete monotonicity vs. monotonicity: a mathematical tool able to sum up all the physical properties 42
- 2.3 OLEDs and Alq$_3$: an organic molecule for photoluminescence 46
- 2.4 The PL emission in the Alq$_3$ molecule 49
- 2.5 Conclusions to Chapter 2 60

3 Dynamical systems and their evolution: mathematical methods and physical interpretations 63
- 3.1 Introduction to modelling dynamical systems . . . 63
- 3.2 Debye or *pure* exponential composition rule . . . 65
  - 3.2.1 Composition rule via Cauchy convolution product . . . 66
  - 3.2.2 Composition rule via Reynolds-Leibnitz theorem . . . 68
- 3.3 One-Parameter Mittag-Leffler composition rule via Cauchy convolution product . . . 72
- 3.4 The general composition rules for anomalous relaxation functions . . . 75
  - 3.4.1 The case of the relaxation function based on the three-parameter Mittag-Leffler function . . . 75
  - 3.4.2 The case of the one-parameter Mittag-Leffler function . . . 77
  - 3.4.3 The case of the (upper) incomplete Gamma function: in the laboratory frame and in the material frame . . . 78
- 3.5 Material time: the counterpart of material frequency in anomalous dispersion models . . . 81
  - 3.5.1 The material Λ transform and the hidden relationship between KWW and HN . . . 84
- 3.6 Evolution equations for relaxation processes in dynamical systems . . . 88
  - 3.6.1 Evolution equation for the one-parameter Mittag-Leffler relaxation 88
  - 3.6.2 Evolution equation for the modified (upper) incomplete Gamma function and its sub-classes . . . 90
- 3.7 Conclusions to Chapter 3 . . . 93

4 Complete monotonicity and special functions in relaxation processes 97
- 4.1 Special functions: an overview. . . . 97
  - 4.1.1 The Mittag-Leffler function . . . 97
  - 4.1.2 The Meijer G-function . . . 99
  - 4.1.3 The motivations behind the investigations on the complete monotonicity . . . 100
- 4.2 Complete monotonicity for the three-parameter Mittag-Leffler function 102
- 4.3 Complete monotonicity for the Meijer G-function . . . 103
  - 4.3.1 Special functions and the *conjectured* theorem . . . 111
  - 4.3.2 A corollary: the complete monotone Meijer G kernel . . . 113
- 4.4 Conclusions to Chapter 4 . . . 115

5 Conclusions 117

Bibliography 121

List of Figures

1.1 Dipole orientation in an unpolarized dielectric between the electrodes of a parallel-plate capacitor. 8

1.2 Dipole orientation in a polarized dielectric between the electrodes of a parallel-plate capacitor. The arrows represent the direction of the electric field **E**. 9

1.3 The real and the imaginary part of the dielectric function (1.21), $\varepsilon'_r(\omega)$ and $\varepsilon''_r(\omega)$ vs. ω. Here we set $\varepsilon_s = 2.4$, $\varepsilon_\infty = 1$, $\omega_0 = 3.94 \cdot 10^2$ THz and $\zeta = 1.71 \cdot 10^2$ THz. 15

1.4 The Kohlrausch-William-Watts (KWW) function for different values of β at $\tau = 1$ in order to highlight the three different trends: the stretched (solid red line), the *pure* (dotted black line) and the compressed (dashed blue line) exponential function. 19

1.5 Cole-Cole plot of (1.33) for different values of the parameters α and γ. The dotted black line is the Debye (D) semicircle. The other three cases are respectively the Cole-Cole (CC, dashed blue line), the Cole-Davidson (CD, long dashed blue line) and the Havriliak-Negami (HN, solid green line). The presence of the symmetry axis (the vertical solid black line) allows to better appreciate the asymmetry characterizing the anomalous behaviour of the Cole-Davidson model and the Havriliak-Negami model. 20

1.6 Relaxation diagrams for the dispersion models: the Havriliak-Negami (HN), the Cole-Cole (CC) and the Cole-Davidson (CD). The empty circles represent the measured imaginary susceptibility $\chi''(\omega)$ for different materials collected in [96]. The labels of the axes refer to the powers used to describe the asymptotic behaviour in Eqs. (1.40) and (1.41). Reprinted from "Stochastic tools hidden behind the empirical dielectric relaxation laws" by A. Stanislavsky and K. Weron, 2017, Report on Progress in Physics, Volume(**80**), 036001. Copyright [2017] by the Name of Copyright Holder. 23

2.1 Electron configurations for a singlet ground state (a); a singlet excited state (b); and a triplet excited state (c). The dashed red box denotes the bound state of an electron and its hole called exciton. The exciton is the emitting center of the luminophore. 26

2.2 Frank-Condon energy diagram. The horizontal lines inside the two curves represent the vibrational energy levels generated by the oscillation of the nuclei in the molecule with respect to their equilibrium positions. However, the allowed transitions according to the selection rules between electronic levels are vertical. It means that the nuclei are assumed to be frozen during the extremely short time (10^{-15} s) needed for the absorption of a photon, so their oscillations can be neglected as stated by the Frank-Condon principle. 27

2.3 Time-dependent behaviour of the material clock (2.2) in the stretched, compressed and laboratory frame. The vertical axis highlights the switching point in the time-behaviour observed in the stretched and compressed case. 30

2.4 Reduced mass term $\mathcal{m}(t)$ at $\tau = 1$ and $M = 1$. 35

2.5 Partial energy diagram showing the fundamental decay rates used to model a photoluminescent system. Excited vibrational levels have been omitted for semplicity. 38

2.6 A graphical illustration for the *domino-effect* algorithm. 45

2.7 Schematic basic configuration of an OLED. 47

2.8 Molecular structure of meridianal and facial isomer of Alq_3. 48

2.9 Optical absorption spectrum (left) and emission spectrum, (right), at room temperature of a 32 nm thick Alq_3 film thermally evaporated on a silica substrate. The arrow indicates the pumping wavelength $\lambda_{\text{exc}} =$ 395 nm. Reprinted from "Singular Photoluminescence Behavior of Alq3 Films at Very Long Decay Times" by G. Baldacchini et al. Journal of Luminescence, 2018, Volume (**193**), 106-113. Copyright [2018] by the Name of Copyright Holder. 49

2.10 Photoluminescence intensity peak of the 140nm thick film alq60 in atmosphere (black square) and in dry box (white square). Reprinted from "Singular Photoluminescence Behavior of Alq3 Films at Very Long Decay Times" by G. Baldacchini et al. Journal of Luminescence, 2018, Volume (**193**), 106-113. Copyright [2018] by the Name of Copyright Holder. 50

2.11 PL intensity of sample alq63-3 decaying in air with a zoom for the time-resolved PL after 10,000 h (black circles). 52

2.12 PL intensity of sample alq65-1 decaying in air with a zoom for the time-resolved PL after 10,000 h (black circles). 53

2.13 The time dependent reduced mass $\mathcal{m}(t)$ (2.12a) of the fourth component of the sample alq63-3. 55

2.14 PL intensity of the sample alq63-3 decaying in air (blue dots) and the time-dependent reduced mass $\mathcal{m}(t)$ (red solid line). 56

2.15 PL intensity of the sample alq63-3 decaying in air (blue dots) and the time-dependent reduced mass $\mathcal{m}(t)$ at different relaxation time corresponding to each component: τ=0.72h blue solid line, τ=332h green solid line, τ=3195h orange solid line and finally τ=13381h red solid line. 56

2.16 PL intensity of the sample alq65-1 decaying in air (blue dots) annealed at 180°C in dry O_2 and the time-dependent reduced mass $\mathscr{m}(t)$ at different relaxation time corresponding to each component: τ=0.61h blue solid line, τ=300h green solid line, τ=2819h orange solid line and finally τ=32,451h red solid line. 57

2.17 PL intensity of sample alq63-3 decaying in Air after $10,000$h (full black circles), best fit (solid red line) by using (2.29) and parameters presented in Table 2.5 and the Prony series approximation of the fourth component by using (2.18) (dashed purple line) and (2.24) (dashed orange line). . . 58

2.18 PL intensity of sample alq65-1 decaying in Air after $10,000$h (full black circles), best fit (solid red line) by using (2.29) and parameters collected in Table 2.5 and the Prony series approximation of the fourth component by using (2.18) (dashed purple line) and (2.24) (dashed orange line). . 58

3.1 A graphical representation of the action of the complex-scaling operator in the Λ transform. As expected, the complex-scaling property shows a behaviour similar to the known scaling property of the Laplace-Fourier transform: a complex-scaling rotation in the time domain implies another one in the opposite direction in the frequency domain. 85

3.2 Cole-Cole plot for the Cole-Cole dispersion model where the angles with respect to the Debye diagrams have been shown. 86

3.3 Comparison between the real and the imaginary parts of (3.70) for different values of the parameters α and β. In the left-hand side (lhs) we have the Havriliak-Negami function (dashed blue line) and in the right-hand side (rhs) we have the Λ transformed function after the action of the complex-scaling operator (solid red line). 87

List of Tables

2.1 Parameters of the two-terms Prony series that approximates the stretched KWW function for several values of β. The last column is the sum of the squared residuals (SSR). 37
2.2 Parameters of the two-terms Prony series that approximates the compressed KWW function for several values of β. The last column is the sum of the squared residuals (SSR). 37
2.3 Parameters of the zero-th and first-order kinetics (two-terms Prony series with $K_2 = 0$) that approximates the compressed KWW function for several values of β. The last column is the sum of the squared residuals (SSR). 43
2.4 Amplitudes, time constants, and KWW parameter β of the four components for the reference not-annealed sample alq63-3 and the sample alq65-1, which has been annealed in dry oxygen at 180°C, retrieved by fitting the experimental data with (2.29). 54
2.5 Amplitude and time constant of the fourth component I_4 for the reference not-annealed sample alq63-3 and alq65-1, which has been annealed in dry oxygen at 180°C, retrieved by fitting the experimental data with (2.29). 58
2.6 Amplitude and time constants of the fourth component I_4 for the reference not-annealed sample alq63-3 and alq65-1, which has been annealed in dry oxygen at 180°C, retrieved by fitting the experimental data with Eq. (19). 59

Motivation for writing the thesis

This thesis investigates the physical mathematical background needed for modelling relaxation processes in complex and disordered systems, highlighting the relation between the physical meaning and the mathematics used to analyse dynamical systems. Different novel methodologies and approaches have been introduced to enlarge the landscape of the possible mathematical methods and intriguing physical interpretations to extricate successfully the complexity that characterizes real physical processes.
In fact, the intrinsic complexity of the anomalous relaxation processes creates barriers that obstacle a comprehensive knowledge.
Problems and open questions as

- the physical origin of the Kohlrausch-Williams-Watts function $e^{-x^{\beta}}$ for $\beta > 0$,
- the role of its singularity,
- the physical interpretation of the complete monotonicity,
- as well as the formulation of the evolution equations

are closely linked to each another. We need only the *correct lens* to see the common thread behind these crucial issues, and this thesis wants to be exactly that lens. And to be sure that it is a useful lens, we need the theory agrees with experiments. Theory and experiments are strongly dependent upon each other.
This is the essence of Science.

Outline of the thesis

The structure of the thesis is explained trying to put in evidence the essential technical points and the main results. The thesis is divided into five interrelated and self-consistent chapters.

Chapter 1 briefly reviews the fundamentals of the classical electromagnetic theory, fixes the notation and the basic formulas that will be used throughout the thesis, and it highlights possible analogies between different models of dielectric permittivity increasing the impact of the results obtained.

In **Chapter 2**, we focus our attention on the Kohlrausch-William-Watts (KWW) function. Despite its popularity and success in modelling relaxation processes, the physical

origin of this function is quite elusive and it is still a matter of debate in the scientific community. In order to bring out its meaning, a phenomenological model based on a second order differential equation has been formulated and articulated into three steps. Firstly, we extricate the complexity due to the anomalous behaviour introducing a different frame: the material frame. This strategic change of perspective favours the emerging of the Physics that can be modelled as a damped harmonic oscillator. Once the usual laboratory frame has been restored, the solution of the differential equation is exactly the KWW function, unveiling its meaning. However, the introduction of this material frame has dragged other interesting results. Analysing the singularity in the second order differential equation, we have the possibility to deepen the problem of the divergence on the first derivative in the stretched KWW function (i.e. for $0 < \beta \leq 1$). The singularity is not as disturbing as it appears. Moreover, considering the Lagrangian and the Hamiltonian associated with the differential equation, we can define a precious physical quantity, the reduced mass, that unveils the dynamics and the physical meaning of the complete monotonicity and monotonicity in modelling relaxation processes.
As a second step, the validation of the phenomenlogical model has been performed framing the results in the context of physicol-chemical reactions. The bi-exponential model commonly used in photoluminescence is a special case of the phenomenological model proposed in this thesis. The bi-exponential model consists in a weighted sum of two exponential functions and it is the result of the approximation in the dynamics of the system.
The last step represents the most meaningful test bench for the model: its predictions with respect to the data collecting in the experiments. Among all the physical system experienced relaxation processes, the photoluminescence from organic molecule as the Tris(8-hydroxyquinoline) alluminium (Alq3) has been considered. The choice of this molecule as a test case is due to on the large amount of available data and the widely applications in Organic Light Emitting Diodes (OLEDs), a spreading technology in our daily life. It should be remarked that the model presents a very general approach and for this it can be used to describe other photoluminescent materials.

Chapter 3 describes and design new methodologies in modelling dynamical systems involved in relaxation processes. Our attention has been focused on the evolutionary problems that can be addressed with the composition rule. We can consider the composition rule as a physical manifestation of the semigroup property governing the evolution of any linear and deterministic system. The definition of the operation needed to compose the relaxation syntagms, that is the relaxation functions on a finite time intervals, is the main issue of the Chapter.
The term *syntagm* is borrowed from linguistics and it means a syntactic autonomous unit that has meaning both alone and when contextualized in an ordered sequence of other syntagms. In this respect, the term *relaxation syntagm* manages to convey its physical meaning in a very natural way. It defines a relaxation function in a finite time interval that can be analysed separately or in a wider time interval when it is composed with other relaxation syntagms.
As it will be illustrated in this Chapter, the composition rule is not so easy task when we consider anomalous behaviours and their anomalous (or non-Debye) relaxation func-

tions. However, we present two different methodologies. The first approach defines the composition rule for the one-parameter Mittag-Leffler function from which it is possible to define an integro-differential relation playing the role of the time evolution equation. The hallmark of this approach is the compelling and logical use of the mathematics.
On the other hand, the issue of the composition rule can be addressed also from a physical point of view. Inspired by Reynolds-Leibnitz theorem, it is possible to define a very general composition rule as a commutator operator that involves a derivative and its inverse operator, that can be bought under the name *anti-derivative.* Being the relaxation syntagms a part of the relaxation function keeping its meaning, the relaxation syntagms are *intensive functions* and for this reason, Reynolds-Leibnitz theorem plays a paramount role as it will be explained in this Chapter. This general composition rule gives a further validation to the model proposed in Chapter 2, since the relaxation can be distorted, compressed or stretched but it always keeps its meaning. This idea inspired a modification of the Fourier transform in order to understand what is the effect of the anomalous behaviour on the frequency domain. The main result of this investigation was the possibility to explain the experimental recurrences of the Havriliak-Negami and KWW function in modelling relaxation processes allowing to completely restore the symmetry from a dynamical point of view between the relaxation and the dispersion models. The Chapter continues briefly illustrating mathematical tools and methodologies we developed in analysing evolutionary problems in a different context: the anomalous diffusion with the fractional Fokker-Planck equation. In fact despite the evident differences between the two processes, i.e. the relaxation and the anomalous diffusion, the mathematical methods share the same backbone. The problem is also addressed in terms of the semigroups theory in order to bring out a connection between the semigroup operator in the differential equation with the Reynolds-Leibnitz composition rule. We need to show that the solution of the second order differential equation arises as a consequence of the action of the semigroup operator to the initial condition. Therefore, a *track* of the semigroup property is embedded in the solution and it confirms that the Reynolds-Leibnitz composition rule is actually a manifestation of the semigroup property.

Chapter 4 is dedicated to the problem concerning the mathematical requirements to be satisfied by complete monotonic functions. As shown in the previous chapters, this property plays a relevant role in the physical and mathematical interpretation of relaxation processes. Therefore the definition of the mathematical requirements to be satisfied by the special functions involved in the description of relaxation processes represents a remarkable issue for the current research. The attention will be focused on the Mittag-Leffler function whose complete monotonicity has been proven keeping as a compass the papers written by Pollard and Wiman. The Chapter continues considering another special function, the Meijer's G-function. Here we formulated a *conjectured theorem* for its complete monotonicity that can be framed in the context of the known literature.

Finally, in **Chapter 5** we will summarize the results of the thesis framing them in a broader context and we will give the future lines of research and development.

Chapter 1

Introduction

In this thesis, the theory of the relaxation processes plays a central role, so it is important to outline the main aspects of the interaction between matter and electromagnetic fields.

All these interactions are described by the macroscopic *Maxwell equations* [144, 145] which at the very beginning were twenty. Only after the simplification carried with the modern vector notation developed by O. Heaviside and J. W. Gibbs [89] all the electromagnetic phenomena were summarized in the well-known set of the four macroscopic Maxwell equations as follows

- ◇ Gauss' law: $$\nabla \cdot \mathbf{D} = \rho \tag{1.1a}$$
- ◇ Ampere's law: $$\nabla \times \mathbf{H} = \mathbf{J} + \frac{\partial \mathbf{D}}{\partial t} \tag{1.1b}$$
- ◇ Faraday's law: $$\nabla \times \mathbf{E} = -\frac{\partial \mathbf{B}}{\partial t} \tag{1.1c}$$
- ◇ Gauss' law for magnetic fields: $$\nabla \cdot \mathbf{B} = 0, \tag{1.1d}$$

where the International System of units (SI units) are assumed throughout.

The Maxwell equations (1.1) are fundamental pillars in the description of the interrelations among quantities that depend on the material medium as the electric displacement $\mathbf{D}$, the magnetic field $\mathbf{H}$ and the ohmic current density $\mathbf{J}$, and quantities that do not depend on the material medium as the electric field $\mathbf{E}$, the magnetic induction $\mathbf{B}$ and the electric charge density ρ.[1]

However, we can reduce the four Maxwell equations to only two equations noting that the current density $\mathbf{J}$ and the charge density ρ are linked together by the so-called continuity equation

$$\frac{\partial \rho}{\partial t} + \nabla \cdot \mathbf{J} = 0,$$

which is obtained taking the divergence of (1.1b) and then, by applying (1.1a). In its turn, the Gauss law (1.1a) can be used to eliminate the unknown electric charge density ρ, by defining it in terms of $\mathbf{D}$ as

---

[1] Only for thoroughness, it is clarified that all field variables are functions of time t and space $\mathbf{x} = (x, y, z) \in \mathbb{R}^3$.

$$\rho := \nabla \cdot \mathbf{D}.$$

Adding the continuity equation to the two remaining Maxwell equations, i.e. Ampere's law (1.1b) and Faraday's law (1.1c), the essential system valid in any material medium still contains unknown vector functions. Thus, to find a self-consistent solution for the electromagnetic field, Maxwell's equations should be supplemented by three relations, known as *constitutive relations.* These equations are not universally valid, but depend upon the properties of the materials under consideration. We can assume that these equations have the form of the following local relations

$$\begin{aligned}
&\diamond \quad \mathbf{D} = \varepsilon \mathbf{E} = \varepsilon_r \varepsilon_0 \mathbf{E},\\
&\diamond \quad \mathbf{J} = \sigma \mathbf{E},\\
&\diamond \quad \mathbf{B} = \mu \mathbf{H} = \mu_r \mu_0 \mathbf{H},
\end{aligned}$$

where

- $\varepsilon := \varepsilon_0 \varepsilon_r$ is the permittivity of the material and its unit is $\frac{\mathrm{C}^2}{\mathrm{Nm}^2}$,
- $\varepsilon_0 = 8.8541878128\ 10^{-12}\ \frac{\mathrm{C}^2}{\mathrm{Nm}^2}$ is the vacuum permettivity,
- ε_r is the relative dielectric permittivity (or simply relative permittivity) and it is dimensionless,
- $\mu := \mu_0 \mu_r$ is the permeability of the material and it is measured in $\frac{\mathrm{H}}{\mathrm{m}}$ or $\frac{\mathrm{kg\ m}}{\mathrm{A}^2\mathrm{s}^2}$,
- $\mu_0 = 4\pi 10^{-7} \frac{\mathrm{kg\ \ m}}{\mathrm{A}^2\mathrm{s}^2}$ is the vacuum permeability,
- μ_r is the relative magnetic permeability that is a dimensionless quantity,
- σ is the specific conductivity of the material and its unit is $\frac{\mathrm{S}}{\mathrm{m}}$ or $\frac{\mathrm{s}^3\ \mathrm{A}^2}{\mathrm{kg\ m}^3}$.

In SI units, the vacuum permittivity ε_0 and the vacuum permeability μ_0 are related to the speed of light in vacuum c as follows:

$$c^2 = \frac{1}{\varepsilon_0 \mu_0}.$$

The constitutive equations allow us to solve the Maxwell system embracing the physical meaning of the quantities introduced which are therefore called *constitutive parameters.* Materials can be classified according to these constitutive parameters, as schematically shown below:

$$\begin{cases} \varepsilon, \mu \text{ are scalars, if the material is isotropic,} \\ \varepsilon, \mu \text{ are } 2^{\text{nd}} \text{ rank tensors, i.e. } \varepsilon_{i,j} = \begin{vmatrix} \varepsilon_{x,x} & \varepsilon_{x,y} & \varepsilon_{x,z} \\ \varepsilon_{y,x} & \varepsilon_{y,y} & \varepsilon_{y,z} \\ \varepsilon_{z,x} & \varepsilon_{z,y} & \varepsilon_{z,z} \end{vmatrix} \text{ or } \mu_{i,j} = \begin{vmatrix} \mu_{x,x} & \mu_{x,y} & \mu_{x,z} \\ \mu_{y,x} & \mu_{y,y} & \mu_{y,z} \\ \mu_{z,x} & \mu_{z,y} & \mu_{z,z} \end{vmatrix}, \\ \text{if the material is anisotropic;} \end{cases}$$

$$\begin{cases} \varepsilon_r > 0 \quad \mu_r > 0 \quad \text{most dielectric materials,} \\ \varepsilon_r < 0 \quad \mu_r > 0 \quad \text{metals, electrical plasmas, thin wire structures ,} \\ \varepsilon_r > 0 \quad \mu_r < 0 \quad \text{gyrotropic magnetic materials as some ferrites,} \\ \varepsilon_r < 0 \quad \mu_r < 0 \quad \text{metamaterials;} \end{cases}$$

$$\begin{cases} \sigma = 0 \quad \text{dielectrics,} \\ \sigma > 0 \quad \text{conductors.} \end{cases}$$

If the constitutive parameters are frequency-dependent, the material is named *dispersive*, as it will be explained in Section 1.1.
Finally, the radiation-matter interaction is accomplished by coupling the Maxwell equations and the Lorentz force acting on a particle of charge q and velocity $\mathbf{v}$ which reads

$$\mathbf{F} = q(\mathbf{E} + \mathbf{v} \times \mathbf{B}),$$

emphasizing how the electromagnetic fields can be related to measurable forces.
At this point, the characterization of the interactions between electromagnetic fields and any medium has been illustrated, so it is possible to fix the relevant tools and the framework in which the investigations will be carried out.

1.1 The zoo of permittivities: ε, ε_0 and ε_r

The dielectric permittivity ε plays an important role in understanding the electromagnetic properties of materials [30, 31, 94, 99, 180] since it affects the propagation of the electric fields influencing their amplitude and phase. In other words, the dielectric permittivity ε is a measure of how the electric field $\mathbf{D}$ behaves while the external field $\mathbf{E}$ interacts with any material.
In particular, measurements of dielectric properties imply measurements of the relative permittivity ε_r that differs from the permittivity ε by the constant vacuum permittivity ε_0:

$$\varepsilon_r(\omega) = \frac{\varepsilon(\omega)}{\varepsilon_0}.$$

The significant role of the relative permittivity can be physically unveiled using two circuital configurations where we integrate a capacitor into a circuit with direct or alternating current. The difference in the two configurations is hidden in the relative dielectric permittivity: it can be considered a constant, or it can be modeled as a complex-valued function depending on the frequency of the applied field:

$$\varepsilon_r(\omega) = \varepsilon'_r(\omega) + i\varepsilon''{}_r(\omega). \tag{1.2}$$

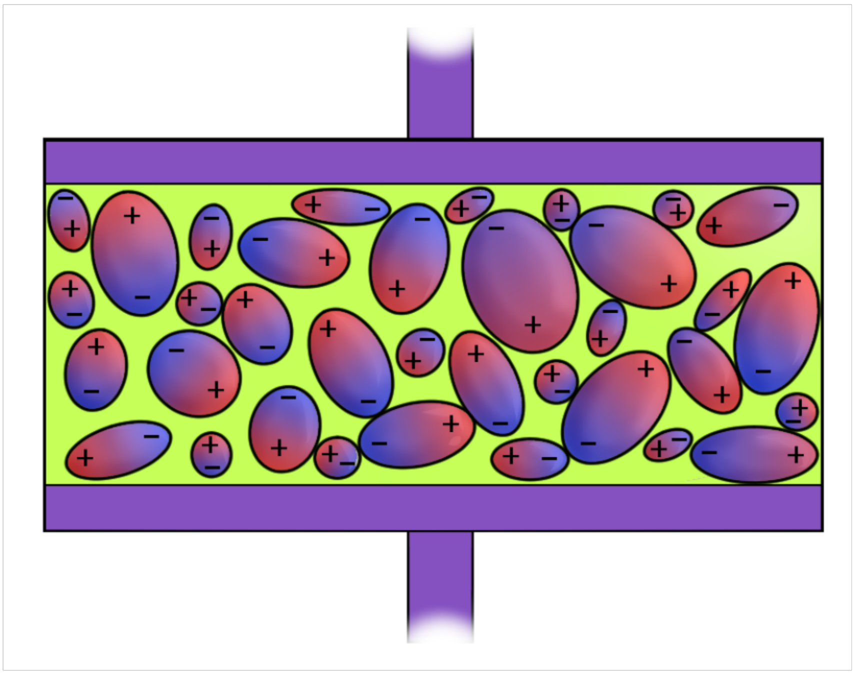

Figure 1.1: Dipole orientation in an unpolarized dielectric between the electrodes of a parallel-plate capacitor.

Firstly, we will consider the case of a direct current circuit (DC), where ε_r is a constant. Here, the amount of charge q stored in a capacitor C is linearly proportional to the electric potential difference ΔV between the electrodes. Thus, we may write

$$q = C|\Delta V|,$$

where C is a positive proportionality constant called *capacitance*.
Physically, capacitance measures the capacity of the electric charge storage for a given difference of potential ΔV. The SI unit of capacitance is the farad (F).
As long as the electric field is switched off and the capacitor is not polarized, the dipoles in the dielectrics have a random orientation, without any resulting pole. It may in principle looks like Fig. (1.1).
After switching on the electric field, the dielectric starts to be polarized and the dipoles organize themselves in chains as shown in Fig. 1.2. Every dipole chain binds in the electrode due to a torsional moment induced by the presence of the field. Thus, when the dipole chains are perfectly aligned, the electrode is able to receive as many new free charge carriers as those the dipole chains have bound without creating an increase of the electric field strength (or the voltage) above that of the starting point. This means a corresponding increase in capacitance.
From a phenomenological point of view, this effect can be described by the introduction of the relative dielectric permittivity ε_r which takes into account the presence of the dielectric material and the consequent increase of its storage capacity unlike the case when there is only vacuum between the electrodes.
So, the capacitance is linked to the relative dielectric permittivity ε_r according to the

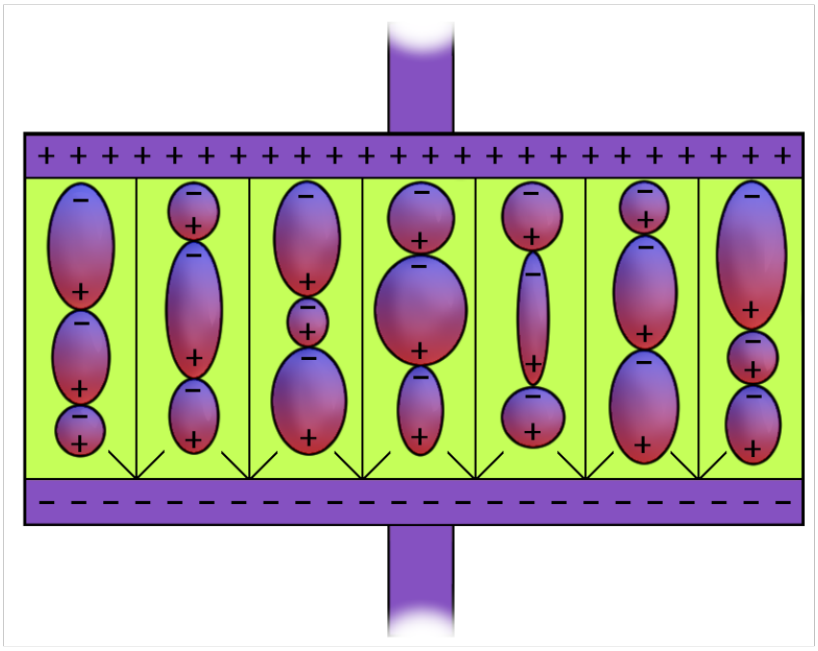

Figure 1.2: Dipole orientation in a polarized dielectric between the electrodes of a parallel-plate capacitor. The arrows represent the direction of the electric field **E**.

following expression

$$\varepsilon_r' = \frac{C}{C_0},$$

where ε_r' is the real part of the relative permittivity ε_r, C_0 is the test capacitance that is the capacitance when among the plates there is only the vacuum.
In case of a parallel-plate capacitor, the test capacitance is

$$C_0 = \varepsilon_0 \frac{A}{d},$$

and, the capacitance C with a dielectric between the electrodes is

$$C = \varepsilon_0 \varepsilon_r' \frac{A}{d},$$

where A and d denote respectively the surface and the distance between the plates of the electrodes. Otherwise, if a time-varying electromagnetic field (i.e. AC voltage) is placed across the same capacitor, the resulting current will be made up of a charging current I_C and a loss current I_L that is related to ε_r. The energy losses in the material are the inherent dissipation of electromagnetic energy in the dielectric material and can be represented as a conductance in parallel with a capacitor. So, the dielectric permittivity gains an imaginary part, and it becomes complex-valued depending on the frequency of the applied field. In (1.2), $\varepsilon_r'(\omega)$ represents the storage or the absorption and $\varepsilon_r''(\omega)$ is the imaginary part which describes the energy loss. The imaginary part of permittivity $\varepsilon_r''(\omega)$ is always greater than zero, and it is usually much smaller than the real part $\varepsilon_r'(\omega)$. The loss factor includes the effects of both dielectric loss and conductivity.

When complex permittivity is drawn as a simple vector diagram, the real and imaginary components are 90° out of phase. The vector $\varepsilon_0\varepsilon_r(\omega)$ forms an angle δ with the real axis (i.e. the axis fixed by $\varepsilon_0\varepsilon_r'(\omega)$). The relative energy loss in a material is the ratio of the energy lost to the energy stored. Mathematically, we conveniently describe the energy losses by means of the so-called electric loss tangent and its loss angle δ:

$$\tan(\delta) = \frac{\varepsilon_r''(\omega)}{\varepsilon_r'(\omega)} = \mathcal{D} = \frac{1}{\mathcal{Q}},$$

where $\mathcal{D}$ denotes the dispersion factor and its inverse, $\mathcal{Q}$ is the quality factor.

For very low-energy loss materials, since $\tan(\delta) \simeq \delta$, the loss tangent can be expressed in angle units, milliradians, or microradians.

The dielectric loss tangent of any material describes quantitatively the dissipation of the electric energy due to different physical processes such as electrical conduction, dielectric relaxation, dielectric resonance and loss from nonlinear processes (such as hysteresis). When measuring the energy loss of a dielectric at a single frequency, in general, it is impossible to get knowledge on their dependence on the frequency. Phenomenologically, they all give rise to just one measurable quantity, namely, the total measured loss tangent. The origin of dielectric losses can also be considered as being related to the time delay between the electric field and the electric displacement vectors (i.e. the dipole rotation).

The definition of the electric displacement $\mathbf{D}$ given by the corresponding constitutive equation reads

$$\mathbf{D}(\mathbf{x}, t) = \varepsilon\mathbf{E}(\mathbf{x}, t) = \varepsilon_r\varepsilon_0\mathbf{E}(\mathbf{x}, t),$$

and it can be regarded as correct only if the medium assumes a time-independent relative permittivity, i.e. $\varepsilon = \varepsilon_0\varepsilon_r$ is a constant. Otherwise, the system is a temporally dispersive medium whose permittivity ε depends on the history of the electric field strength. In such a case, the displacement and the electric fields are related by the convolution

$$\mathbf{D}(\mathbf{x}, t) = \varepsilon_0\mathbf{E}(\mathbf{x}, t) + \varepsilon_0 \int_{-\infty}^{t} dt'\ \mathbf{E}(\mathbf{x}, t')\chi(t - t'). \tag{1.3}$$

In the right-hand side of (1.3) there are two contributions: the first term represents the free-space response which contains the vacuum permittivity ε_0, and the second term is the time domain polarization vector $\mathbf{P}(\mathbf{x}, t)$, that is the material response described by the susceptibility kernel $\chi(t)$:

$$\mathbf{P}(\mathbf{x}, t) = \varepsilon_0 \int_{-\infty}^{t} dt'\ \mathbf{E}(\mathbf{x}, t')\chi(t - t'). \tag{1.4}$$

Thus, we can recast the electric displacement (1.3) in a more compact form using (1.4) as follows

$$\mathbf{D}(\mathbf{x}, t) = \varepsilon_0\mathbf{E}(\mathbf{x}, t) + \mathbf{P}(\mathbf{x}, t).$$

The convolution form used for defining the displacement $\mathbf{D}(\mathbf{x}, t)$ in (1.3) and the polarization $\mathbf{P}(\mathbf{x}, t)$ in (1.4) implies the causality. In other words, the values of the displacement $\mathbf{D}(\mathbf{x}, t)$ and the polarization $\mathbf{P}(\mathbf{x}, t)$ at the present time t depend only on the values assumed by the electric field $\mathbf{E}(\mathbf{x}, t)$ at a time prior and equal to t.

1.2 Relaxation and dispersion: complementary concepts

The term *relaxation* means the irreversible process of a perturbed system towards a novel equilibrium state. When a system in equilibrium is disturbed by an external field, that system is pushed out of equilibrium. We deal with a relaxation process only if the time needed to reach a new equilibrium state is longer than the time of interaction with external field. The time delay, usually denoted with τ, is the *relaxation time* which characterizes the system previously influenced by an external field. In fact it represents the delay in the response of a system due to the changes of the external field. So, the relaxation time τ could be considered as a distinctive mark of a physical process under examination.

The description of relaxation is achieved in the time domain introducing the relaxation function $\Psi(t)$ accounting for the pulse decay and the pulse response function $\phi(t)$ linked to

$$\phi(t) = -\frac{d}{dt}\Psi(t), \quad t \geq 0.$$

In case the external field is an electric field $\mathbf{E}$ and the system is a dielectric (or a dielectric material)[2], the relaxation process is called *dielectric relaxation process*. Unlike what happen in conductor materials, electrical charges do not flow into the material, but they are slightly shifted from their average or equilibrium position causing the polarization of the dielectric. After switching off the external dielectric field, the polarization starts to decay.
Once introduced the definitions of the static permittivity ε_s

$$\varepsilon_s = \varepsilon_r(\omega \to 0) \tag{1.5}$$

and the optical permittivity ε_∞

$$\varepsilon_\infty = \varepsilon_r(\omega \to \infty), \tag{1.6}$$

we can make evident the relation between the relaxation function $\Psi(t)$ (or the pulse response function $\phi(t)$) with the normalized complex permittivity

$$\hat{\varepsilon}(\omega) := \frac{\varepsilon_r(\omega) - \varepsilon_\infty}{\varepsilon_s - \varepsilon_\infty} \tag{1.7}$$

or with the normalized complex susceptibility

$$\hat{\chi}(\omega) = 1 - \hat{\varepsilon}(\omega). \tag{1.8}$$

---

[2] A dielectric is an electrical insulator that can be polarized by an electric field.

As shown in [66], the Fourier transform $\mathcal{F}$ on the real positive line

$$\tilde{F}(\omega) = \mathcal{F}[f(t);\omega] = \int_0^\infty dt\ f(t)e^{-i\omega t}$$

or equivalently the Laplace transform $\mathcal{L}$, i.e.

$$\hat{F}(s) = \mathcal{L}[f(t);s] = \int_0^\infty dt\ f(t)e^{-st},$$

relate both the time-dependent function $\Psi(t)$ and $\phi(t)$ with the normalized complex permittivity $\hat{\varepsilon}(\omega)$ and susceptibility $\hat{\chi}(\omega)$.
The replacement in favour of the Laplace parameter $s = i\omega$ compacts the notation of the two transforms and define the following correspondences for the relaxation function

$$\begin{aligned}\Psi(t) &= 1 - \mathcal{L}^{-1}\left[\frac{1}{s}\hat{\chi}(s);t\right] = \mathcal{L}^{-1}\left[\frac{1}{s} - \frac{1}{s}\hat{\chi}(s);t\right]\\ &= \mathcal{L}^{-1}\left[\frac{1}{s}\hat{\varepsilon}(s);t\right],\end{aligned} \tag{1.9}$$

and the pulse response function or relaxation response

$$\phi(t) = \mathcal{L}^{-1}\Big[\hat{\chi}(s);t\Big] = \mathcal{L}^{-1}\Big[1 - \hat{\varepsilon}(s);t\Big]. \tag{1.10}$$

This fact opens the possibility to address the analysis both in the time domain with the relaxation function $\Psi(t)$ (or the pulse response function $\phi(t)$) and in the frequency domain with the dispersion model and its spectrum defined by the normalized complex permittivity $\hat{\varepsilon}(\omega)$. This possibility occurs when dielectrics are considered as passive and casual linear systems [66]. Analysing the complex dielectric permittivity $\hat{\varepsilon}(\omega)$, we define the dielectric spectrum that can be presented in two equivalent ways. Usually the real and the imaginary components of the complex permittivity are plotted vs. the frequency in logarithmic scale. The lines obtained are respectively named dispersion and absorption curves. The second method plots the imaginary component of the dielectric permittivity $\hat{\varepsilon}''(\omega)$ with respect to the real one $\hat{\varepsilon}'(\omega)$. The result is a semicircle whose symmetry depends strictly on the relaxation process considered. Such plots are called the Cole-Cole plots [38] or Argand's diagrams of dielectric constant [6]. Examples of the Cole-Cole plots can be found in Fig. 1.5 of Section 1.3.

As last remark, we emphasize that the normalized complex dielectric permittivity $\hat{\varepsilon}(\omega)$ - as well as the normalized complex susceptibility $\hat{\chi}(\omega)$ - satisfies the Hermitian symmetry property

$$\hat{\varepsilon}(-\omega) = \hat{\varepsilon}^*(\omega),$$

or equivalently,

$$\begin{aligned}\hat{\varepsilon}'(-\omega) &= \hat{\varepsilon}'(\omega),\\ \hat{\varepsilon}''(-\omega) &= -\hat{\varepsilon}''(\omega)\end{aligned}$$

since the permittivity is the Fourier transformed function of the relaxation $\Psi(t)$ that is a real function.

To conclude, dispersion models can classify the relaxation of different polarization. For this reason, relaxation models are a useful approach to investigate dielectric dispersion.
The State of Art of dispersion models and relaxations is based on three well-known pillars, which are nowadays spreading in photonics, plasmonics and in dielectrics: the Lorentz model, the Debye model and the Drude model.

1.3 Dispersion models and Debye relaxation

The Dutch physicist H. A. Lorentz was able to grasp the essence of the polarization phenomena introducing a model for describing the behaviour of a wide range of dispersive materials, as dilute or dense gases, metals, semiconductors, and even dielectrics[3]. This model is based on the concept of a mass-spring system, and it is able to describe the behaviour of the polarization and the permittivity in the dispersive materials. In presence of the external electric field, the electrons surrounding the nuclei in the atoms react by vibrating like damped harmonic oscillators, creating a small separation or displacement between the centres of positive and negative charges denoted by $\mathbf{x}(t)$. Their motion is the result of the superposition of different effects, which take into account the forces involved in the system. Applying the Newton law, the differential equation which rules the Lorentz dispersion model is

$$m_e \frac{d^2\mathbf{x}(t)}{dt^2} = -m_e\zeta\frac{d\mathbf{x}(t)}{dt} - m_e\omega_0^2\mathbf{x}(t) - e\mathbf{E}(t), \tag{1.11}$$

where

- ◇ $\mathbf{F}_{tot} = m_e\frac{d^2\mathbf{x}(t)}{dt^2}$ represents the total force acting on the electrons which causes their oscillatory motion, and m_e denotes the mass of the electron;
- ◇ $\mathbf{F}_D = -m_e\zeta\frac{d\mathbf{x}(t)}{dt}$ is a friction force due to multiparticle interactions as the collisions between electrons, the interaction between electrons and the lattice or even to the radiative emission determining global losses with a consequent damping of the system. Here, ζ denotes the damping factor and $\frac{d\mathbf{x}(t)}{dt}$ is the velocity of the electron;
- ◇ $\mathbf{F}_R = -m_e\omega_0^2\mathbf{x}(t)$ plays the role of a restoring spring force due to the positive charges in the nucleus that oscillate with a natural resonant frequency ω_0;
- ◇ $\mathbf{F}_{Ext} = -e\mathbf{E}(t)$ is an external driving force originated by the applied local electric field.

---

[3] The Lorentz dispersion model can be used also for describing the the magnetization if the magnetic field has been applied to the material instead of the electric field as described in the text. In fact, the magnetic field can speed up or slow down the motion of the electrons around the nucleus producing a variation on the magnetic momentum dipole.

The electric field $\mathbf{E}(t)$ and the electron displacement $\mathbf{x}(t)$ can be written respectively in a complex notation

$$\mathbf{E}(t) = \Re[\mathbf{E}_0 e^{\pm i\omega t}] = \mathbf{E}_0 \cos(\omega t),$$
$$\mathbf{x}(t) = \Re[\mathbf{x}_0 e^{\pm i\omega t}] = \mathbf{x}_0 \cos(\omega t),$$

where $\mathbf{x}_0$ and E_0 are in general complex constants. The solution of (1.11) in the Fourier space reads

$$\tilde{\mathbf{x}}(\omega) = -\frac{e}{m_e}\frac{1}{(\omega_0^2 - \omega^2) + i\omega\zeta}\tilde{\mathbf{E}}(\omega). \tag{1.12}$$

The above result is useful to calculate the polarization density, or simply the polarization of the material, which is given by the electron density n_e (per unit volume) times the polarization due to a single electron:

$$\mathbf{P}(t) = n_e p(t) = -e n_e \mathbf{x}(t). \tag{1.13}$$

Multiplying both sides of (1.12) by $-en_e$ and then, taking the Fourier transform of (1.13), we define the polarization in terms of the frequency as

$$\tilde{\mathbf{P}}(\omega) = \frac{e^2 n_e}{m_e}\frac{1}{\omega_0^2 - \omega^2 + i\omega\zeta}\tilde{\mathbf{E}}(\omega). \tag{1.14}$$

The factor ${\omega_p}^2 = \frac{e^2 n_e}{m_e \varepsilon_0}$ is the plasma frequency squared, so (1.14) can be written as

$$\tilde{\mathbf{P}}(\omega) = \frac{\omega_p^2}{\omega_0^2 - \omega^2 + i\omega\zeta}\varepsilon_0\tilde{\mathbf{E}}(\omega). \tag{1.15}$$

Comparing the definition of the polarization in the frequency domain

$$\tilde{\mathbf{P}}(\omega) = \tilde{\chi}(\omega)\varepsilon_0\tilde{\mathbf{E}}(\omega),$$

with (1.15), and solving for $\tilde{\chi}(\omega)$, yields

$$\tilde{\chi}(\omega) = \frac{\omega_p^2}{\omega_0^2 - \omega^2 + i\omega\zeta}. \tag{1.16}$$

Replacing the above definition of susceptibility (1.16) in

$$\varepsilon(\omega) = \varepsilon_0(1 + \tilde{\chi}(\omega)),$$

the permittivity of the material at the frequency ω can defined as follows

$$\varepsilon(\omega) = \varepsilon_0\Big(1 + \frac{\omega_p^2}{\omega_0^2 - \omega^2 + i\omega\zeta}\Big). \tag{1.17}$$

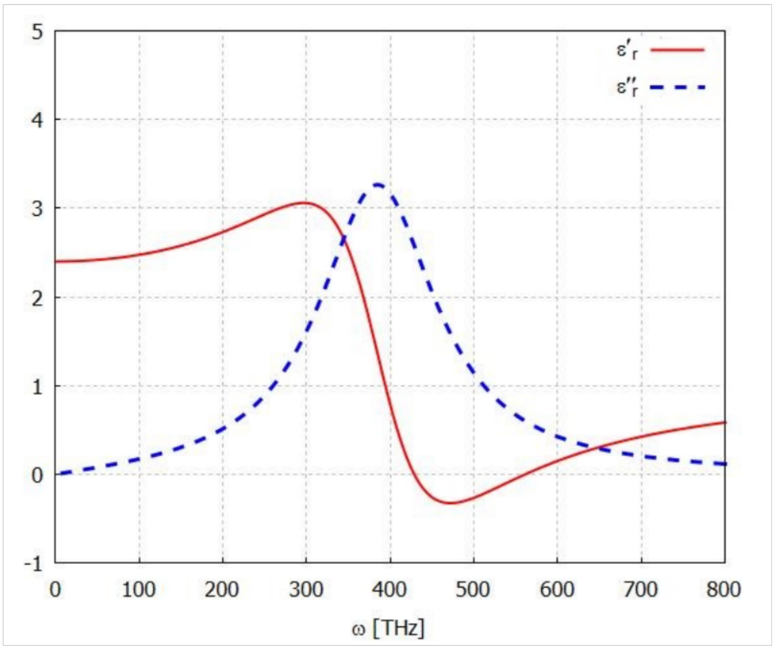

Figure 1.3: The real and the imaginary part of the dielectric function (1.21), $\varepsilon_r'(\omega)$ and $\varepsilon_r''(\omega)$ vs. ω. Here we set $\varepsilon_s = 2.4$, $\varepsilon_\infty = 1$, $\omega_0 = 3.94 \cdot 10^2$ THz and $\zeta = 1.71 \cdot 10^2$ THz.

Finally, the Lorentz relative permittivity $\varepsilon_r(\omega)$ is defined as

$$\varepsilon_r(\omega) = 1 + \frac{\omega_p^2}{\omega_0^2 - \omega^2 + i\omega\zeta}, \tag{1.18}$$

and then, its real and imaginary components read

$$\varepsilon_r'(\omega) = 1 + \frac{\omega_p^2(\omega_0^2 - \omega^2)}{(\omega_0^2 - \omega^2)^2 + \omega^2\zeta^2} \qquad , \tag{1.19a}$$

$$\varepsilon_r''(\omega) = \frac{\omega_p^2 \omega\zeta}{(\omega_0^2 - \omega^2)^2 + \omega^2\zeta^2}. \tag{1.19b}$$

The form of the imaginary part of the permittivity, $\varepsilon''(\omega)$, is often referred to as a Lorentzian function as it is clearly visible from Fig. 1.3. This figure illustrates the behaviour of the real and imaginary part of the permittivity $\varepsilon(\omega)$. Note that $\varepsilon'(\omega)$ has its maximum at the resonant frequency ω_0.
Resorting to the definitions of static permittivity (1.5), and the optical permittivity (1.6), and applying them to (1.19), we obtain

$$\begin{aligned} \varepsilon_s &= \varepsilon(\omega \to 0) = 1 + \frac{\omega_p^2}{\omega_0^2} \\ \varepsilon_\infty &= \varepsilon(\omega \to \infty) = 1 \end{aligned} \tag{1.20}$$

and consequently, we define the complex dielectric function ε_r as follows

$$\varepsilon_r(\omega) = \varepsilon_\infty + \frac{(\varepsilon_s - \varepsilon_\infty)\omega_0^2}{\omega_0^2 - \omega^2 + i\omega\zeta}. \tag{1.21}$$

Considering that the difference between the static permittivity and the optical dielectric constant, $\varepsilon_s - \varepsilon_\infty$, denoted by $\Delta\varepsilon$ is called the strength of the relaxation process, the complex dielectric function $\varepsilon_r(\omega)$ in (1.21) can be written as below

$$\varepsilon_r(\omega) = \varepsilon_\infty + \frac{\Delta\varepsilon\ \omega_0^2}{\omega_0^2 - \omega^2 + i\omega\zeta}. \tag{1.22}$$

Among the variations of the Lorentz model, there are two well-known special cases: the Drude model and the Debye model.

The Lorentz model (1.11) reduces to the Drude model given by the equation

$$m_e \frac{d^2\mathbf{x}(t)}{dt^2} = -m_e\zeta\frac{d\mathbf{x}(t)}{dt} - e\mathbf{E}(t), \tag{1.23}$$

when the restoring force $\mathbf{F}_R$ is neglected. This condition is fulfilled if the conduction electrons can be considered free, therefore the Drude model makes excellent predictions about the nature of the conduction electrons in metals and in plasma [8, 51].
The permittivity of the material based on the Drude model is

$$\varepsilon_r(\omega) = 1 - \frac{\omega_p^2}{\omega^2 - i\omega\zeta}.$$

The other variant of the Lorentz model (1.11) is the Debye model that describes systems composed by an ideal and non-interacting ensemble of freely rotating dipoles induced by an alternating external electric field [31, 46, 47, 172].
It is possible to model the response of dipoles, that have a natural frequency ω_0, in terms of the displacement between positive and negative charges

$$m_e\zeta\frac{d\mathbf{x}(t)}{dt} = -m_e\omega_0^2\mathbf{x}(t) - e\mathbf{E}(t). \tag{1.24}$$

Comparing the differential equation which rules the Debye model (1.24) with the one of the Drude model (1.23), it is possible to highlight the following features.
In the Drude model, the electrons are free to move and this justifies why the restoring force term is missing in (1.23), whereas in the Debye model (1.24), the second order derivative can be dropped out. The physical assumption behind this mathematical simplification is rooted in the relaxation processes: the presence of a high friction that causes the damping tones down the contribution of the inertia force.
It is therefore possible to oversee the acceleration of the dipoles without much error.
The equation of motion (1.24) leads to the following dielectric function

$$\varepsilon_r(\omega) = \varepsilon_\infty + \frac{\omega_p^2}{\omega_0^2 + i\zeta\omega}. \tag{1.25}$$

Replacing $\zeta = \tau\omega_0^2$ and

$$\Delta\varepsilon = \varepsilon_s - \varepsilon_\infty = \frac{\omega_p^2}{\omega_0^2}$$

in (1.25), it is possible to write the Debye dielectric function as below

$$\varepsilon_r(\omega) = \varepsilon_\infty + \frac{\Delta\varepsilon}{1 + i\omega\tau}. \tag{1.26}$$

Debye assumed that the polarization decays exponentially with a single relaxation time τ, after the removal of the external electric field. In the time domain, the counterpart of the dispersion relation (1.26) is the Debye relaxation

$$\Psi(t) = e^{-\frac{t}{\tau}}, \tag{1.27}$$

and consequently its dielectric response function is

$$\phi(t) = \frac{e^{-\frac{t}{\tau}}}{\tau}. \tag{1.28}$$

For many systems - except for example ferroelectric materials, water in liquid state and weak solution of polar liquids in non-polar solvents [172], the Debye relaxation (1.27) (or its response function (1.28)) does not sufficiently describe the experimental data since the relaxation behaves not-exponentially. This implies taking into account the distribution of relaxation times in formulating relaxation laws, now named non-Debye or anomalous relaxation laws. Consequently, the response function (1.28) and the complex dielectric permittivity (1.26) can be expressed in terms of a distribution function G for the relaxation time τ:

$$\Psi(t) = \int_0^\infty d\tau\ G(\tau) e^{-\frac{t}{\tau}} \tag{1.29}$$

and

$$\hat{\varepsilon}(\omega) = \int_0^\infty d\tau\ \frac{G(\tau)}{1 + i\omega\tau}. \tag{1.30}$$

Here, the distribution function $G(\tau)$, which satisfies the normalization condition $\int_0^\infty G(\tau)d\tau = 1$, can be regarded as the fraction of polarization processes where relaxation times range between $\log(\tau)$ and $\log(\tau) + d(\log(\tau))$ and it satisfies the following normalization condition

$$\int_\infty^\infty d(\log(\tau))\ G(\log\tau) = 1. \tag{1.31}$$

It is quite hard to obtain the actual distribution of relaxation times. In the last decades, many phenomenological relaxation and dispersion models have been developed starting from the Debye dispersion model (1.26) and the relaxation function (1.28), paving the way to a new branch of physics: the so-called anomalous or non-Debye relaxation models.

1.4 Non-Debye or anomalous relaxation and dispersion models

The most important and popular anomalous models are the Kohlrausch-Williams-Watts (KWW) function [112, 198] and the Havriliak-Negami model [66, 76, 87] with its variants the Cole-Cole [38] and the Cole-Davidson [44]. Recently, the Hilfer excess-wings model [92, 93] and the Jurlewicz-Weron-Stanislavsky (JWS) model [100] have been added to the list of anomalous models.

The most popular function used to fit the time-domain relaxation data which do not obey the simple exponential law, is the Kohlrausch-Williams-Watts (KWW) function [112, 198]

$$\Psi(t) = e^{-\left(\frac{t}{\tau}\right)^{\beta}}, \tag{1.32}$$

where τ is the characteristic relaxation time constant, and the parametric exponent denoted by the Greek letter β is non-negative and its range can be divided as follows:

- ◇ $0 < \beta < 1$,
- ◇ $\beta = 1$,
- ◇ $\beta > 1$.

The value $\beta = 1$ denotes the *pure* exponential function that is a watershed case for the behaviour of the KWW function. If $\beta \in (0, 1)$, the KWW function is called *stretched* exponential function since it decays slower than the exponential function ($\beta = 1$) as shown in Fig. 1.4. For $\beta > 1$, the function runs faster then a pure exponential function as illustrated in Fig. 1.4, and therefore it is called *compressed* exponential function.
We can appreciate the meaning behind the choice of the names considering Fig. 1.4 where the three different trends are shown: the stretched, the *pure* and the compressed exponential behaviour. The KWW relaxation function (1.32) appropriately models the intricate behaviour of liquids [55, 65, 110, 111, 151, 184, 201], glasses [128, 162, 163], biological tissues [113], dielectric materials and especially the folding of proteins [84]. This ubiquitous feature promotes the consideration of the Kohlrausch-Williams-Watts function as a *universal model* for describing the relaxation behaviour in the time domain.
The exceptionally wide range of applications of the KWW function overcomes the field of physics and it spreads throughout the sciences. In fact, in probability theory and statistics [153], the KWW exponential function is known as the complementary cumulative Weibull distribution [50] or as reciprocal Weibull distribution in [152]. In mathematics, the KWW function can be also defined as the Laplace transform of the Lévy stable distribution [26, 73, 167].

On the other hand, in 1967, Havriliak and Negami proposed a two parameters phenomenological formula in the frequency regime in order to take into account the asymmetry and the amplitude of the dielectric dispersion curve [87] and their formula

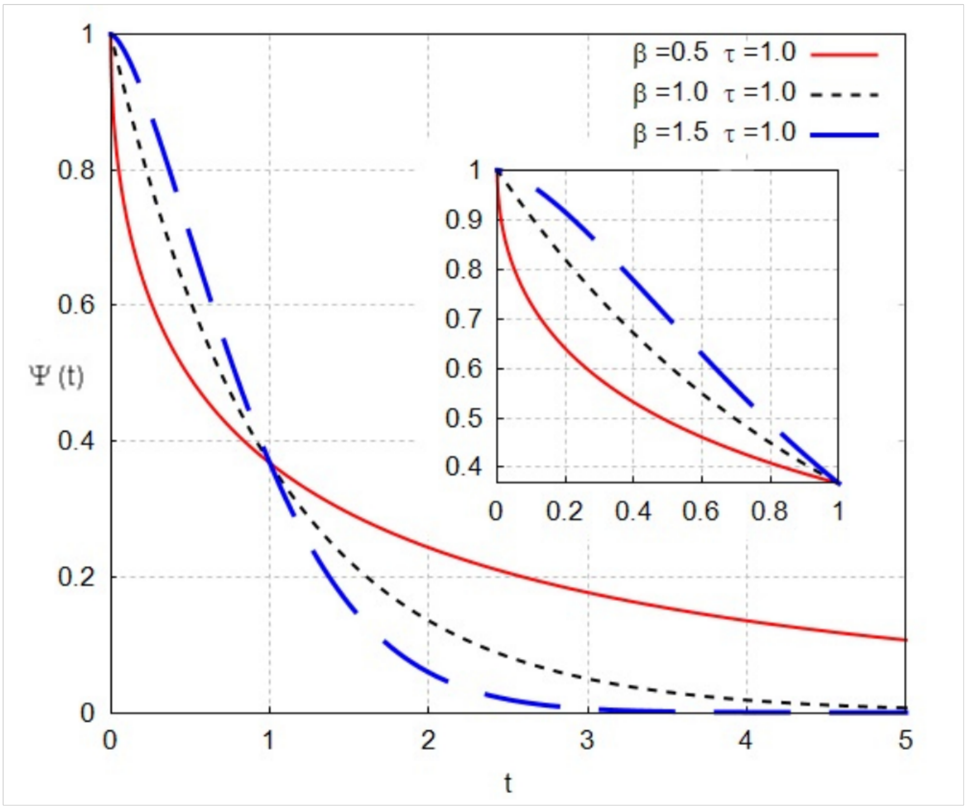

Figure 1.4: The Kohlrausch-William-Watts (KWW) function for different values of β at $\tau = 1$ in order to highlight the three different trends: the stretched (solid red line), the *pure* (dotted black line) and the compressed (dashed blue line) exponential function.

reads:

$$
\begin{aligned}
\hat{\varepsilon}(\omega) &= \frac{\varepsilon_r(\omega) - \varepsilon_\infty}{\Delta\varepsilon} \\
&= \frac{1}{[1 + (i\omega\tau)^\alpha]^\gamma},
\end{aligned}
\tag{1.33}
$$

nowadays well-known as Havriliak-Negami model.
Here $\Delta\varepsilon = \varepsilon_s - \varepsilon_\infty$ is the relaxation strength of the process, ε_s and ε_∞ are respectively the low and high frequency limit of the dielectric permittivity and the parameters α and γ range according to $0 < \alpha \leq 1$ and $0 < \gamma \leq 1$. These two phenomenological parameters make the shape of the relaxation peak more pliable compared to the Debye model (1.26). The parameter γ takes into account the asymmetry of the dispersion curve whereas α its broadness. All that we know about α and γ comes from experiments as well as their ranges. In order to appreciate how these phenomenological parameters influence the relaxation curve, Fig. 1.5 collects the Cole-Cole plot of (1.33) for different choices of the parameters.

The real and the imaginary part of the Havriliak-Negami dielectric function (1.33)

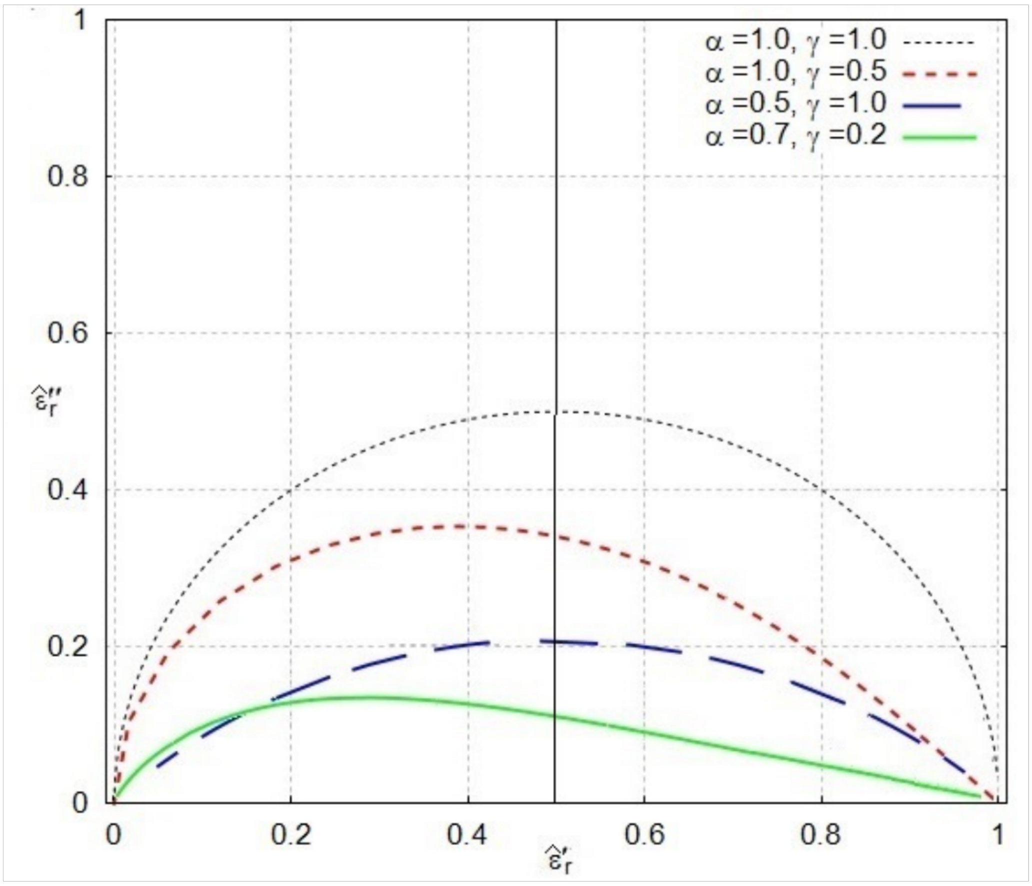

Figure 1.5: Cole-Cole plot of (1.33) for different values of the parameters α and γ. The dotted black line is the Debye (D) semicircle. The other three cases are respectively the Cole-Cole (CC, dashed blue line), the Cole-Davidson (CD, long dashed blue line) and the Havriliak-Negami (HN, solid green line). The presence of the symmetry axis (the vertical solid black line) allows to better appreciate the asymmetry characterizing the anomalous behaviour of the Cole-Davidson model and the Havriliak-Negami model.

are

$$\begin{aligned} \varepsilon'_r(\omega) &= \varepsilon_\infty + \Delta\varepsilon \frac{\cos(\gamma\vartheta)}{\left[1 + 2(\omega\tau)^\alpha \cos(\frac{\pi\alpha}{2}) + (\omega\tau)^{2\alpha}\right]^{\frac{\gamma}{2}}} \\ \varepsilon''_r(\omega) &= \Delta\varepsilon \frac{\sin(\gamma\vartheta)}{\left[1 + 2(\omega\tau)^\alpha \cos(\frac{\pi\alpha}{2}) + (\omega\tau)^{2\alpha}\right]^{\frac{\gamma}{2}}}, \end{aligned} \tag{1.34}$$

where

$$\vartheta = \arctan\left(\frac{(\omega\tau)^\alpha \sin(\frac{\pi\alpha}{2})}{1 + (\omega\tau)^\alpha \cos(\frac{\pi\alpha}{2})}\right), \tag{1.35}$$

and the relaxation time, related to the critical frequency ω_0, is

$$\tau = \frac{1}{\omega_c}\left[\tan\left(\frac{\pi}{2(\gamma+1)}\right)\right]^{\frac{1}{1-\alpha}}. \tag{1.36}$$

From the Havriliak-Negami dispersion model (1.33), other two anomalous dispersion models stand out considering special choices for its parameters: the Cole-Cole dispersion model and the Cole-Davidson dispersion model; obviously in the last instance the Debye dispersion model.
Fixing $\gamma = 1$ in (1.33), we obtain the Cole-Davidson dispersion model

$$\hat{\varepsilon}(\omega) = \frac{\varepsilon_r(\omega) - \varepsilon_\infty}{\Delta\varepsilon} = \frac{1}{1 + (i\omega\tau)^\alpha}. \tag{1.37}$$

whose real and imaginary parts are

$$\begin{aligned} \varepsilon'_r(\omega) &= \varepsilon_\infty + \Delta\varepsilon \frac{1 + (\omega\tau)^\alpha \cos(\frac{\pi\alpha}{2})}{1 + 2(\omega\tau)^\alpha \cos(\frac{\pi\alpha}{2}) + (\omega\tau)^{2\alpha}} \\ \varepsilon''_r(\omega) &= \Delta\varepsilon \frac{(\omega\tau)^\alpha \sin(\frac{\pi\alpha}{2})}{1 + 2(\omega\tau)^\alpha \cos(\frac{\pi\alpha}{2}) + (\omega\tau)^{2\alpha}}. \end{aligned} \tag{1.38}$$

The other special case is the Cole-Davidson dispersion model and it steps out from the Havriliak-Negami dispersion model when α is set equal to 1. As we have done with the Cole-Cole dispersion model, the real and imaginary parts of the Cole-Davidson are

$$\begin{aligned} \varepsilon'_r(\omega) &= \varepsilon_\infty + \Delta\varepsilon \frac{\cos(\gamma \arctan(\omega\tau)\ )}{\left[1 + (\omega\tau)^2\right]^{\frac{\gamma}{2}}} \\ \varepsilon''_r(\omega) &= \Delta\varepsilon \frac{\sin(\gamma \arctan(\omega\tau)\ )}{\left[1 + (\omega\tau)^2\right]^{\frac{\gamma}{2}}}. \end{aligned} \tag{1.39}$$

In Fig. 1.5, the Cole-Cole model preserves the symmetry that characterizes the Debye model but its semicircle is dampened compared to the Debye one. Conversely, the other two anomalous behaviours, the Cole-Davidson model and the Havriliak-Negami model, are skewed with respect to the symmetry axis. Taking into account these peculiarities, it is licit to suppose that there are two different origins for the anomalous behaviour: one carried out by the Cole-Cole model and the other one by the Cole-Davidson model. Obviously, the Havriliak-Negami model merges both the two types of anomalies as it is a generalization of the previous two. We will unveil the nature of the different anomalies considering the presence or the absence of symmetry and connecting this aspect to the dynamics of the systems itself in a framework that restores the symmetry between the frequency and the time domains in the light of the harmonic oscillator.

It is worth to note that the relaxation parameters in these non-Debye models (i.e. Havriliak-Negami model and its special cases) are extracted upon fitting the experimental data providing a deeper understanding of the anomalous behaviour. However, it is important to point out that the physical meaning behind these parameters is very limited although the success of these methods.

After analysing dielectric properties of many insulating and semiconducting materials [96–99] using a logarithmic scale, Jonscher formulated a universal law for dielectric relaxation models.

As Jonscher stated in [97], the higher frequency branch follows the fractional power law $\hat{\varepsilon}(\omega) \simeq (i\omega)^{n-1}$, where n is a number almost near zero.

The frequency dependencies of dielectric permittivity follow a common universal pattern for almost all the materials. Here below the universal response behaviour:

$$\begin{array}{lllll} \omega < \omega_p & \varepsilon_r''(\omega) \simeq \omega^m & \text{and} & \varepsilon_r'(\omega) \simeq 1 - \varepsilon''(\omega) \\ \omega > \omega_p & \varepsilon_r''(\omega) \simeq \omega^{n-1} & \text{and} & \varepsilon_r'(\omega) \simeq \omega^{n-1}. \end{array} \tag{1.40}$$

The frequency ω_p is to be found temperature dependent. According to this universal law, the deviation from the Debye behaviour could be described by the functional relation

$$\varepsilon_r''(\omega) = \frac{A}{(\frac{\omega}{\omega_p})^{-m} + (\frac{\omega}{\omega_p})^{1-n}}, \tag{1.41}$$

whereas $\varepsilon'(\omega)$ is derived numerically from the Kramers-Krönig relations. The exponentials m and n fall in the range between 0 and 1. Despite having certain universal behaviours, such as the above-mentioned two fitting functions (1.40) and the Jonscher functional relation (1.41), their origins are not entirely clear yet [99, 156, 157]. To emphasize the universality of the asymptotic dependence highlighted in (1.40), it is possible to consider Fig. 1.6 where the circles represent the imaginary part of the permittivity for different materials according to their behaviour at high and low frequency limit.

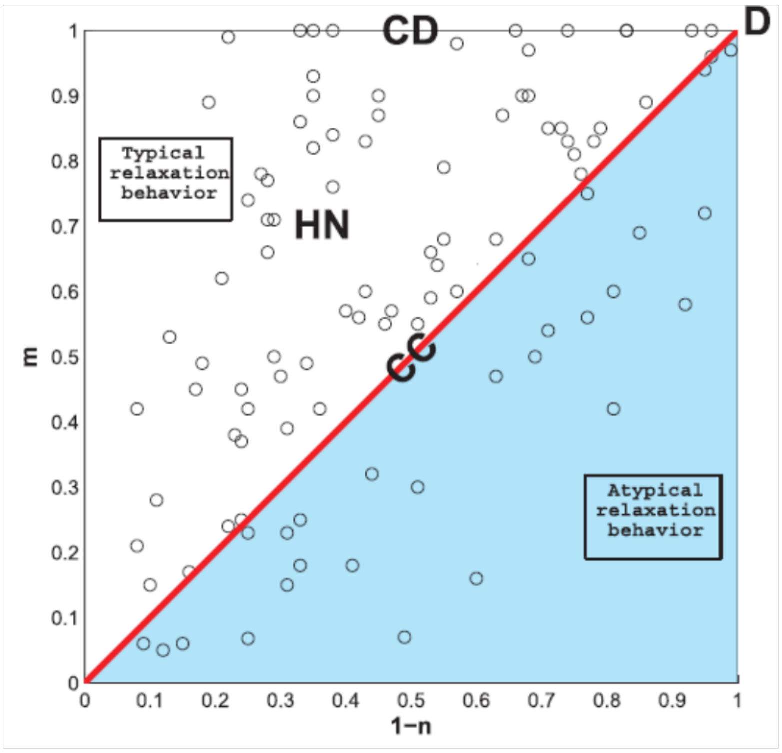

Figure 1.6: Relaxation diagrams for the dispersion models: the Havriliak-Negami (HN), the Cole-Cole (CC) and the Cole-Davidson (CD). The empty circles represent the measured imaginary susceptibility $\chi''(\omega)$ for different materials collected in [96]. The labels of the axes refer to the powers used to describe the asymptotic behaviour in Eqs. (1.40) and (1.41). Reprinted from "Stochastic tools hidden behind the empirical dielectric relaxation laws" by A. Stanislavsky and K. Weron, 2017, Report on Progress in Physics, Volume(**80**), 036001. Copyright [2017] by the Name of Copyright Holder.

Chapter 2

Photoluminescence for shining a light on anomalous relaxation processes

2.1 Basic concepts and mechanisms in photoluminescence

Photoluminescence (PL) is the emission of light from atoms or functional groups in chemical compounds as a result of the absorption of the electromagnetic radiation. The prefix *photo-* reveals the nature of the underlying mechanism [146]: the photoexcitation. From now on, the emitters will be called *luminophores*, since these atoms or functional groups are responsible for luminescence [130]. The term photoluminescence embraces both fluorescence and phosphorescence. In other words, the class of PL processes can be divided into two main categories based on the nature of the excited state. As the Pauli's exclusion principle affirms [103, 159], a pair of electrons occupying the same electronic ground state must have opposite spins — see Fig. 2.1(a). Such a state is called singlet since the net angular momentum is zero and the emitted photon has a single spectral line. After absorbing a photon, the electron in the singlet ground state is promoted by photoexcitation to a higher energy level leaving in the ground state a positively charged electron hole. The photoexcitation of the electron in the luminophore generates a bound state composed by an electron and its hole called *exciton*. The exciton can be in a triplet or in a singlet state and its relaxation gives rise to the luminescence via electron-hole recombination. It is hence evident that the difference between the fluorescence and the phosphorescence is in the spin multiplicity that characterizes the electrons in the ground state and in the excited one.

The PL takes the name of *fluorescence* in case the light emission arises from a singlet excited state [189]. In fluorescence, the electron absorbs the electromagnetic wave (generally in the ultraviolet range) and it moves into an excited state, as schematically shown in Fig. 2.1(b). Here, the electron in the ground state is paired to the electron of opposite spin in the photoexcited state. However, the energy suddenly acquired by the photoexcited electron is quickly dispersed in approximately 10ns since this electron is in a particular unstable state. The equilibrium can be reached emitting a photon in the visible light range.

As mentioned, the other PL process is the *phosphorescence*, and it can be observed

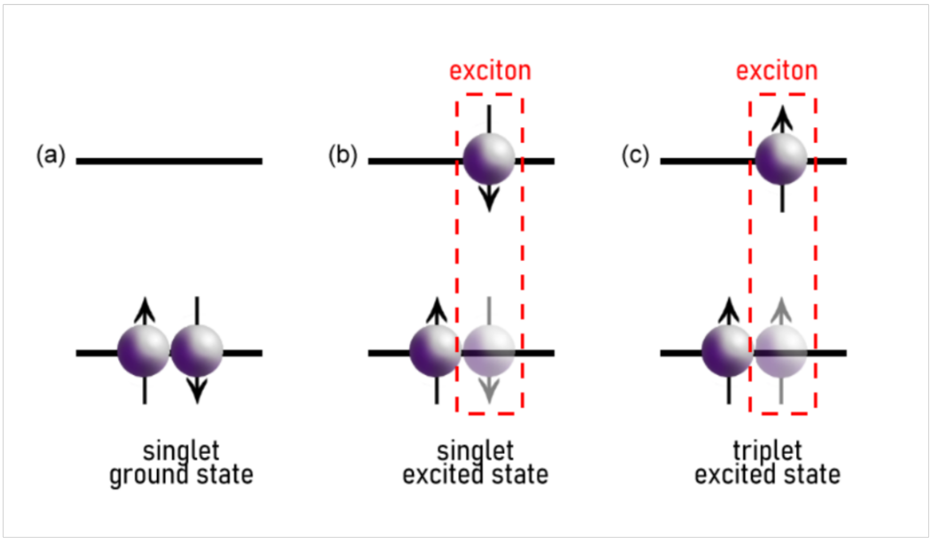

Figure 2.1: Electron configurations for a singlet ground state (a); a singlet excited state (b); and a triplet excited state (c). The dashed red box denotes the bound state of an electron and its hole called exciton. The exciton is the emitting center of the luminophore.

when the excited electron is in a triplet state after the photoexcitation as shown in Fig. 2.1(c): the electron in the photoexcited state has the spin orientation of the electron in the ground state [63]. Even in this PL process, the spin multiplicity of the excited state strictly influences the amount of time necessary for emitting the radiation. In phosphorescence, the range of this amount of time could be from few milliseconds to even hours after the photoexcitation of the initial ground state. The delay in the emission is due to the fact that the electron does not reach directly the ground state after its de-excitation, but it stops into an intermediate state (i.e. the triplet state) from which the probability of falling to the ground state is extremely low. In other words, the emission rate is much slower than singlet transitions. However, these transitions become more probable when a significant interaction between the spin angular momentum and the orbital angular momentum is observed, for example in the presence of heavy atoms. Furthermore, solutions rich in paramagnetic species, such as molecular oxygen O_2, increase the transition probability between two electronic states with different spin multiplicity, the so-called intersystem crossing, making these spin transitions more probable [129, 158].The presence of the oxygen favours the mixing between the triplet state and the singlet state of organic molecules and consequently, the intersystem crossing occurs.

The difference between these two PL mechanisms can be better appreciated considering the following energy diagram illustrated in Fig. 2.2 which is known as the Frank-Condon energy diagram [39, 62]. The Frank-Condon energy diagram shows how transitions can occur to different vibrational levels, resulting in characteristic shapes for the excitation and emission spectra, as schematically shown in Fig. 2.2.

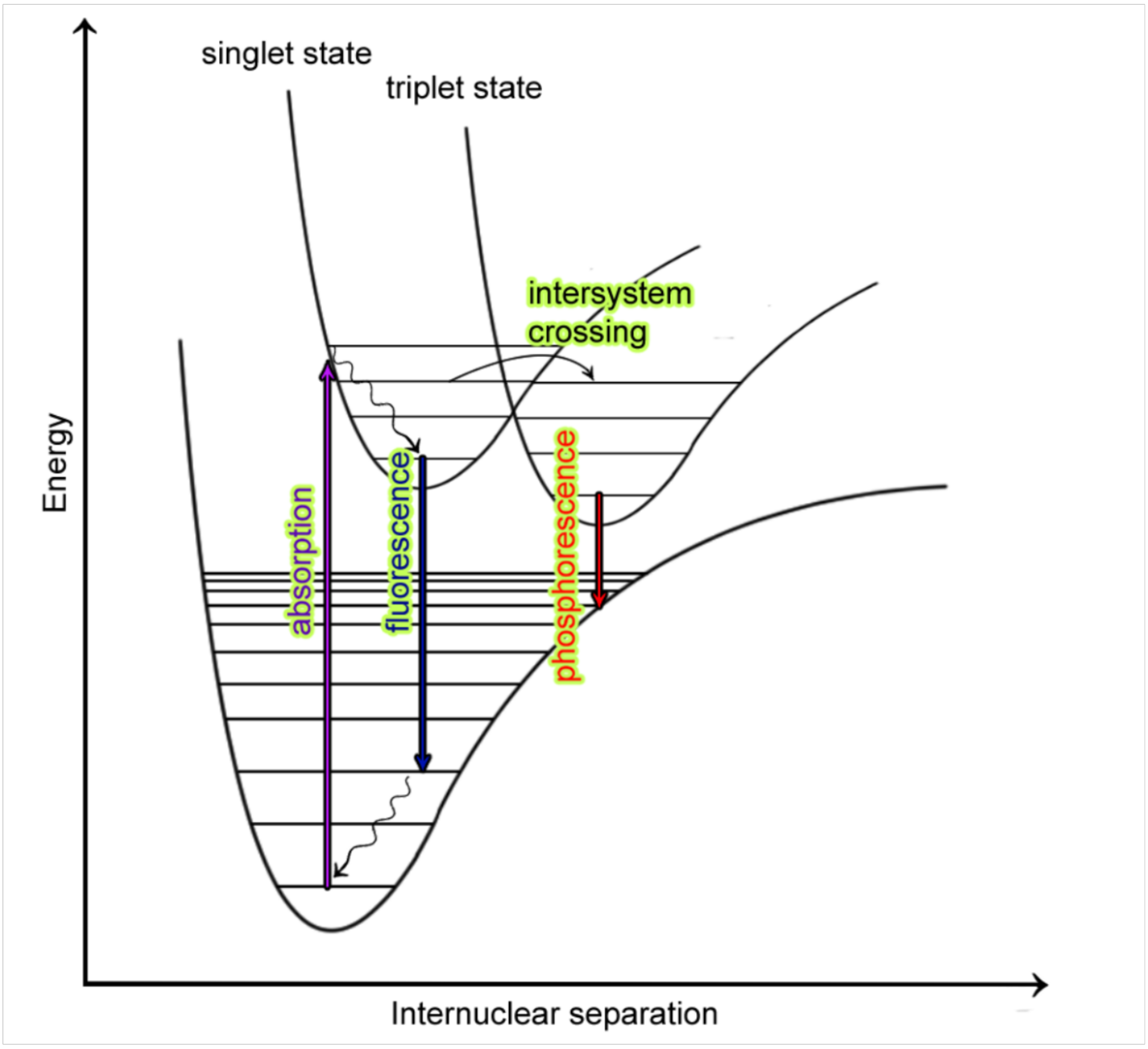
singlet state
triplet state
intersystem crossing
Energy
absorption
fluorescence
phosphorescence
Internuclear separation

Figure 2.2: Frank-Condon energy diagram. The horizontal lines inside the two curves represent the vibrational energy levels generated by the oscillation of the nuclei in the molecule with respect to their equilibrium positions. However, the allowed transitions according to the selection rules between electronic levels are vertical. It means that the nuclei are assumed to be frozen during the extremely short time (10^{-15} s) needed for the absorption of a photon, so their oscillations can be neglected as stated by the Frank-Condon principle.

2.2 Time-resolved photoluminescence

As time passes, the initial number of luminophores $n(0)$ begins to decrease. The luminophores will be quenched as the excitons relax, and they will not emit luminescence anymore leaving the system free to evolve towards equilibrium. All the luminophores are considered to be identical, and their excitons can be in a triplet or in a singlet state, playing the role of the excited emitter. To describe the PL emission, the relaxation function of the luminophores is a key notion and in the most general case, it is defined as a fraction between the numbers of luminophores at a specific time $n(t)$ and the initial number of luminophores $n(0)$.

The aim of this Section is to introduce a phenomenological model based on a second-order differential equation for describing the dynamics underling the relaxation of the luminophores, as we illustrated in [123]. A preview of the advantages of this model that will be described throughout the Chapter are summarized here below.

- ◇ Firstly, the model restores the symmetry from a dynamical point of view with dispersion models presented in Chapter 1. In fact, we describe the dynamical system as a damped harmonic oscillator introducing a second order differential equation with time-dependent coefficients whose solution is the Kohlrausch-Williams-Watts function. This model not only restores the parallelism with the Lorentz dispersion model, but it paves the way to a novel approach in relaxation processes. As it will be explained in Chapter 3, a novel transform bridges the solution of the model and its generalization to a driven damped harmonic oscillator (i.e. a generalized Kohlrausch-Williams-Watts function) with the Havriliak-Negami model.
- ◇ Secondly, the model gives a clear physical interpretation not only for the Kohlrausch-Williams-Watts (KWW) function, but it unveils the role of the complete monotonicity and simple monotonicity in relaxation processes. These mathematical properties are strictly linked to the nature of the dynamics experienced by the system during relaxation.
- ◇ Moreover, the model solves the problem of the infinite relaxation rate at the origin that affects the first derivative of the stretched KWW function. This singular point is not intrinsic to the physical system, but it is only nested in the frame. For this reason, the role of the frame is vital in the correct interpretation of the anomalous behaviours.
- ◇ Last and not least, this model generalizes the bi-exponential model (i.e. a model described by the weighted sum of two exponential functions) used in photoluminescence and explains the anomalous behaviours and dynamics observed in the experiments. The proposed model and its predictions are validated in different environmental conditions and for a wide time-range of measurements (more than six years of measurements).

2.2.1 Part I: the material clock frame

The necessity to introduce a second order model is linked to the frictional and restoring nature of the forces acting on the system. The radiative friction or resistance is the retarding force acting on charges when the electromagnetic radiation is emitted during a PL process. The consequence is the ineluctable decreasing of the energy and the damping of oscillations. It is important to remark that the damping of the oscillations occurs not only as the result of the emission, but also as the result of the collisions with other oscillators and of the decelerating effect of the surrounding medium. The presence of the restoring force is due to the Coulomb attraction between the positive and negative charges that constitute the bound state in the excitons.

Despite the simplified analysis of the forces acting on the system, the relaxation still exhibits complex and nonlinear behaviours that complicate the investigations on the material response and properties. The key notion to understand this anomalous behaviour is to change the perspective with the introduction of a new frame, called material frame, that is different from the *classical* laboratory one and centred in the material itself. The anomalous behaviour has been enclosed in the flexible scale of the material frame. Such a scale can *stretch* and *compress* the system giving an insight of what happens from the point of view of the material during the relaxation, focusing the attention on the dynamics which finally results to be simplified. According to this approach, during the relaxation process the material follows its own *clock*, called the *material clock* or *material time*, which is in general different from the one set in the laboratory [52, 60, 90, 141, 148, 155, 177, 186]. The material clock represents the time measured by a clock, whose rate itself changes: it can accelerate or decelerate. Consequently, in the laboratory, the relaxation processes evolve with a different speed as the system ages. The material clock embeds the thermal history dependence at the origin of the anomalous behaviour

$$t^* = \int_0^t \frac{dx}{a(\mathcal{T}(x) - \mathcal{T}_0)}, \tag{2.1}$$

where $a(\mathcal{T}(x)-\mathcal{T}_0)$ is a time-dependent function of the temperature of the system, $\mathcal{T}(x)$ is the current temperature and $\mathcal{T}_0$ is the reference temperature. The only requirement on $a(\mathcal{T}(x) - \mathcal{T}_0)$ is to be non-negative to ensure that the material time t^* can never go backwards with the increasing of the laboratory time t. Such a transformation implies that the relaxation that occurs over time t with time dependent relaxation time τ in the real time domain is equal to what occurs in the material time domain with constant relaxation time. To model how the material clock t^* marks the time, we have to define the function $a(\mathcal{T}(x) - \mathcal{T}_0)$ in terms of the (inverse) Arrhenius equation in order to explicit how the material time depends on the absolute temperature:

$$\begin{aligned} a(\mathcal{T}(x) - \mathcal{T}_0) : &= \frac{1}{\beta\tau^{\beta-1}}\; e^{(1-\beta)\frac{E}{R}\left(\frac{1}{\mathcal{T}(x)}-\frac{1}{\mathcal{T}_0}\right)} \\ &= \frac{1}{\beta\tau^{\beta-1}} e^{(1-\beta)\log\left(\frac{x}{\tau}\right)} \\ &= \frac{x^{1-\beta}}{\beta}, \end{aligned}$$

Here above, the symbol E denotes the activation energy and R is the gas constant defined as $R := \mathcal{N}_A\ k_B$ where $\mathcal{N}_A$ is the Avogadro number and k_B is the Boltzmann

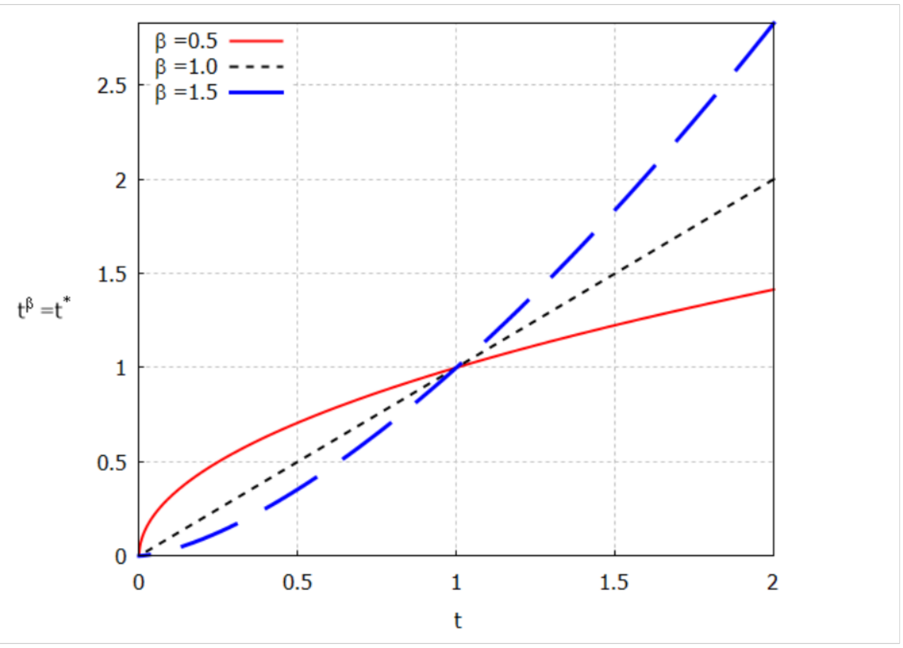

Figure 2.3: Time-dependent behaviour of the material clock (2.2) in the stretched, compressed and laboratory frame. The vertical axis highlights the switching point in the time-behaviour observed in the stretched and compressed case.

constant. The equivalence between

$$\frac{E}{R}\Big(\frac{1}{\mathcal{T}(x)}-\frac{1}{\mathcal{T}_0}\Big)=\log(\frac{x}{\tau})$$

directly follows considering the logarithmic version of the Arrhenius law. Once the function a has been defined, the material clock assume the following form (2.1):

$$t^* = \int_0^t dx\,\frac{\beta}{x^{1-\beta}} = t^\beta. \tag{2.2}$$

The material clock captures all the anomalous behaviours including re-configurations, the relaxation times distribution, the nonlinear response and also effects as ageing and rejuvenation.

As it appears from Fig. 2.3, the concept of the material clock can be visualized by comparing it with the linear behaviour. Here, the values of the exponent β can be split into two ranges: $0 < \beta < 1$ (solid blue line) and $\beta > 1$ (dashed red line) where the case $\beta = 1$ is the linear time (dotted black line) in the laboratory frame, and it represents the only case where the clock rate is constant.
If β belongs to the first range (i.e. $\beta \in (0, 1)$), which from now on will be called the stretched range, the time flows initially slowly than the time in the laboratory. After crossing the intersection with the linear time line, the time in the material starts to speed up and increase almost linearly. In this case, the material clock stretches the timescale. On the other hand, if $\beta > 1$, the material clock compresses the timescale: the passing of time is faster at the beginning and then, for $t > 1$ it slows down its rate

as shown in Fig. 2.3. This explains the name "compressed range", when β assumes values greater than 1.
Taking into account the material frame and the forces acting on the system, the relaxation dynamics can be described by the following initial value problem:

$$\begin{aligned}
&\frac{d^2n(t^*)}{dt^{*2}} + \frac{2\zeta}{\tau^*}\frac{dn(t^*)}{dt^*} + \frac{n(t^*)}{\tau^{*2}} = 0 \\
&n(0) = n_0 \\
&\frac{dn(t^*)}{dt^*}|_{t^*=0} = -\frac{\zeta n_0}{\tau^*},
\end{aligned} \tag{2.3}$$

where $\tau^* = \tau^\beta$. The parameter ζ is the damping ratio, and it critically determines the evolution of the system. Mathematically, the presence of the damping term in the differential equation for $n(t)$ changes the form of the solution so that the oscillations are perturbed or even dramatically attenuated. The damping harmonic oscillator can be:

- ◇ overdamped ($\zeta > 1$): the system exponentially decays to a steady state without oscillating. The return to equilibrium is slower then the critically damped case;
- ◇ critically damped ($\zeta = 1$): the system returns to a steady state as quickly as possible without oscillating;
- ◇ underdamped ($0 < \zeta < 1$): the system oscillates with a slightly different frequency than the undamped case ($\zeta = 0$) where the amplitude gradually decreases to zero.

The solution of the second order differential equation (2.3) reads:

$$n(t^*) = n_0 e^{-\zeta \frac{t^*}{\tau^*}} \cos\Big(\frac{t^*}{\tau^*}\sqrt{1-\zeta^2}\Big). \tag{2.4}$$

Considering the increment of the material clock chosen (2.2)

$$\frac{d}{dt^*} = \frac{1}{\beta t^{\beta-1}}\frac{d}{dt},$$

the differential equation (2.3) can be written in the laboratory frame as follows

$$\begin{aligned}
&\frac{d^2n(t)}{dt^2} + \Big(\frac{1-\beta}{t} + \frac{2\zeta\beta t^{\beta-1}}{\tau^\beta}\Big)\frac{dn(t)}{dt} + \frac{\beta^2 t^{2\beta-2}}{\tau^{2\beta}} n(t) = 0. \\
&n(0) = n_0 \\
&\frac{dn(t)}{dt}|_{t=0} = \begin{cases} 0 & \text{for } \beta > 1 \\ -\frac{\zeta n_0}{\tau} & \text{for } \beta = 1 \\ \infty & \text{for } 0 < \beta < 1 \end{cases}
\end{aligned} \tag{2.5}$$

and its solution now reads

$$n(t) = n_0 e^{-\zeta\left(\frac{t}{\tau}\right)^{\beta}} \cos\Big(\frac{t^{\beta}}{\tau^{\beta}}\sqrt{1-\zeta^2}\Big). \tag{2.6}$$

Assuming that the system returns to equilibrium as fast as possible, i.e. the system has been critically damped ($\zeta = 1$), the solution of the initial value problem (2.5), i.e. (2.6), reduces to the Kohlrausch-Williams-Watts (KWW) function:

$$n(t) = n_0 e^{-\left(\frac{t}{\tau}\right)^{\beta}}. \tag{2.7}$$

We should focus the attention on the initial conditions of the initial value problems in both the frames. The first condition results to be the same of the initial value problem in the material frame:

$$n(t^*)|_{t^*=0} = n(t)|_{t=0} = n_0,$$

as expected since the initial number of the luminophores should be the same in any frame. On the other hand, the second initial condition presents a variety of behaviours according to the value of the β parameters. All these behaviours are a consequence of the choice of the frame, and in order to support this idea we highlight how this initial condition in the laboratory frame is linked to the material frame. Mathematically, we have

$$\frac{dn(t)}{dt} = \frac{dn(t^*)}{dt^*}|_{t^*=t^{\beta}} + \frac{\zeta + \sqrt{1-\zeta^2}\,\tan\Big(\frac{t^{\beta}}{\tau^{\beta}}\sqrt{1-\zeta^2}\Big)}{\tau^{\beta}}(1-\beta t^{\beta-1})n(t),$$

and for $\zeta = 1$, we obtain

$$\frac{dn(t)}{dt} = \frac{dn(t^*)}{dt^*}|_{t^*=t^{\beta}} + \frac{(1-\beta t^{\beta-1})}{\tau^{\beta}}n(t).$$

Thus, the two relaxation rates differ by a term which accounts for the change of the frames: from the laboratory frame to the material frame and vice versa. At $t = 0$, it is possible to recover the initial conditions previously defined for the respective frames. The presence of this extra term supports our idea that the frame plays a key role in a clear understanding of the dynamics. To be sure that the singularity does not affect the physics, we analyse the nature of the singularity in the coefficients of the differential equation.

The coefficient in front of the first order derivative in (2.5) represents the time-dependent frictional term in the laboratory frame and its form is a direct consequence of the material clock chosen (2.2):

$$P(t) := \Big(\frac{1-\beta}{t} + \frac{2\zeta\beta t^{\beta-1}}{\tau^{\beta}}\Big), \tag{2.8}$$

whereas, the coefficient in front of $n(t)$ is

$$Q(t) := \frac{\beta^2 t^{2\beta-2}}{\tau^{2\beta}}. \tag{2.9}$$

Both of these coefficients are singular for $t = 0$. This singularity influences the derivatives of the KWW function. However, the singularity is not particularly disturbing, in fact it is classified as a regular singularity [25, 95, 115, 171, 173]. In other words, $P(t)$ diverges no more rapidly than $\frac{1}{t}$ and $Q(t)$ diverges no more rapidly than $\frac{1}{t^2}$. We remark that the singularity appears when we come back to the laboratory frame, and it does not exist in the material frame. We therefore suspect that it is a *coordinate* singularity, i.e. a singularity that is nested in the choice of the frame and therefore, it can be erased.

At this point, we focus our attention on the time-dependent frictional term $P(t)$. It is important to investigate the role of this term in the dynamics of the system so we need to find a related physical quantity in order to unveil the mechanism behind the anomalous behaviour.

From a mesoscopic point of view, the quenching of the luminophores occurs when the excitons relax via electron-hole recombination. The mass of the luminophores during its emitting-life changes because of the *cloud* of virtual particles such as phonons, photons and also others particles as the more reactive species in the atmosphere that surrounds and interact with the exciton. Here, the laboratory damping coefficient in front of the first order derivative (2.5) is the key tool to interpret correctly the experimental results. It is therefore important to investigate the role of this term in the dynamics of the system finding a related physical quantity in order to unveil the mechanism behind the anomalous behaviour. The problem can be formulated introducing the Lagrangian $\mathscr{L}$ of a harmonic oscillator:

$$\mathscr{L} = \frac{1}{2}\mathscr{m}(t)\Big(\frac{dn(t)}{dt}\Big)^2 - \frac{1}{2}\mathscr{m}(t)\omega^2(t)n^2(t), \tag{2.10}$$

where $\mathscr{m}(t)$ and $\omega(t)$ denote respectively the reduced mass and the frequency of the system that are both time-dependent functions and lastly, $n(t)$ represents the generalized coordinate that defines uniquely the system. Applying the Lagrange equation, we obtain a differential equation describing the relaxation dynamics as a damped harmonic oscillator in terms of its time-dependent reduced mass $\mathscr{m}$ and time-dependent frequency $\omega(t)$

$$\frac{d^2n(t)}{dt^2} + \frac{\dot{\mathscr{m}}(t)}{\mathscr{m}(t)}\frac{dn(t)}{dt} + \omega^2(t)n(t) = 0, \tag{2.11}$$

where $\dot{\mathscr{m}}$ is the time derivative of the reduced mass $\mathscr{m}$. Comparing the differential equation obtained from the analysis in the material frame (2.5) with the one derived from the Lagrangian formalism (2.11), we get an explicit expression for the time-dependent reduced mass $\mathscr{m}(t)$ and frequency $\omega(t)$:

$$\mathscr{m}(t) = Mt^{1-\beta}e^{2\zeta\left(\frac{t}{\tau}\right)^{\beta}}, \tag{2.12a}$$

$$\omega(t) = \frac{\beta^2 t^{2\beta-2}}{\tau^{2\beta}}. \tag{2.12b}$$

Before investigating the key role of the reduced mass $\mathscr{m}(t)$ in the dynamics, we remark once again the correctness of the result since the expression of the Hamiltonian $\mathcal{H}$ of this dynamical system given by

$$\mathcal{H} = t^{1-\beta}e^{2\zeta\left(\frac{t}{\tau}\right)^{\beta}}\left[\frac{M}{2}\left(\frac{dn(t)}{dt}\right)^2 + \frac{M}{2}\frac{\beta^2 t^{2\beta-2}}{\tau^{2\beta}}n^2(t)\right] \tag{2.13}$$

generalizes the Caldirola-Kanai Hamiltonian $\mathcal{H}_{\mathrm{CK}}$ [33, 101] that emerge fixing $\beta = 1$:

$$\mathcal{H}_{\mathrm{CK}} = e^{2\zeta\left(\frac{t}{\tau}\right)}\left[\frac{M}{2}\left(\frac{dn(t)}{dt}\right)^2 + \frac{M}{2\tau^2}n^2(t)\right]. \tag{2.14}$$

As it is evident, the Caldirola-Kanai Hamiltonian $\mathcal{H}_{\mathrm{CK}}$ retains a time dependent reduced mass $\mathscr{m}(t) = Me^{2\zeta\left(\frac{t}{\tau}\right)^{\beta}}$ but for $\beta = 1$ the frequency is merely constant $\omega = \frac{1}{\tau^2}$. On the other hand, the Hamiltonian $\mathcal{H}$ has both a time-dependent mass and frequency. The importance of the time-dependent reduced mass $\mathscr{m}(t)$ in the dynamical equations lies in the fact that it shows the presence of damping or/and pumping mechanisms probing the inertia of the system that is proportional to the decay rate. The time evolution of the reduced mass $\mathscr{m}(t)$ gives a physical insight of the dynamics during the relaxation. In Fig. 2.4, we illustrated the reduced mass $\mathscr{m}(t)$ for different values of the β parameter.

Firstly, let us consider the special case $\beta = 1$ where the reduced mass $\mathscr{m}(t)$ is logaritmically constant in the first part of its evolution. Here the luminophores are quenched at the same rate and the surrounding environment does not have any influence on the dynamics of the system. In other words, the cloud of virtual particle, as phonons and photons, generated by the radiation emitted by the luminophores do not obstacle the luminescence. As t approaches to τ, the reduced $\mathscr{m}(t)$ starts to increase its value and it implies that the dynamics is governed by a damping mechanism. Otherwise, if $\beta < 1$, the dynamical system present a more real behaviour. From the very beginning, the luminophores interact with the cloud of virtual particles. This cloud deforms the initial situation creating micro-environments and configurations that causes a distribution of relaxation time. These deformations around the luminophores can be modelled as traps where the excited particles are captured and then released. Despite the difference between the aforementioned cases, the dynamics is essentially the same and it is named *single* dynamics. The luminophores decay in parallel: the fastest decay earlier and all the other follow according to a hierarchical order based on the relaxation time. On the other hand the dynamics of the luminophores described by the KWW function with $\beta > 1$ is *dual*. In other words, the dynamics is governed by a serial

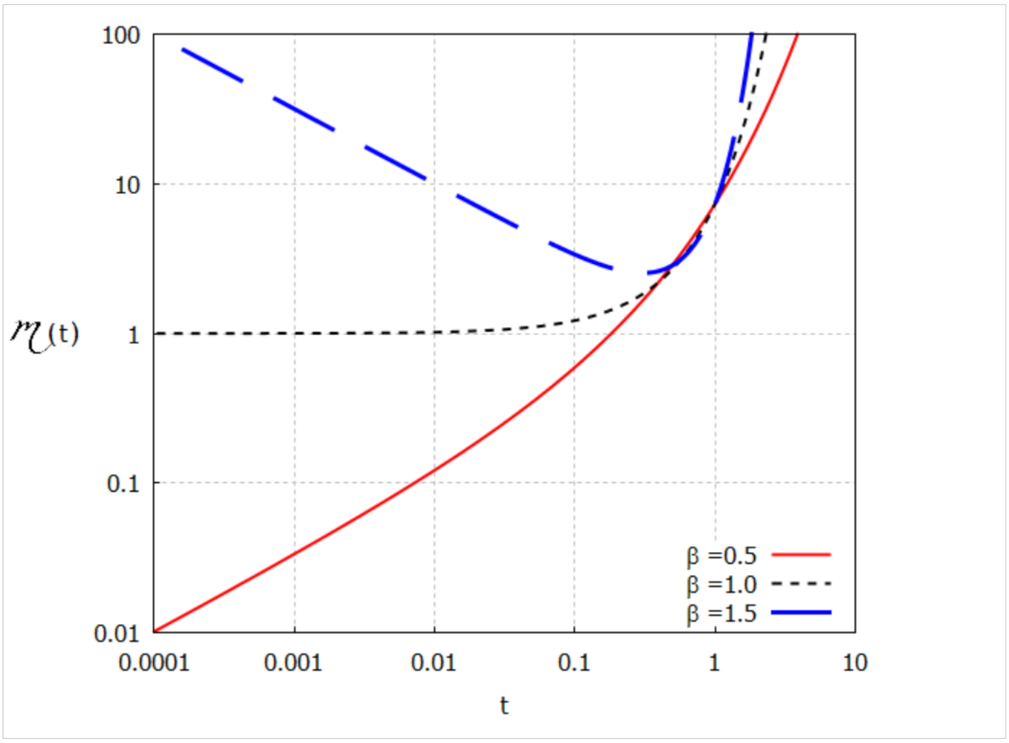

Figure 2.4: Reduced mass term $\mathpzc{m}(t)$ at $\tau = 1$ and $M = 1$.

mechanism as a consequence of the markedly different behaviour of the reduced mass. In the compressed range, the reduced mass has a convexity which is absent in the other two cases. The convexity is a hallmark of the dual dynamics. The dashed blue curve in Fig. 2.4 initially decreases until $\frac{t}{\tau} = 1$ when the reduced mass reaches its minimum. The decreasing of the reduced mass implies that a pumping mechanism is active. The system favours the emission and the luminophores populates the singlet excited state. However, as time passes, the pumping mechanism is damped and at the minimum of the reduced mass, we reach a sort of equilibrium. The luminophores behave ideally and emit radiation freely. According to this phenomenological model, the minimum of the reduced mass should correspond to a plateau in the luminescence, i.e. a time interval in which the luminescence seems to be constant (in the double log plot). Physically, the presence of the plateau can be explained as a reconfiguration or reorganization of the molecules: the nature of the luminophores has been changed from the triplet to the singlet state. As the reduced mass cross the minimum, the dynamics has its turning point and the damping mechanism takes the lead. Now, the luminescence dramatically decreases as the reduced mass increases its value. In conclusion to this Section, there are two possible classes of luminophores which can be distinguished on the basis of their origin modelled by the two KWW functions. In order to adduce evidence for the single and dual dynamics, the problem must be considered in the framework of the physico-chemical interpretation.

2.2.2 Part II: the KWW function as a sum of PL decays

As was evident in Section 2.2.1, two mechanisms govern the dynamics of the PL emission depending on the range of the parameter β and therefore there should be two different origins for the damping. The aim of this Subsection is to find these differences expanding in series the KWW function via the so-called Prony series [49, 203]. This series reproduces quite faithfully the behaviour of the KWW function using a finite sum of N simple exponential functions

$$e^{-\left(\frac{t}{\tau}\right)^{\beta}} \sim \sum_{i=0}^{N} A_i e^{-K_i t}, \tag{2.15}$$

weighted by the coefficients A_i that should only satisfy the following constraint:

$$\sum_{i=0}^{N} A_i = 1. \tag{2.16}$$

Under the condition (2.16), the parameters A_i and K_i should minimize the sum of the squared residuals (SSR) between the KWW function and the Prony series. The SSR is a relevant index describing the quality of the approximation obtained by the least squared method. The more the SSR index is small, the more the Prony series approximate the KWW function. Concerning even a simple two terms Prony series, it is possible to obtain a sufficiently high-quality approximation and both KWW functions clearly can show its own peculiarities.

The choice to use the Prony series instead of more sophisticated results known in literature as [73, 161, 167] is due to the fact that we need only two terms in order to show how the proposed model not only generalizes the bi-exponential model used for modelling relaxation processes, but it improves the physical interpretation of experimental data and quantities in the light of the results obtained in Section 2.2.1.

The stretched KWW function ($0 < \beta < 1$) can be quite well approximated by the two-terms Prony series (2.15) provided that K_i and A_i are real and positive parameters satisfying the condition (2.16). In Tab. 2.1, there are collected few examples of the stretched KWW function approximated by the two-terms Prony series (2.15) with the corresponding values of SSR. An interesting feature emerged from Tab. 2.1 is that the K_i parameters differ by several order of magnitude. Such difference increases as β tends to zero. Another aspect that it should be noted is the sign of the coefficients A_i: all the coefficients are positive and this is not a mere numerical coincidence as it will be explained in Section 2.2.3.

Concerning the compressed KWW function, the two terms Prony series can be considered a satisfactory approximation also in this case, as confirmed by the values of the SSR in Tab. 2.2. Contrary to what occurs for the stretched KWW function, the terms in the Prony series, which is approximating the compressed exponential function, can assume both positive and negative signs. Another difference between the stretched and the compressed Prony series is the values of the decay rates (or the inverse of a relaxation time). In Tab. 2.2, the two components have almost the same values of the K_i parameters, whereas, as previously remarked, in Tab. 2.1 the discrepancy needs

Table 2.1: Parameters of the two-terms Prony series that approximates the stretched KWW function for several values of β. The last column is the sum of the squared residuals (SSR).

β	parameters				SSR
	A_1	A_2	K_1	K_2	
0.1	0.906071	0.0939289	0.356131	$1.0391\ 10^{-5}$	10.9237
0.2	0.891382	0.108618	0.71233	$2.1053\ 10^{-3}$	$5.24985\ 10^{-1}$
0.3	0.808055	0.191945	1.2683	$3.1232\ 10^{-2}$	$3.25275\ 10^{-2}$
0.4	0.749713	0.250287	1.56817	$9.9424\ 10^{-2}$	$4.84242\ 10^{-3}$
0.5	0.694155	0.305845	1.73787	$1.9646\ 10^{-2}$	$9.52931\ 10^{-4}$
0.6	0.63105	0.36895	1.83565	$3.1490\ 10^{-1}$	$1.99314\ 10^{-4}$
0.7	0.552047	0.447953	1.88862	$4.5187\ 10^{-1}$	$3.83391\ 10^{-5}$
0.8	0.445005	0.554995	1.90991	$6.0787\ 10^{-1}$	$5.68391\ 10^{-6}$
0.9	0.284997	0.715003	1.90434	$7.8697\ 10^{-1}$	$4.29233\ 10^{-7}$

several order of magnitude to be filled. However, expanding the KWW function into

Table 2.2: Parameters of the two-terms Prony series that approximates the compressed KWW function for several values of β. The last column is the sum of the squared residuals (SSR).

β	parameters				SSR
	A_1	A_2	K_1	K_2	
1.1	9.27217	-8.27217	0.79703	0.773835	$8.98102\cdot 10^{-5}$
1.2	13.827	-12.827	0.758224	0.73983	$4.28344\cdot 10^{-4}$
1.3	18.1737	-17.1737	0.741702	0.726466	$9.96678\cdot 10^{-4}$
1.4	19.5284	-18.5284	0.734959	0.719935	$1.7287\cdot 10^{-3}$
1.5	21.9199	-20.9199	0.731631	0.717709	$2.55749\cdot 10^{-3}$
1.6	22.4522	-21.4522	0.730799	0.716776	$3.42634\cdot 10^{-3}$
1.7	23.8176	-22.8176	0.730602	0.717073	$4.2894\cdot 10^{-3}$
1.8	24.809	-23.809	0.730919	0.717692	$5.11091\cdot 10^{-3}$
1.9	27.0386	-26.0386	0.731071	0.718768	$5.86421\cdot 10^{-3}$
2.0	26.5933	-25.5933	0.731862	0.719196	$6.53116\cdot 10^{-3}$

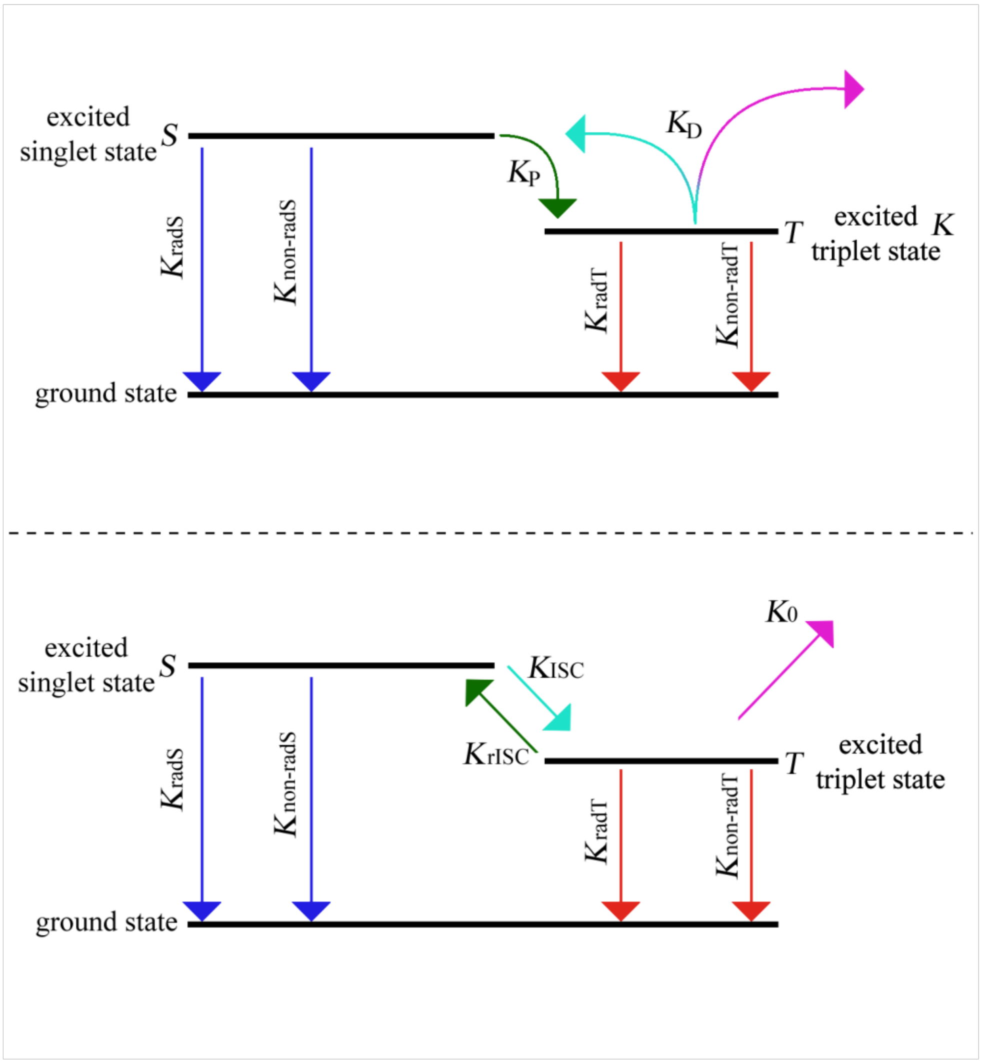
excited singlet state
S
K_D
K_P
T
excited triplet state
K
K_radS
K_non-radS
K_radT
K_non-radT
ground state
K_0
excited singlet state
S
K_ISC
K_rISC
T
excited triplet state
K_radS
K_non-radS
K_radT
K_non-radT
ground state

Figure 2.5: Partial energy diagram showing the fundamental decay rates used to model a photoluminescent system. Excited vibrational levels have been omitted for semplicity.

a Prony series does not allow an immediate understanding of the physical meaning and role of A_i and K_i. The key to unlock the physical meaning behind the above observations is to introduce the physical-chemical interpretation based on the kinetic equations. The physical-chemical interpretation of the PL emission based on the kinetic equations allows us to consider few decay pathways, the one showed in Fig. 2.5. The time evolution of the excited luminophores in singlet and triplet states is given by the following coupled equations modelled using the scheme shown in Fig. 2.5:

$$\begin{cases} \dfrac{dn_S(t)}{dt} = -K_S \; n_S(t) + K_D \; n_T(t), \qquad n_S(0) = m \\ \dfrac{dn_T(t)}{dt} = K_P \; n_S(t) - K_T \; n_T(t), \qquad n_T(0) = n, \end{cases} \tag{2.17}$$

where

- $n_S(t)$ is the fraction of the luminophores in the singlet excited state at the time t whereas $n_S(0) = m$ denotes the initial fraction of luminophores at $t = 0$;

- $n_T(t)$ is the fraction of the luminophores in the triplet excited state at time t. Here, the triplet state is a *special* trap where the excited electron can be caught after inverting its spin $n_T(0) = n$ is the initial fraction of luminophores at $t = 0$ that populate the triplet state;

- $K_{\text{rad } S}$ and $K_{\text{non-rad } S}$ denote the radiative and non-radiative rates from S to the ground state S_0, respectively. $K_{\text{rad } S}$ determines the rate of the fluorescent emission $(= \frac{1}{\tau_F})$;

- $K_{\text{rad } T}$ and $K_{\text{non-rad } T}$ are the radiative and non-radiative rates characterizing the transition from the triplet state T to the ground state S_0, respectively. $K_{\text{rad } T}$ determines the rate of the phosphorescent emission;

- K_P is the total trapping rate, and it coincides with the intersystem crossing rate $K_{\text{ISC}} = \dfrac{1}{\tau_{\text{ISC}}}$, that is the rate at which the triplet state has been populated by the singlet exicited state;

- K_D is the total de-trapping rate, and it is defined as the difference between the reverse intersystem crossing rate $K_{\text{rISC}} = \dfrac{1}{\tau_{\text{rISC}}}$ (i.e. the re-population of the singlet excited state from the triplet one) and the triplet-trap rate K_0. K_0 is the rate at which the excited triplet state is impoverished via interaction with an external trap due to the presence of more active species as the molecular oxygen.

The system (2.17) can be solved for both excited states. However, since we are interested in the fluorescence intensity emission that is proportional to the number of luminophores in S, we will consider only the solution that describes the time evolution of the number of the luminophores in that excited state. The form of the solution is a bi-exponential function of the form

$$n_S(t) = A_1 \, e^{-K_1 \, t} + A_2 \, e^{-K_2 \, t}, \tag{2.18}$$

where K_i denotes the total decay rates and the coefficients A_i are defined as follows

- $K_1 = \dfrac{K_S + K_T + \sqrt{(K_S - K_T)^2 + 4K_D K_P}}{2}$;

- $K_2 = \dfrac{K_S + K_T - \sqrt{(K_S + K_T)^2 + 4K_D K_P}}{2}$

- $A_1 = \dfrac{m(K_S - K_T) + m\sqrt{(K_S - K_T)^2 + 4K_D K_P} - 2K_D n}{2\sqrt{(K_S - K_T)^2 + 4K_D K_P}}$

- $A_2 = \dfrac{-m(K_S - K_T) + m\sqrt{(K_S - K_T)^2 + 4K_D K_P} + 2K_D n}{2\sqrt{(K_S - K_T)^2 + 4K_D K_P}}$.

The coefficients A_1 and A_2 result to be normalized as we divide $n_S(t)$ by the initial condition $n_S(0) = m$. The decay rates should respect the constraints listed below in order to match the experiments:

$$K_S > K_T \geq 0, \tag{2.19a}$$
$$K_{\text{ISC}} >> K_S \tag{2.19b}$$
$$K_{\text{rISC}} >> K_T \tag{2.19c}$$
$$K_{\text{ISC}} >> K_{\text{rISC}} \tag{2.19d}$$
$$K_{\text{non-rad T}} >> K_{\text{rad T}}. \tag{2.19e}$$

The singlet decay rate K_S is greater than the triplet decay rate K_T (2.19a), as expected due to the fact that the fluorescent emission is a faster light-emitting process than the phosphorescence. The constraint on the intersystem crossing (2.19b) (or the reverse intersystem crossing (2.19c)) prevails on the de-activation of the excited states explaining the excitons crossover between S and T states. However, as established by Hund's rule [57], the triplet state T is always energetically lower than the singlet excited state S, therefore the intersystem crossing is more favourable then the reverse process (2.19d). To guarantee the reverse intersystem crossing, two requests should be fulfilled: the energy split ΔE_{ST} between S and T should be small and an endothermic process, as the thermal activation, should be involved to overcome the energy gap. Under these requirements, the S state can be re-populated with a delay as compared to the time needed to populate the S state directly via photoexcitation.
The last constraint (2.19e) imposes a *direction* to the competition between the non-radiative and radiative decay rates: $K_{\text{non-rad T}} >> K_{\text{rad T}}$. This inequality can explain the not-observed phosphorescence at room temperature.
However, it is important to underline that the reverse intersystem crossing decay rate K_{rISC} is strongly dependent from the temperature according to an Arrhenius law [18, 64, 190]:

$$K_{\text{rISC}} = Ce^{-\frac{\Delta E}{k_B \mathcal{T}}}, \tag{2.20}$$

where C is the prefactor related to the spin-orbit coupling, ΔE is the singlet-triplet energy gap, $k_B = 8.617333262\ 10^{-5} \frac{\text{eV}}{K}$ is the Boltzmann constant and $\mathcal{T}$ is the temperature measured in Kelvin. Therefore, the de-trapping rate K_D, defined as a difference between K_{rISC} and K_O, can be both positive or negative and it plays an important role in the interpretation of what KWW function governs the dynamics of the system. K_D influences the sign of coefficients A_1 and A_2. For any combination of the signs, the sum of the coefficients A_1 and A_2 always reduces to the unity, so it results that the bi-exponential function (2.18) is normalized. Such a normalization imposed on the coefficients of the solution (2.18) hides the constraint $A_1 + A_2 = 1$ which is the same constraint imposed on the coefficients of the Prony series to approximate the stretched and the compressed KWW function.
Taking into account the previous mathematical considerations on the Prony series as an approximation to the KWW function, the attention should be focused on the physical meaning. For this reason, we will firstly resort to an ideal experiment and then, when the meaning of the terms in the Prony series has been understood, we can consider a

real physical system.
After switching off the initial photoexcitation, all the luminophores are caught in the singlet excited state. Mathematically, the initial conditions for the system (2.17) are $S(0) = m$ and $T(0) = 0$. The luminophores decay and relax to the ground state according to (2.18) when $n = 0$:

$$\begin{aligned} n_S(t) = & \frac{m\ e^{-\frac{t}{2}(K_S+K_T+\sqrt{(K_S-K_T)^2+4K_DK_P})}(K_S - K_T + \sqrt{(K_S-K_T)^2+4K_DK_P})}{2\sqrt{(K_S-K_T)^2+4K_DK_P}} \\ & + \frac{m\ e^{-\frac{t}{2}(K_S+K_T-\sqrt{(K_T-K_S)^2+4K_DK_P})}(K_T - K_S + \sqrt{(K_S-K_T)^2+4K_DK_P})}{2\sqrt{(K_S-K_T)^2+4K_DK_P}}. \end{aligned} \tag{2.21}$$

As in the general case, the normalization of the coefficients result as we divide the solution by the initial condition $n_S(0) = m$. As depicted in Fig. 2.5, the luminophores in the excited singlet state S decay to the ground state or to the triplet excited state T, which is initially empty and therefore it begins to be populated via intersystem crossing. Whatever the path chosen by the excitons, the singlet excited state is depleted in any case. In this situation, both A_1 and A_2 assume only positive values and respect the normalization condition (2.16). This result perfectly frames the physical situation: the singlet excited state is decaying via intersystem crossing or to the ground state (directly or after being captured a bit longer, explaining the differences between the order of magnitude in the decay rates), whereas the reverse intersystem crossing and the other radiative and non-radiative pathways are present but still *asleep*. Combining all the information: the positiveness of both coefficients and the aforementioned decay routes, the dynamics is dominated by a damping mechanism and the bi-exponential model is therefore modelled with a stretched KWW function.
At this point, both excited states are populated and then, other paths illustrated in Fig. 2.5 are available. The conditions on the parameters involved in the definition of A_1 and A_2 to be satisfied are:

$$K_S > K_T \geq 0, \tag{2.22a}$$
$$K_D = K_{\text{rISC}} - K_O \leq 0 \tag{2.22b}$$
$$K_P > 0 \tag{2.22c}$$
$$K_P \leq \frac{(K_S - K_T)^2}{4K_D}. \tag{2.22d}$$

Compared to the previous situation, the reverse intersystem crossing plays a more relevant role. As $K_{\text{rISC}} = K_O$, the bi-exponential models for the fluorescence from the singlet excited state reduces to a simple mono-exponential function. This implies the presence of a *plateau* in the double-log plot highlighting a re-configuration of the luminophores: a change of their spin. As the temperature goes down, K_{rISC} tends to zero, whereas the triplet-trapping rate grows up due to the increasing of the concentration of the quenchers $K_D = K_{\text{rISC}} - K_O < 0$, and then the damping mechanism dominates the dynamics.

To validate the approach, we consider a special case of the system (2.17): when the triplet and the singlet states are in quasi-equilibrium, that is the rate of production of the triplet state is zero. The presence of the pumping mechanism is neglected if the non-radiative triplet-trap decay rate K_O is more competitive than the reverse intersystem crossing rate K_{rISC}: the concentration of the quenchers starts to be enough influential on the dynamics of the system. The pumping mechanism has just stopped its action, $K_D < 0$, and the decay of the number of luminophores is unstoppable. Under these conditions, the system (2.17) can be reduced to

$$\begin{cases} \dfrac{dn_S(t)}{dt} = -K_S\, n_S(t) - K_O\, n_T(t), & n_S(0) = m \\ \dfrac{dn_T(t)}{dt} = 0, & n_T(0) = n. \end{cases} \tag{2.23}$$

The solution of the system (2.23) reads

$$n_S(t) = \left(m + \frac{K_O}{K_S} n\right) e^{-K_S t} - \frac{K_O}{K_S} n. \tag{2.24}$$

As expected, it can be rewritten in terms of a two terms-Prony series (2.15) where the parameters and coefficients are obviously

- ◇ $K_1 = K_S$ and $A_1 = m + \dfrac{K_O}{K_S} n$,
- ◇ $K_2 = 0$ and $A_2 = -\dfrac{K_O}{K_S} n$,

and fulfil the constraint (2.16) imposed on the Prony series coefficients once we normalize the result. We can separate the solution (2.24) into two contributions. The zero-th order kinetics is a constant rate that is dependent on the concentration of luminophores in the triplet state, whereas it is independent on the concentration of the luminophores in the singlet excited state. The first-order kinetics is directly proportional to the concentration of luminophores in the singlet state. To validate the assumptions about the Prony series presented above, the solution (2.24) should behave as a compressed KWW function since the A_i coefficients involved in the series expansion have always opposite sign. The values of the parameters, coefficients and the corresponding SSR, which evaluates how good is the overlapping between the compressed KWW function and the Prony series, are summarized and collected in Tab. 2.3. The sum of the squared residuals ranges between $10^{-4} \div 10^{-3}$ confirming a good agreement between the two approaches. The solution is consistent with the one obtained in [15].

2.2.3 Part III: complete monotonicity vs. monotonicity: a mathematical tool able to sum up all the physical properties

The term *component* is used to indicate the ordinate spatial aggregation inside the class of the luminophores that shows the same PL degradation decay (i.e. the same value of β) and consequently, also the same dynamics. Concerning the results obtained up

Table 2.3: Parameters of the zero-th and first-order kinetics (two-terms Prony series with $K_2 = 0$) that approximates the compressed KWW function for several values of β. The last column is the sum of the squared residuals (SSR).

β	parameters		SSR
	A	K	
1.1	$2.09995{\cdot}10^{-7}$	1.03288	$3.76718{\cdot}\ 10^{-4}$
1.2	$3.53297{\cdot}10^{-7}$	1.06063	$1.26035{\cdot}\ 10^{-3}$
1.3	$4.54678{\cdot}10^{-7}$	1.08409	$2.40555{\cdot}\ 10^{-3}$
1.4	$5.28605{\cdot}10^{-7}$	1.10393	$3.66868{\cdot}\ 10^{-3}$
1.5	$5.83922{\cdot}10^{-7}$	1.1207	$4.96133{\cdot}\ 10^{-3}$
1.6	$6.26239{\cdot}10^{-7}$	1.13483	$6.22604{\cdot}\ 10^{-3}$
1.7	$6.59223{\cdot}10^{-7}$	1.14669	$7.4234{\cdot}\ 10^{-3}$
1.8	$6.85322{\cdot}10^{-7}$	1.15659	$8.52553{\cdot}\ 10^{-3}$
1.9	$7.06193{\cdot}10^{-7}$	1.16477	$9.51321{\cdot}\ 10^{-3}$
2.0	$7.22969{\cdot}10^{-7}$	1.17146	$1.03749{\cdot}\ 10^{-2}$

to now, there are two classes of luminophores: one described by the stretched KWW function and the other one by the compressed KWW function. The introduction of these components inside the classes do not imply a long-range spacial grouping but it describes ensembles whose elements are locally distributed on the entire system. The phenomenological intuition on the aggregation in components, which influences the behaviour of the luminophores relaxation, can be interpreted in the light of the crucial mathematical properties of monotonicity and complete monotonicity.

These properties can be used as catalysts for collecting all the physical features illustrated in the previous subsections.

Here below there are the definitions that we will use [149]:

> **Definition 2.2.1.** Let (a, b) be an interval on the real axis, and $f(x)$ be a real valued function defined on (a, b). The function is called monotonically increasing, if for all x_1 and $x_2 \in (a, b)$ such that $x_1 \leq x_2$, $f(x_1) \leq f(x_2)$, so f preserves the order. Likewise, a function is called monotonically decreasing if, whenever $x_1 \leq x_2$, then $f(x_1) \geq f(x_2)$, so it reverses the order.
> In case the above inequality is strict, the function is called strictly increasing (or decreasing).

> **Definition 2.2.2.** Let (a, b) be an interval on the real axis, and $f(x)$ be a real valued function defined on (a, b). The function $f(x)$ is said to be convex if for any x_1 and $x_2 \in (a, b)$, and $0 \leq \lambda < 1$, we have
>
> $$f[(1-\lambda)x_1 + \lambda x_2] \leq (1-\lambda)f(x_1) + \lambda f(x_2).$$

This inequality is called Jensen's inequality.
If the above inequality is strict whenever $x_1 \neq x_2$ and $0 < \lambda < 1$, the function is called strictly convex.

Definition 2.2.3. Let (a, b) be an interval on the real axis, and $f(x)$ be a real valued function defined on (a, b). The function $f(x)$ is said to be concave if for any x_1 and $x_2 \in (a, b)$, and $0 \leq \lambda < 1$, we have the following Jensen's inequality

$$f[(1-\lambda)x_1 + \lambda x_2] \geq (1-\lambda)f(x_1) + \lambda f(x_2).$$

If the above inequality is strict whenever $x_1 \neq x_2$ and $0 < \lambda < 1$, the function is called strictly concave.

Definition 2.2.4. Let (a, b) be an interval on the real axis and $f(x)$ be a convex function. Then $f(x)$ is continuous on the interior of that interval.
Comparing the definitions of convex function and concave function, it is evident that the results obtained for convex function can be modified into results for concave functions by multiplication of -1 and vice versa. As a last remark, concave and convex functions may be not continuous everywhere, but the point of discontinuity have to be on the boundary of the interval.

Definition 2.2.5. For our purposes, we can simplify the definition 2.2.2, if the function is differentiable.
The differentiable function f defined on an open interval (a, b) is convex on (a, b) if and only if

$$f(x_1) - f(x_2) \geq f'(x_2)(x_1 - x_2) \tag{2.25}$$

for all $x_1 \in (a, b)$ and $x_2 \in (a, b)$ such that $x_1 > x_2$ and is concave on (a, b) if and only if

$$f(x_1) - f(x_2) \geq f'(x_2)(x_1 - x_2) \tag{2.26}$$

for all $x_1 \in (a, b)$ and $x_2 \in (a, b)$;

Preposition 2.2.1. A twice-differentiable function $f(x)$ defined on the interval (a, b) is convex if and only if $f"(x) \geq 0$ for all x in the interior of (a, b) and vice versa, it is named concave if and only if $f"(x) \leq 0$ for all x in the interior of (a, b).
In case the above inequality are strict, we have strict convexity and strict concavity respectively in the interval (a, b). The proof of the second preposition can be found in [175].

Definition 2.2.6. A real valued function $f(x)$, defined on an interval $I = (a, b) \in \mathbb{R}$, is called complete monotone on $I = (a, b)$, if the function f has derivatives of all orders and satisfies the condition

$$(-1)^n f^{(n)}(t) \geq 0, \ n \in \mathbb{N}_0, \ n \in I, \tag{2.27}$$

where $f^{(n)}$ represents the n-th derivative with respect to t. Therefore, a complete monotone function is non-negative as it is immediate to conclude considering the case $n = 0$ in (2.27).

By applying the above definitions and properties, the compressed KWW function satisfies the requirement needed to be a monotonic function, whereas the stretched KWW function is completely monotone. In this last case, the proof can be obtained either via Laplace transform and Bernstein theorem or applying the algorithm presented here below. If the KWW function (or more generally a relaxation function) satisfies the following properties:

- it is positive, strictly convex and decreasing ;
- it is said to be of class $C^n(I, \mathbb{R})$ in $(0, \infty)$ is an open subset of the real number $\mathbb{R}$;

and if we consider the above prepositions on convex and concave functions we establish a "domino-effect" algorithm that guarantees the complete monotonicity if the relaxation function is positive, strictly convex and decreasing. A graphical illustration is represented in Fig. 2.6.

The stretched KWW function describes the class of completely monotone luminophores.

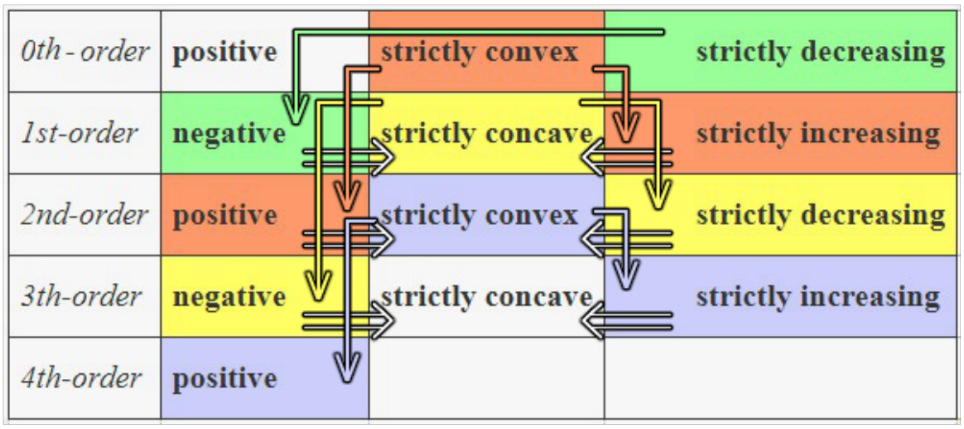

0th - order	**positive**	**strictly convex**	**strictly decreasing**
1st-order	**negative**	**strictly concave**	**strictly increasing**
2nd-order	**positive**	**strictly convex**	**strictly decreasing**
3th-order	**negative**	**strictly concave**	**strictly increasing**
4th-order	**positive**		

Figure 2.6: A graphical illustration for the *domino-effect* algorithm.

The complete monotonicity reveals the single nature of the PL emission decay: only the damping mechanism governs the overall dynamics. This aspect is important because it guarantees that the luminophores in the class follow parallel decay routes, or in other words the damping mechanism dominates on the time-evolution PL decay resulting into parallel *daughters* pathways, i.e. the fluorescence decay and the intersystem crossing (see Fig. 2.5). Here, the luminophores follow pathways that exist from the beginning: the fluorescent decay, the non-radiative excited singlet decay and the intersystem crossing. Other possibilities are still not active. It means that the luminophores do not interact with other species, as molecular dioxygen or more active molecules in the environment when the dynamics is ruled by a complete monotone relaxation function.

On the other hand, the compressed exponential function models the class of monotone luminophores that is governed by a serial or strictly sequential decay process. Here, the dynamics has a dual nature: there is a pumping mechanism followed by a damping mechanism, as obtained analysing the reduced mass $\mathcal{m}$ in the compressed range. The serial nature of the monotonic decay can be physically appreciated by the presence

of a plateau in the luminescent emission. This plateau testifies the re-organization experienced by the class of monotone function and it is a remarkable difference from the class of complete monotone luminophores. The monotone dynamics described by the compressed KWW function is not a *self-consistent* process as the stretched KWW decay but it has to follow the latter in case of photoexcitation of the sample since the pathways involved are activated only after the damping mechanism ruled by the stretched KWW function. In fact the photoexcitation allows populating only the singlet excited state and therefore the compressed KWW function can start only when the triplet state is populated. Here, the number of the quenchers or their concentration grows up in the sample, so their influence becomes more and more important until the decay is unstoppable and increasingly faster with the consequent degradation of the sample itself. The destructive effect of the increasing concentration of the quenchers has been observed considering the Prony series expansion of the KWW function where the main differences characterizing the two classes of luminophores clearly emerged: in the Prony series of the stretched KWW function all the terms are positive whereas in the Prony series that approximates the compressed KWW function there are also negative terms. The negative terms in the compressed Prony series approximation are related to the quenching of the luminophores by the molecular dioxygen present during the PL measurements. These very reactive species can impoverish the triplet state detrapping the excited electron and favouring the de-activation of the state preventing the fluorescent emission.
The next step is to consider a physical system that can be used as a test-case for the approach: the PL emission of the Tris(8-hydroxyquinoline)aluminum molecule, or briefly the Alq_3 molecule. The relaxation of the excitons described by the KWW relaxation function $\Psi(t) = e^{-\left(\frac{t}{\tau}\right)^{\beta}}$ can be related to the decay of the number of the luminophores that can be experimentally probed by measuring the photoluminescence decay curve. From a mathematical point of view, we define the following notation:

$$\Psi(t) = \frac{n(t)}{n(0)} := I(t). \tag{2.28}$$

Without loss of generality, this approach can be also applied for other photoluminescent molecules.

2.3 OLEDs and Alq_3: an organic molecule for photoluminescence

In the last 30 years, photonics experienced a technological revolution as a result of an intense research activity that played a key role in designing a new class of light-emitting devices based on organic materials: OLEDs [32, 67, 134, 183]. Organic light-emitting diodes, or shortly OLEDs, are now a reality in many practical applications (as flat panel displays) and they are extremely competitive compared to devices made by inorganic semiconductors [20]. OLEDs are optoelectronic devices in which the active layers are organic thin films sandwiched between a transparent conducting anode and a metallic cathode as shown in Fig. 2.7.

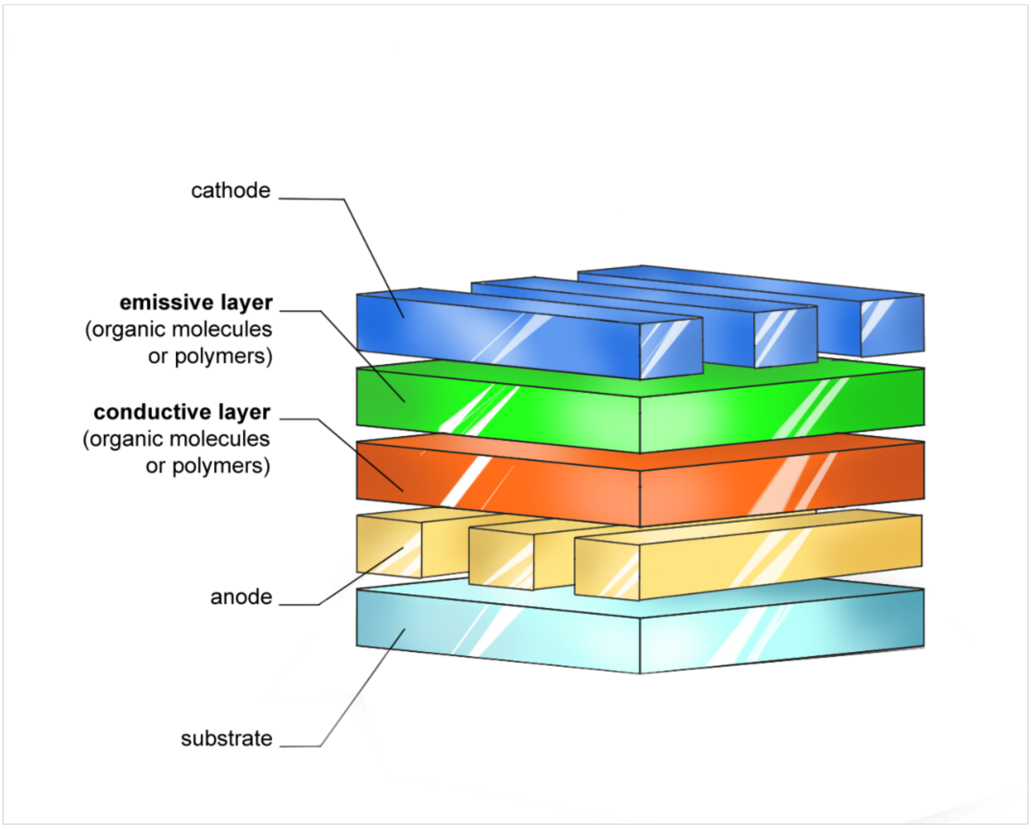
cathode
emissive layer
(organic molecules or polymers)
conductive layer
(organic molecules or polymers)
anode
substrate

Figure 2.7: Schematic basic configuration of an OLED.

A wide interest in organic materials for application in OLEDs began with the pioneering work of Tang and Van Slyke in 1987 [191], where the first high-luminance low-voltage driven device is based on the molecule Alq$_3$.

Tris(8-hydroxyquinoline)aluminum, Alq$_3$, is one among many metal chelates well known since a long time in the analytic literature under the name of metal oxinates. Its condensed formula is $Al(C_9H_6NO)_3$ where the compound in parenthesis is known as 8-Hydroxyquinoline or Quinoline, which has been formerly used as a precipitating or chelating agent to separate metals, and as a parent compound to make anti-malaria drugs, fungicides, biocides, alkaloids, dyes, rubber chemicals and flavouring agents, present in medicinal, agricultural and industrial applications, and lately in optoelectronics. Alq$_3$ is a coordination complex wherein aluminum is bonded in a bidentate manner to the conjugate base of three Quinoline ligands, as in Fig. 2.8. However, it is not a planar molecule and it forms two different geometric isomers, meridianal and facial, and it has been found that thin films of it are constituted mainly of meridianal isomers.

After 30 years of research in OLEDs, Alq$_3$ is still one of the most commonly used electron-transporting layers and luminescent materials in OLEDs. Indeed, it is essential to study the luminescence properties of this low molecular weight organic material in order to produce good OLED devices. For that purpose, PL measurements were performed in various samples in a systematic way.

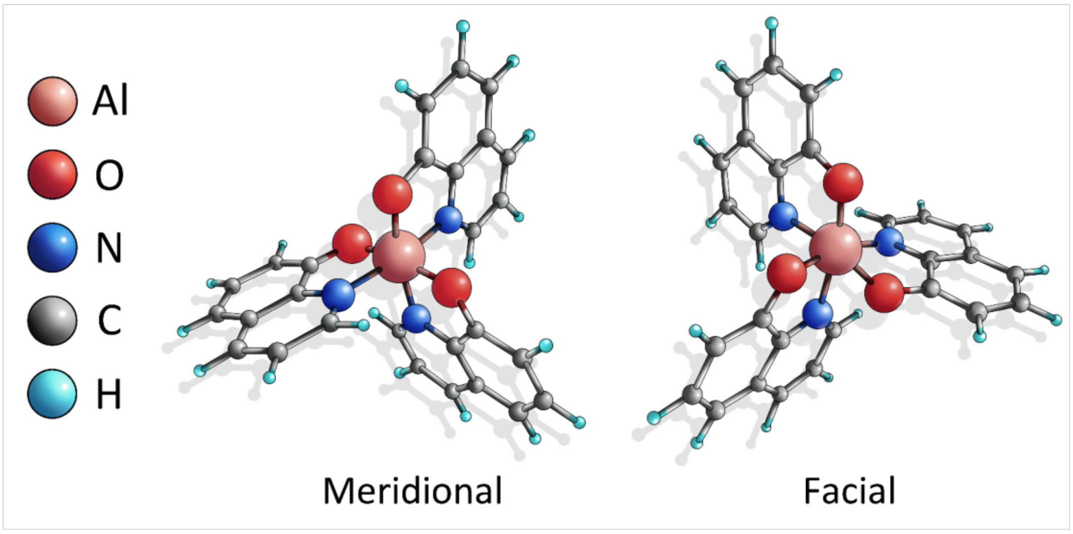

Figure 2.8: Molecular structure of meridianal and facial isomer of Alq_3.

Alq_3 has different absorption bands for wavelengths less than 450nm and it shows the typical bell-shaped emission peaked at 540nm when a photoexcitation is driven under pumping at 395nm. Hence, Alq_3 is a luminescent material in the green light region, as illustrated in Fig. 2.9. The green emission is commonly used in OLED devices.

Due to their thermal stability, Alq_3 is usually deposited in the OLED structures by using the thermal evaporation technique in vacuum.

In this case, the evaporation rate plays an importance role to control the surface morphology of the thin film and enhance the luminescence efficiency of the Alq_3-based OLED. Additionally, the thermal evaporation method allows the thin film of Alq_3 to be either an emissive or an electron transporting layer in a multi-layer structure OLED.

Unfortunately, as any other organic material, a film of Alq_3 is extremely sensitive to temperature and atmospheric exposure. Such an exposure produces non-emissive species acting as luminescence quenchers. The encapsulation of the sample is an attempt to contrast the degradation: the lifetime is extended but its final demise is an unavoidable destiny.

Figure 2.10 illustrates the experimental PL peak intensity of a 140nm thick film of Alq_3, sample alq60, as a function of time in atmosphere and in a dry box: actually, they are two samples evaporated in the same batch and therefore nominally equal. The data show that the sample in the dry box degrades more slowly than the sample in the atmosphere. In fact, comparing the half-life of the two films, it is evident how influential the presence of atmospheric exposure and temperature are. In the sample alq60 kept in a dry box the half-life is reached approximately at 6300h, whereas in the same sample alq60 decaying in atmosphere the half-life is at 1000h.

Figure 2.10 also shows that PL intensity decays in both samples at different rates as time increases. Indeed, in the first 1000h the rate is much faster than after that, and overall the two decays cannot be described by a pure exponential trend that would have been linear in a semi log representation. The two solid curves in Fig. 5 are best fits of the experimental data with a sum of exponential functions that will be introduced

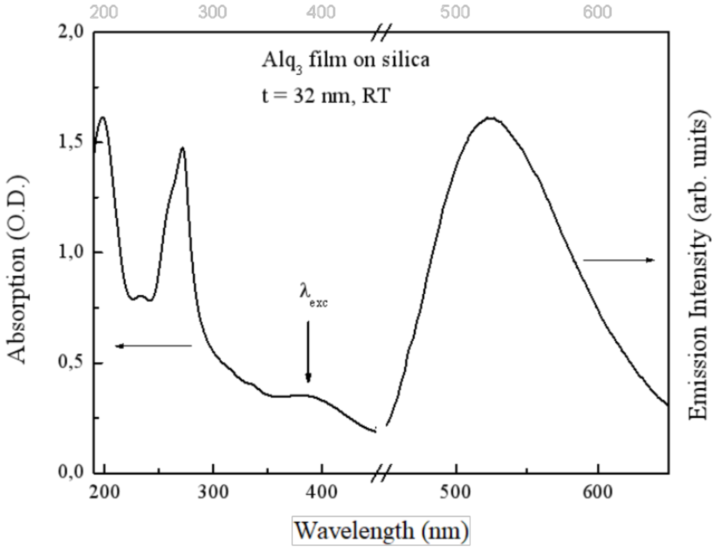

Figure 2.9: Optical absorption spectrum (left) and emission spectrum, (right), at room temperature of a 32 nm thick Alq$_3$ film thermally evaporated on a silica substrate. The arrow indicates the pumping wavelength $\lambda_{exc} = 395$ nm. Reprinted from "Singular Photoluminescence Behavior of Alq3 Films at Very Long Decay Times" by G. Baldacchini et al. Journal of Luminescence, 2018, Volume (**193**), 106-113. Copyright [2018] by the Name of Copyright Holder.

later on.

Anyway, on the basis of its promising applications in optoelectronics, many studies have been focused on the optimization of the device performance with respect to efficiency, long-term stability, as above, and charge transfer properties.

Among many technical approaches, thermal annealing was discovered to be very effective in influencing the above properties.

The thermal annealing is a heat treatment process which alters the microstructure of a material in order to change its mechanical and/or electrical properties. The thermal annealing of the emissive layer in an OLED improves incredibly not only the efficiency of the devices but also the PL emission and the lifetime contrasting the degradation for very long time, more than 10,000h.

However, in spite of advances in Alq$_3$ based devices, the knowledge and understanding of the optical properties of Alq$_3$ and its chemical and environmental stability is still limited, a situation that requires further studies.

2.4 The PL emission in the Alq$_3$ molecule

The aim of this Section is to use the approach delineated in Section 2.2 and in [123] to explain the PL intensity decay of the Alq$_3$ molecule. As presented in [12–15], the PL intensity decay can be described with a multi-exponential model based on the KWW

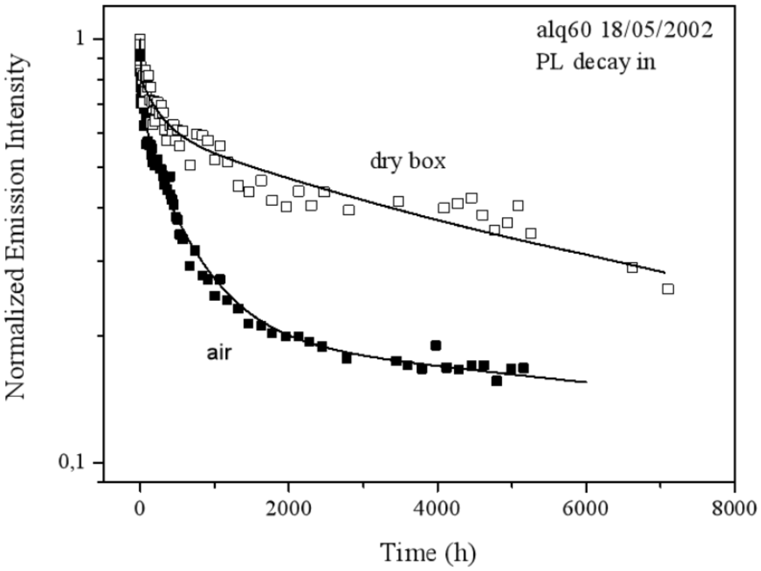

Figure 2.10: Photoluminescence intensity peak of the 140nm thick film alq60 in atmosphere (black square) and in dry box (white square). Reprinted from "Singular Photoluminescence Behavior of Alq3 Films at Very Long Decay Times" by G. Baldacchini et al. Journal of Luminescence, 2018, Volume (**193**), 106-113. Copyright [2018] by the Name of Copyright Holder.

functions, the so-called four components model:

$$I(t) = \sum_{i=1}^{4} I_i e^{-\left(\frac{t}{\tau_i}\right)^{\beta_i}}, \qquad (2.29)$$

where the total intensity $I(t)$ consists of four components characterized by three parameters I_i, β_i and τ_i, which respectively represent the amplitude, the KWW parameter and the constant time of the i-th component. In order to satisfy the normalization condition to the overall process, the four component model (2.29) should respect the following constraint imposed on the sum of the amplitudes

$$\sum_{i=1}^{4} I_i = I_1 + I_2 + I_3 + I_4 = 1. \qquad (2.30)$$

Here, the amplitudes of the components depend on the physical and chemical conditions during the thermal evaporation and annealing processes, whereas the characteristic times depend on the environmental conditions.
Figures 2.11 and 2.12 illustrate the normalized intensity emission (black circles) of the reference sample alq63-3 and of the sample alq65-1, which is annealed in dry oxygen at 180°C. The solid red line represents the best fit of the experimental data by using (2.29), whereas the dashed lines are the components. The inserts of Figs. 2.11-2.12 display with magnification the end tail of the normalized PL emission. Only the fourth component is still surviving in the very long time range.
Comparing the intensity decay of the two samples, it is evident that the thermal treatment significantly improved the PL emission: the normalized emission intensity in the reference sample alq63-3 at 50,000h is about $3 \cdot 10^{-5}$, whereas is 0.02 in the annealed sample alq65-1, almost three orders of magnitude bigger! More detailed information is contained in the retrieved amplitudes and time constants of the four components collected in Table 2.4.
From a strictly numerical point of view, the process of annealing produced these remarkable consequences:

- ◇ I_1 and I_2 are the same within the standard deviation (4%),
- ◇ I_3 decreases from 51% to 27%,
- ◇ I_4 increases from 17% to 45%,
- ◇ τ_4 increases from 7200h to 30,398h,

which clearly reflect the sizeable increment in the intensity and duration of the luminescence.

Another consequence of the thermal annealing is the rearrangement of the components, which is better deduced by observing the behaviour of the components (dashed lines) illustrated in Figs. 2.11 and 2.12. In the reference sample alq63-3, the order among the components has not been preserved during the photoluminescent decay. Up to a hundred hours, the order of the intensity arranged from the lowest to the highest

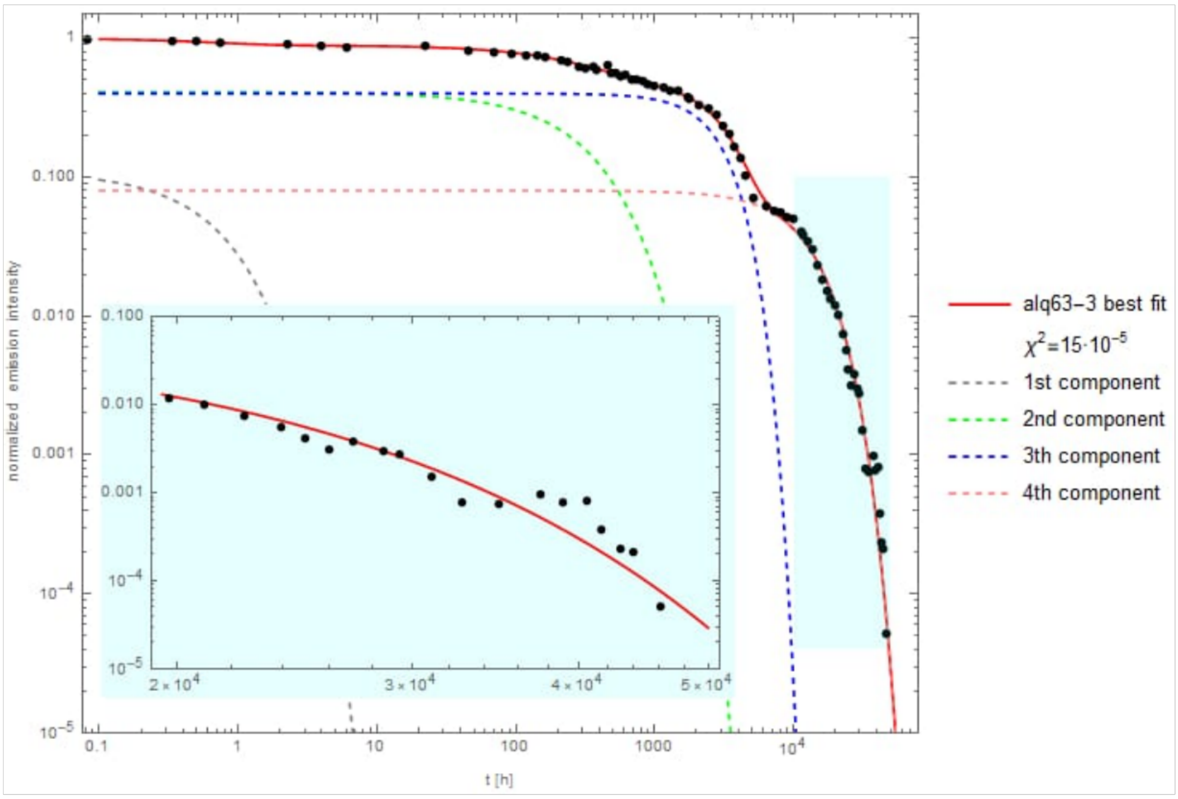

Figure 2.11: PL intensity of sample alq63-3 decaying in air with a zoom for the time-resolved PL after 10,000 h (black circles).

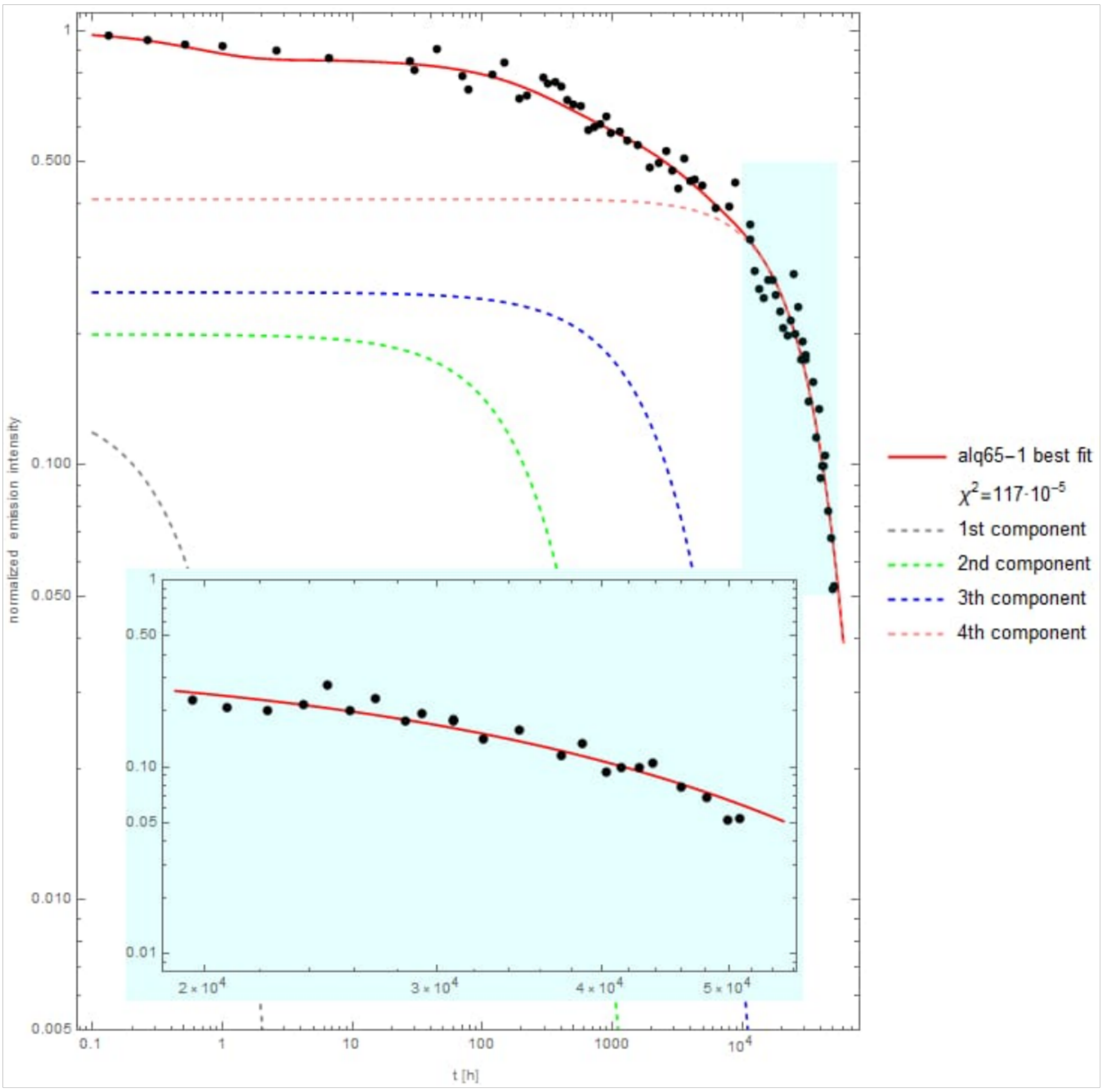

Figure 2.12: PL intensity of sample alq65-1 decaying in air with a zoom for the time-resolved PL after 10,000 h (black circles).

is I_1, I_4, I_2 and finally I_3. Between 100h and 1500h, I_2 and I_4 swap. Only after 6000h the order is restored, as remarked in Fig. 2.11. Instead, in annealed sample alq65-1 all four components are perfectly organized from the very beginning till the end of the PL decay, i.e. from a fraction of a second to 50,000h, as remarked in Fig. 2.12. However, the fourth component in alq65-1, as in alq63-3, is described by a compressed KWW function that is a simply monotone function: a re-organization or re-configuration has been expected in both the samples.

Table 2.4: Amplitudes, time constants, and KWW parameter β of the four components for the reference not-annealed sample alq63-3 and the sample alq65-1, which has been annealed in dry oxygen at 180°C, retrieved by fitting the experimental data with (2.29).

Sample	Amplitude (%)				Time constant(s^{-1})				β				$\chi^2(10^{-5})$
	I_1	I_2	I_3	I_4	τ_1	τ_2	τ_3	τ_4	β_1	β_2	β_3	β_4	
alq63-3	11	41	40	8	0.72	332	3195	13381	1	1	2	1.57	15
alq65-1	14	20	25	41	0.61	300	2819	30,398	1	1	1	1.39	117

Once we understand how many components are needed for describing the profile of the PL emission and the best fit function for interpolating the experimental data, we apply our model to investigate the hidden dynamics in terms of pumping and damping mechanism behind the abrupt decreasing observed at the end of the time evolution of the photoluminescent intensity, see Figs. 2.11 and 2.12, and the negative bump in sample alq63-3 around 5000h, see Fig. 2.11. Knowing the time behaviour of the reduced mass (2.12a), it is possible to establish if the pumping or the damping mechanism is acting on the system and then observe how it influences the luminescence. Figure 2.13 represents the time evolution of the reduced mass $\mathscr{m}(t)$ for the I_4 component in the alq63-3. The choice to consider the fourth component is due to the fact that it is the only component in the very long time range that still survives (see inserts of Figs. 2.11 and 2.12). This allows us to observe clearly the mechanism behind the intensity decay in a physical system in order to apply it to the whole range of data validating our approach and hypothesis. Once the minimum of the function $\mathscr{m}(t)$, i.e. the turning point at 4514h in Fig. 2.13, has been exceeded, the reduced mass $\mathscr{m}(t)$ starts to increase and so, the damping mechanism dominates the dynamics of the system. The first derivative with respect to time of the reduced mass should be analysed in order to find the exact time instant when the damping takes the place of the pumping mechanism and the plateau of the luminescence should appear. In a neighbourhood of $3000\text{h} < t < 5000\text{h}$, the PL intensity is expected to be almost constant. As shown in Fig. 2.14, we found the expected plateau. As explained in Section 2.2.2, this phenomenon is due to the fact that the values of the triplet-trapping rate K_O and the reverse intersystem crossing rate K_{rISC} are approximately equal. The system is in a quasi-equilibrium and the decay slows down according to a pure exponential behaviour that appears as a plateau in the normalized PL intensity. As K_O overcomes definitely K_{rISC}, the concentration of the quenchers cannot be neglected any more and becomes the main influential responsible

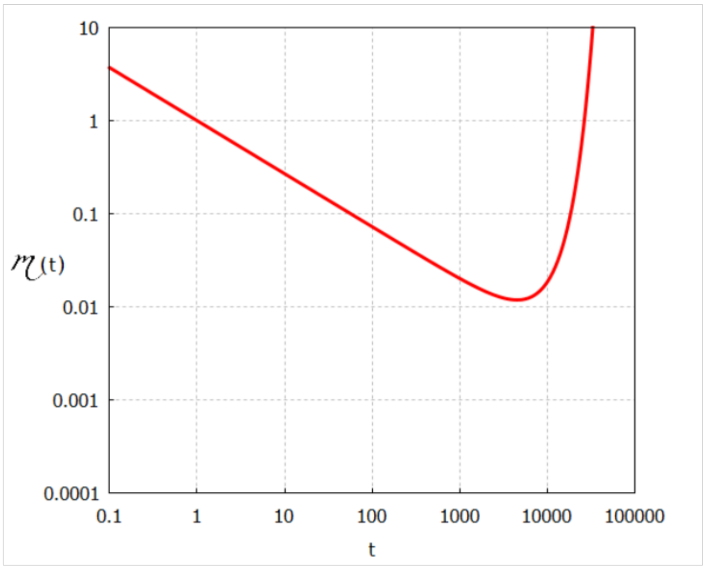

Figure 2.13: The time dependent reduced mass $\mathscr{m}(t)$ (2.12a) of the fourth component of the sample alq63-3.

for the abrupt decreasing in the PL intensity observed in proximity of t=10,000h. The dynamics hidden behind the whole intensity emission can be analysed evaluating the time-dependent reduced mass $\mathscr{m}(t)$ for each component that highlights the range of the influence of each component in the PL decay. With the knowledge of the time behaviour of the reduced mass, it is possible to predict the presence and the position of the plateau. To support this idea, it is useful to compare all the curves of the reduced mass with the data collected concerning the reference sample alq63-3 as shown in Fig. 2.15. Each solid line represents the reduced mass corresponding to each component. The presence of the *knee*, borrowing the term from high-energy physics, can be explained as the result of the superposition of the effects determined by all the components. The appearance of the "knee" is due to the damping effect of the first three components and the pumping of the last one. It is also crucial for the reliability of the model to observe that the faintest decrease in photoluminescence around 2000h has been identified by the minimum of the third component. However, it is less evident than the *knee* since there is still living the fourth component and its pumping mechanism is active at that moment. After $10,000$h all the reduced masses contribute as a damping mechanics explaining the abrupt decay observed. From $10,000$h the pumping and the quasi-equilibrium phase have been overcome and the system starts to rapidly "quench" the luminescence giving a physical interpretation to this sudden decreasing of the luminescence: there are no other (relevant) components in this time range that are pumping against the decreasing of all four components. Analogous results have been obtained also for the sample alq65-1 (see Fig. 2.12, Fig. 2.16 and Tab. 2.4), but they have been reported here for sake of conciseness.

However, as observed in Section 2.2.3, the compressed KWW function is not complete monotone and this fact, according to our phenomenological model, indicates that the dynamics is dual and therefore, it should be another reconfiguration, or in other words another plateau has been expected. In fact, the presence of the compressed exponential

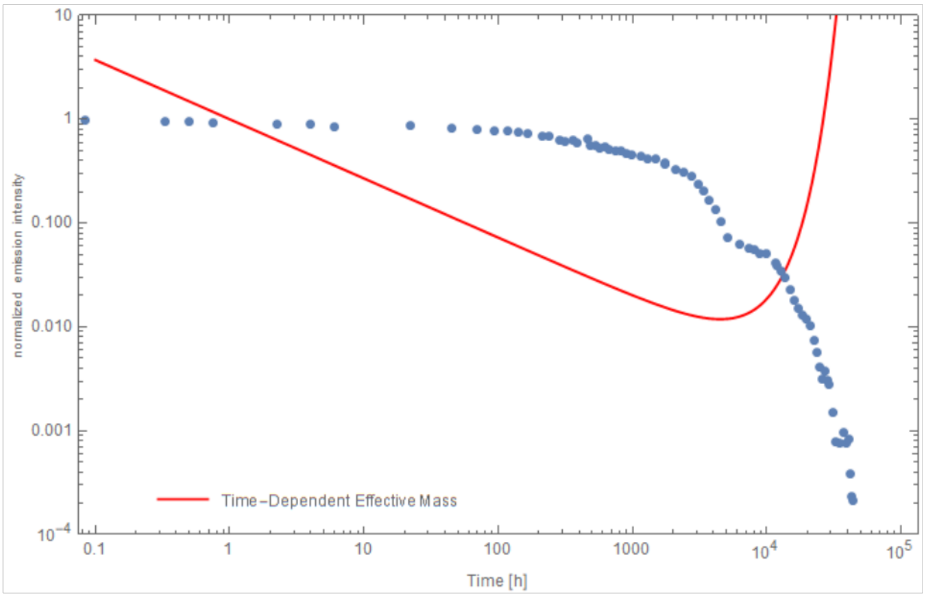

Figure 2.14: PL intensity of the sample alq63-3 decaying in air (blue dots) and the time-dependent reduced mass $\mathscr{m}(t)$ (red solid line).

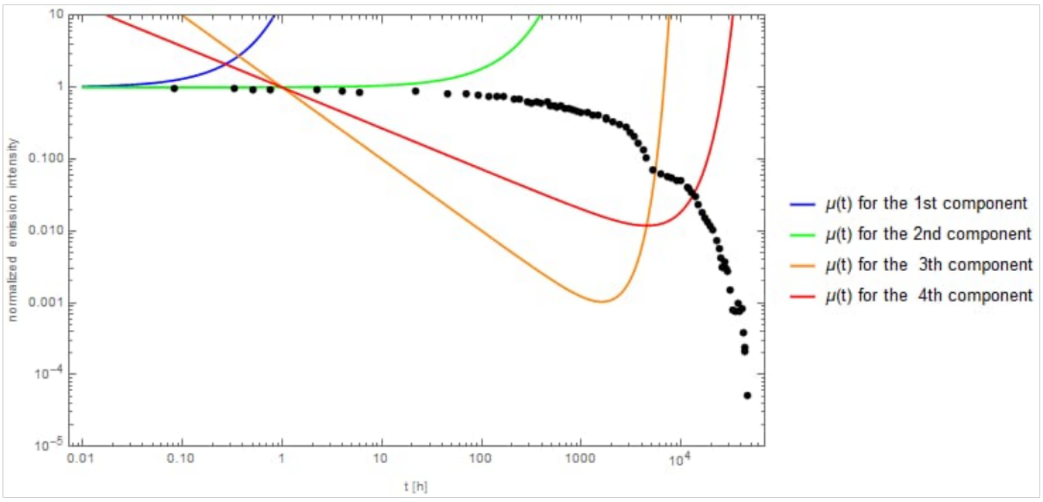

Figure 2.15: PL intensity of the sample alq63-3 decaying in air (blue dots) and the time-dependent reduced mass $\mathscr{m}(t)$ at different relaxation time corresponding to each component: τ=0.72h blue solid line, τ=332h green solid line, τ=3195h orange solid line and finally τ=13381h red solid line.

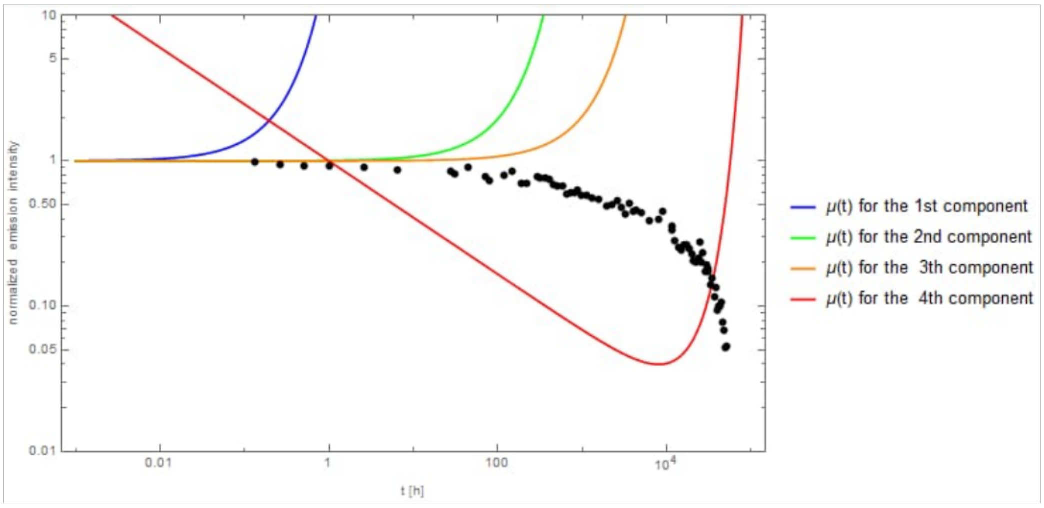

Figure 2.16: PL intensity of the sample alq65-1 decaying in air (blue dots) annealed at 180°C in dry O_2 and the time-dependent reduced mass $\mathscr{m}(t)$ at different relaxation time corresponding to each component: τ=0.61h blue solid line, τ=300h green solid line, τ=2819h orange solid line and finally τ=32,451h red solid line.

β means that there is a disorder or an heterogeneity in the system (i.e. the increasingly cumbersome presence of the molecular oxygen), which implies the increasingly faster decay and consequently, the pressing degradation of the Alq$_3$ sample. This plateau has been expected since the number of the quenchers has been increased but meanwhile also the number of the luminophores that are still active has decreased, therefore the rate of decay K_O slowed down. So, it is possible to gain again a quasi-equilibrium situation: $K_D = 0$ that physically explain the presence of the plateau.

This plateau, which until now had gone unnoticed, "appears" at $t = 40,000$h and it gives a physical evidence of our model. A similar observation emerges also for the annealed sample. The thermal annealing allowed to even out differences between the plateau and the following damping in the decay till $30,000$h as it can be observed in Fig. 2.12, but this unnoticed plateau results to be evident even if less than what is observed in the reference sample alq63-3, and it approximately occurs at the same time, approximately $40,000$h.

It should be also highlighted that the time that elapses between the plateau during the PL degradation gives an indirect measurement of the *pumping* time range needed to populate the singlet excited state. A better overview can be obtained by considering also the kinetics equation approach. This allows us to give a further evidence of the correctness of the interpretation. Figures 2.17 and 2.18 illustrate how the theoretical fits defined via two-terms Prony series (i.e. the bi-exponential model used in photoluminescence (2.18) and its approximation (2.24)) can match the data of the reference sample alq63-3 and the annealed one, alq65-1.

Table 2.5: Amplitude and time constant of the fourth component I_4 for the reference not-annealed sample alq63-3 and alq65-1, which has been annealed in dry oxygen at 180°C, retrieved by fitting the experimental data with (2.29).

sample	annealing	parameters		
		A	K_S	K_D
alq63-3	none	0.15	$0.12\ 10^{-3}$	$0.62\ 10^{-7}$
alq65-1	dry O_2	0.40	0.013	$67.0\ 10^{-7}$

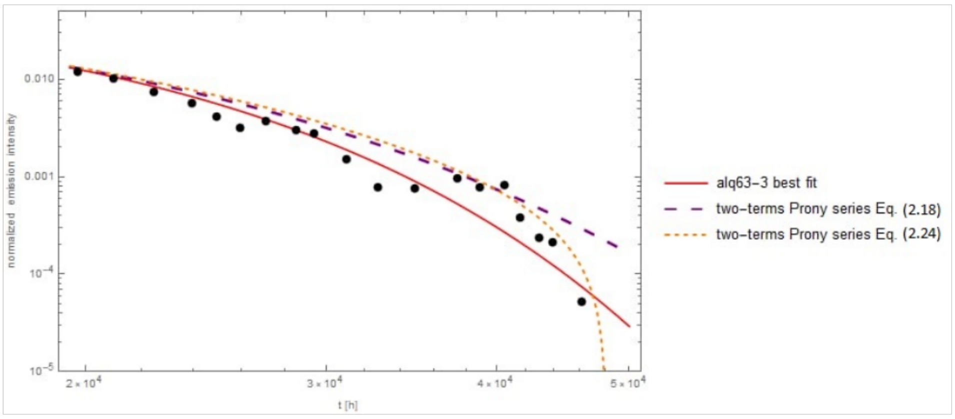

Figure 2.17: PL intensity of sample alq63-3 decaying in Air after 10, 000h (full black circles), best fit (solid red line) by using (2.29) and parameters presented in Table 2.5 and the Prony series approximation of the fourth component by using (2.18) (dashed purple line) and (2.24) (dashed orange line).

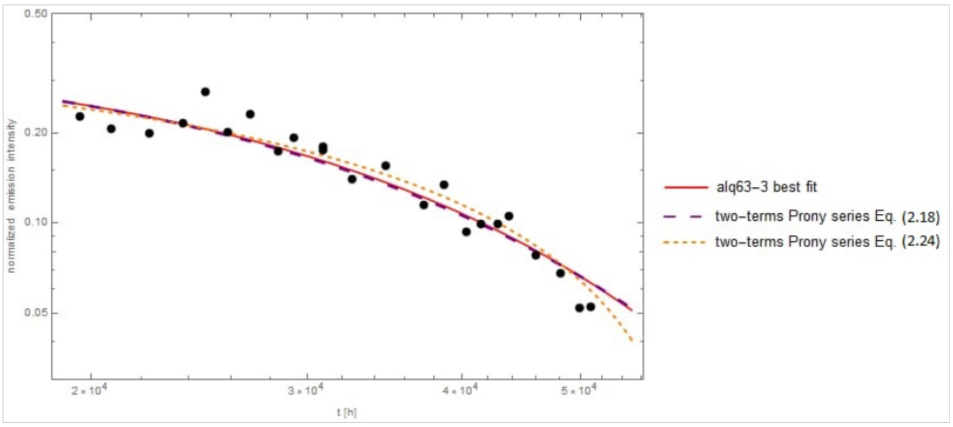

Figure 2.18: PL intensity of sample alq65-1 decaying in Air after 10, 000h (full black circles), best fit (solid red line) by using (2.29) and parameters collected in Table 2.5 and the Prony series approximation of the fourth component by using (2.18) (dashed purple line) and (2.24) (dashed orange line).

It is immediately observed that the two-terms Prony series is a reliable approximation tool for the KWW function even for a physical real system, so confirming the mathematical results obtained exploiting the minimum square method in Section 3.

In particular the two term Prony series (2.24) with only damping mechanisms active seems to be in better agreement with the experimental data. The parameters of the Prony series (2.24) obtained from the best fit are reported in Table 2.5.

Table 2.6: Amplitude and time constants of the fourth component I_4 for the reference not-annealed sample alq63-3 and alq65-1, which has been annealed in dry oxygen at 180°C, retrieved by fitting the experimental data with Eq. (19).

Prony series approximation parameters			
samples	amplitude(%)	$K_S[10^{-3}\mathrm{s}^{-1}]$	$K_D[10^{-7}\mathrm{s}^{-1}]$
alq63-3	15	0.12	$0.62\ 10^{-7}$
alq65-1	40	0.013	$67.0\ 10^{-7}$

It should be noted that the best fit (solid red line) and the Prony approximation (2.24) (dashed orange line) tend to overlap. Indeed, the discrepancies between the two lines is no larger than 0.0005! The fitting values in Table 2.5 are in accordance with the ones collected in Table 3 in reference [15], where the singlet decay rate K_S is equal to $\frac{1}{\tau_4}$ and K_O is equal to the parameter α_4 introduced in [15]. Framing these values in the physical context of the excited states sketched in Fig. 2.5, it is possible to interpret the α parameter introduced in [15] as the triplet-trap decay rate due to more reactive species as the molecular oxygen that inhibits the luminophores. Finally, the dashed purple lines in Figs. 2.17 and 2.18 represent the solution in terms of the two-terms Prony series, i.e. the usual bi-exponential model in photoluminescence, (2.18) and it is drawn not only to highlight the quality of the underlying assumptions in (2.24) but it also helps in the identification of the unnoticed plateau. The compressed KWW function (red solid line) and the kinetics equation approximation (blue dashed line) are confining the last plateau in Fig. 2.17. The plateau at 4500h can represent a transition from an amorphous to crystalline phase transition, or in other words an early stage of the crystalline phase α, whereas the last plateau at $40,000$h can be associated with the so-called α phase transition. In conclusion, the damping mechanism, which dominates the decay after the fourth component in both samples, may be counteracted by the pumping effect generated by a fifth component. Since this fifth component appears only after 50,000h and its intensity is extremely low, approximately it is 10% less than the corresponding amplitude of the fourth component, it is possible to truncate the model up to the fourth component.

2.5 Conclusions to Chapter 2

The relaxation of various physical systems has been found to follow the Kohlrausch-Williams-Watts (KWW) function, as for example in glass-forming liquids [201], glassy materials [162, 163] and in the luminescent decay in solid state matter [12, 15, 29, 36, 42, 61, 125, 126, 181]. Although the qualitative agreement between the experimental data and the theoretical fit based on the KWW function, its physical meaning is quite elusive. In order to find out this meaning, we outlined a phenomenological model based on a second order differential equation. The model has been articulated into three steps.

Firstly, the anomalous relaxation governed by the KWW function has been simplified by choosing an alternative frame, called material frame, where the relaxation behaves ideally thanks to the introduction of the so-called material clock. This clock marks the time in a different way from the laboratory one: it can slow down or accelerate the passing of time embedding the deviations from the *pure* and mono-exponential behaviour that the system experienced during the relaxation. The main result of this step is the definition of a second order differential equation describing a damped harmonic oscillator characterized by a time-dependent reduced mass $\mathscr{m}(t)$ and a time-dependent frequency $\omega(t)$. The introduction of a time-dependent reduced mass $\mathscr{m}(t)$ in the laboratory frame unveils the relaxation dynamics distinguishing the stretched KWW function from the compressed KWW function on the base of their influence on the dynamics of the system. There are two dynamics: a pumping and a damping mechanism. The stretched KWW function is governed only by a damping mechanism, whereas the compressed KWW function describes a dual dynamics where both these mechanisms occur. In case of dual dynamics, the main features in the time-resolved photoluminescence are the faster than exponential decay and the presence of a plateau in the photoluminescent intensity emission in correspondence of the minimum of the reduced mass $\mathscr{m}(t)$. The plateau appears when a quasi-equilibrium is established between the pathways followed by the luminophores during their relaxation. The quasi-equilibrium can be considered as a quasi-phase transition.

In the second step, the analysis is worked out approximating the KWW function via Prony series. This approximation paves the way to an interesting result: it highlights the origin of the KWW function as a superposition of the photoluminescent decay pathways and it gives further evidences of the differences between the two KWW functions. The stretched KWW function can be approximated by a sum of simple exponential functions whereas the compressed KWW function has in its series expansion both positive and negative terms. The presence of the negative terms is due to the fact that the luminophores, i.e. the emitting centres, are quenched after interacting with more active species as the molecular dioxygen O_2 in the atmosphere.

The third part of our approach consists in the introduction of the mathematical concept of monotonicity and complete monotonicity. These mathematical properties are able to sum up all the physical properties, features and results found in the analysis of the relaxation giving a physical insight of their importance in modeling relaxation processes.

Among all the physical system experienced relaxation processes, the photoluminescence from organic molecules as the Tris(8-hydroxyquinoline)alluminium ($\mathrm{Alq_3}$) has been considered. The choice of this molecule as a test-case is based both on the large amount of data available and the widely applications of this material in organic light-emitting diodes (OLEDs), a spreading technology in our daily life. However, it is important to emphasize that our phenomenological model can be extended and generalized also to other photoluminescent materials. The large amount of data allowed to have a complete overview on the time-resolved PL emission giving the possibility to have a good test-case for the approach proposed.

In conclusion, we want to focus the attention on the advantages carried out by the phenomenological model proposed. In addition to being consistent with the known literature, and to framing the physical meaning of the KWW function always keeping in mind the role in the dynamics of the complete monotonicity, the proposed model solved the problem of the singularity at the origin classifying it as a *coordinate* singularity. Last but not least, it restored the symmetry from a dynamical point of view between the dispersion and the relaxation models that are both described by a damped harmonic oscillator (or a driven damped harmonic oscillator as shown in Chapter 3).

Chapter 3

Dynamical systems and their evolution: mathematical methods and physical interpretations

3.1 Introduction to modelling dynamical systems

A *dynamical system* is a mathematical model that describes how a real system evolves in time in terms of a differential equation once the physics governing the system has been abstracted from the complexity nested in real processes.
As described in Chapter 2 and in [123], the analysis of a complex system is successfully performed changing the perspective using a material frame, that is a frame equipped with a clock that marks the time differently from the one set in the laboratory. The choice of a different frame favours the emerging of the physics and consequently, a clearer description of the luminophores relaxation as a second order differential equation whose physical meaning is inscribed in the framework of a damped harmonic oscillator.
More generally, we state that the relaxation functions are solutions of evolutionary problems emerging within relevant mathematical treatments that include fractional calculus [78], operational methods [23, 24] and the theory of exponential operators and semigroups [116].
Our investigation on the properties of the relaxation functions and their evolutionary problems starts with the composition rule.
The term *composition rule* was introduced for the first time in [78] and it refers to a binary and associative operation that composes relaxation functions imitating the semigroup property [5, 56, 57, 68].
Mathematically, the composition rule reads

$$\Psi(t, t_1) \circ \Psi(t_1, t_0) = \Psi(t, t_0), \tag{3.1}$$

where t_0 and t denote the initial and the final endpoints in the time interval considered whereas t_1 is an intermediate (or dummy) time instant ranging between t_0 and t which splits the evolution into two parts, lastly $'\circ'$ denotes the binary and associative composition operation.
Here, $\Psi(t, t_0)$ is the relaxation function in the time interval $[t_0, t]$ and it is built from

$\Psi(t,t_1)$ and $\Psi(t_1,t_0)$ that from now on are called relaxation function syntagms or shortly *relaxation syntagms.* The relaxation syntagms are analogous or identical subsets of the overall relaxation function in the respective time intervals $[t_0,t_1]$ and $[t_1,t]$ that can exist alone or be part of an ordered sequence aimed to obtain a description ranging in a wider time interval. In other words, the time-ordered ensemble of these syntagms reproduces the evolution of the system in the whole time interval.

The notation used in (3.1) is consistent with the one presented in Chapter 1, that is the function $\Psi(t)$ is the relaxation function defined in $[0,t]$.

As shown in Chapter 2, we defined the relaxation function $\Psi(t)$ in $[0,t]$ as the fraction of relaxing centres at time t with respect to the initial number of relaxing centres at $t=0$:

$$\Psi(t) := \frac{n(t)}{n(0)}. \tag{3.2}$$

As a mean to highlight that we consider relaxation syntagms, we will add square brackets to the right-hand side of (3.2) that evoke the square parentheses of the time intervals and so, the meaning of the relaxation syntagm is clearly stated:

$$\Psi(t) := \left[\frac{n(t)}{n(0)}\right]. \tag{3.3}$$

In this way we emphasize how the composition rule reflects the composition of the underlying time interval on which each relaxation syntagm has been defined.

Resorting to the above definition of relaxation function (3.3), we can recast the composition rule (3.1) in $[t_0,t]$ in terms of the fraction of relaxing centres at time t with respect to the number of relaxing centres at a general starting time instant t_0 as the result of the composition of the relaxation syntagms:

$$\left[\frac{n(t)}{n(t_1)}\right] \circ \left[\frac{n(t_1)}{n(t_0)}\right] = \left[\frac{n(t)}{n(t_0)}\right]. \tag{3.4}$$

The two definitions, (3.1) and (3.4), are equivalent.

A system that satisfies the composition rule is deterministic, and it can be physically interpreted as follows.

Imagine you have a couple of observers that analyses the same system from a different point of view. The evolution of the system does not change if the composition rule is fulfilled. This is the fundamental requirement to be considered when modelling a dynamical system.

The aim of this Chapter is to describe and design new methodologies, approaches, and results in modelling dynamical systems. The idea is to address the problem of modelling the evolution of relaxation processes from different perspectives, so we enlarge the landscape of possible mathematical methods and physical interpretations to simplify the complexity that characterizes the relaxation processes.

As previously described, we firstly design the methodologies to obtain the composition rule for the relaxation functions of physical interest in complex processes. The composition rule offers an alternative tool to solve the initial value problems in terms of ordinary, partial or fractional differential equations framed in the context of the theory of exponential operators and semigroups.

3.2 Debye or *pure* exponential composition rule

In this Section we design the methodology for the time syntagms' composition through mixed types of research techniques taking the advantages of the Debye relaxation that is the simplest case:

$$\Psi_D(t) = e^{-\frac{t}{\tau}}, \tag{3.5}$$

where τ is the relaxation time.
In order to simplify the notation in the following calculations, we assume a dimensionless definition for the time variable: $\frac{t}{\tau} = T$.
According to this notation the Debye relaxation function (3.5) now reads:

$$\Psi_D(T) = e^{-T}. \tag{3.6}$$

As described in Section 3.1, the time interval $[T_0, T]$ is split up in two subsets, $[T_0, T_1]$ and $[T_1, T]$, and therefore we define the Debye relaxation (3.6) associated to all these time intervals

$$\begin{aligned}
\Psi_D(T, T_0) &= \left[\frac{n(T)}{n(T_0)}\right]_D = e^{-(T-T_0)}, \\
\Psi_D(T, T_1) &= \left[\frac{n(T)}{n(T_1)}\right]_D = e^{-(T-T_1)}, \\
\Psi_D(T_1, T_0) &= \left[\frac{n(T_1)}{n(T_0)}\right]_D = e^{-(T_1-T_0)}.
\end{aligned} \tag{3.7}$$

The composition rule for the Debye relaxation has the following form, where $'\circ'$ is the unknown binary and associative operation that composes the relaxation syntagms

$$\begin{aligned}
\Psi_D(T, T_1) \circ \Psi_D(T_1, T_0) &= \left[\frac{n(T)}{n(T_1)}\right]_D \circ \left[\frac{n(T_1)}{n(T_0)}\right]_D \\
&= e^{-(T-T_1)} \circ e^{-(T_1-T_0)} \\
&= e^{-(T-T_0)} \\
&= \left[\frac{n(T)}{n(T_0)}\right]_D \\
&= \Psi_D(T, T_0).
\end{aligned} \tag{3.8}$$

In the Debye case (3.8), the composition rule is evidently fulfilled replacing the $'\circ'$ operation with the multiplication, as shown here below:

$$\begin{aligned}\Psi_D(T,T_1)\cdot\Psi_D(T_1,T_0) &= \left[\frac{n(T)}{n(T_1)}\right]_D \cdot \left[\frac{n(T_1)}{n(T_0)}\right]_D\\ &= e^{-(T-T_1)}\cdot e^{-(T_1-T_0)}\\ &= e^{-(T-T_0)}\\ &= \left[\frac{n(T)}{n(T_0)}\right]_D\\ &= \Psi_D(T,T_0).\end{aligned} \tag{3.9}$$

However, the anomalous (or non-Debye) relaxations cannot satisfy the composition rule if the associative and binary $'\circ'$ operation is the multiplication. And accordingly, we have to introduce a more general $'\circ'$ operation to compose anomalous relaxation processes.

3.2.1 Composition rule via Cauchy convolution product

A first possibility to generalize the Debye composition rule is to follow the methodology we illustrated in [78, 79]. Focusing the attention on the terms involved in the $'\circ'$ operation, we can define an *ad hoc* operation aimed to validate the composition rule (3.8). In order to consider only the strictly necessary factors involved in the $'\circ'$-operation, we perform the series expansion of each relaxation syntagm and we get

$$\begin{aligned}\Psi_D(T,T_1)\circ\Psi_D(T_1,T_0) &= \left[\frac{n(T)}{n(T_1)}\right]_D \circ \left[\frac{n(T_1)}{n(T_0)}\right]_D\\ &= e^{-(T-T_1)} \circ\ e^{-(T_1-T_0)}\\ &= \sum_{k=0}^{\infty}(-1)^k\frac{(T-T_1)^k}{\Gamma(k+1)}\circ\sum_{r=0}^{\infty}(-1)^r\frac{(T_1-T_0)^r}{\Gamma(r+1)}\\ &= \sum_{r=0}^{\infty}(-1)^r\sum_{k=0}^{r}\frac{(T-T_1)^k}{\Gamma(k+1)}\circ\frac{(T_1-T_0)^{(r-k)}}{\Gamma(r-k+1)},\end{aligned} \tag{3.10}$$

where in the last line we use the series identity named Cauchy convolution product [81]

$$\sum_{k=0}^{\infty}\sum_{r=0}^{\infty}a_{k,r} = \sum_{r=0}^{\infty}\sum_{k=0}^{r}a_{k,r-k}. \tag{3.11}$$

Now we introduce the *ad hoc* definition for the Debye relaxation

$$(T-T_1)^k\circ(T_1-T_0)^{(r-k)} = \frac{\Gamma(k+1)\Gamma(r-k+1)}{\Gamma(r+2)}(T-T_0)^r \tag{3.12}$$

that can be replaced in (3.10) so we obtain

$$\begin{aligned}
\Psi_D(T,T_1)\circ\Psi_D(T_1,T_0) &= \left[\frac{n(T)}{n(T_1)}\right]_D \circ \left[\frac{n(T_1)}{n(T_0)}\right]_D \\
&= e^{-(T-T_1)} \circ\ e^{-(T_1-T_0)} \\
&= \sum_{r=0}^{\infty}(-1)^r \sum_{k=0}^{r} \frac{(T-T_1)^k}{\Gamma(k+1)} \circ \frac{(T_1-T_0)^{(r-k)}}{\Gamma(r-k+1)} \\
&= \sum_{r=0}^{\infty}(-1)^r \sum_{k=0}^{r} \frac{(T-T_0)^r}{\Gamma(r+2)} \\
&= \sum_{r=0}^{\infty}(-1)^r \frac{(T-T_0)^r}{\Gamma(r+1)} \\
&= e^{-(T-T_0)} \\
&= \left[\frac{n(T)}{n(T_0)}\right]_D \\
&= \Psi_D(T,T_0)
\end{aligned} \tag{3.13}$$

and thus, the composition rule for the relaxation syntagms is fulfilled.
The *ad hoc* definition (3.12) is the starting point for building an integro-differential evolution equation for the Debye process (3.6). The first step is to write (3.12) in its integral form

$$(T-T_1)^k \circ (T_1-T_0)^{r-k} = \frac{1}{T-T_0}\int_{T_0}^{T} dT_1 (T-T_1)^k \cdot (T_1-T_0)^{r-k} \tag{3.14}$$

and then, we replace the above definition (3.14) of the $'\circ'$ operation in (3.10).
After swapping the series with the integral, we obtain

$$\begin{aligned}
\Psi_D(T,T_1)\circ\Psi_D(T_1,T_0) &= \left[\frac{n(T)}{n(T_1)}\right]_D \circ \left[\frac{n(T_1)}{n(T_0)}\right]_D \\
&= \sum_{r=0}^{\infty}(-1)^r \sum_{k=0}^{r} \frac{1}{T-T_0}\int_{T_0}^{T} dT_1\ \frac{(T-T_1)^k \cdot (T_1-T_0)^{(r-k)}}{\Gamma(k+1)\Gamma(r-k+1)} \\
&= \int_{T_0}^{T} \frac{dT_1}{T-T_0} \sum_{r=0}^{\infty}(-1)^r \sum_{k=0}^{r} \frac{(T-T_1)^k (T_1-T_0)^{r-k}}{\Gamma(1+k)\Gamma(1+r-k)}.
\end{aligned} \tag{3.15}$$

Once again we resort to the identity (3.11) in order to point out the two Debye relaxations in each time syntagms

$$\begin{aligned}
&\int_{T_0}^{T} \frac{dT_1}{T-T_0} \sum_{r=0}^{\infty} (-1)^r \sum_{k=0}^{r} \frac{(T-T_1)^k (T_1-T_0)^{r-k}}{\Gamma(1+k)\Gamma(1+r-k)} \\
&= \int_{T_0}^{T} \frac{dT_1}{T-T_0} \sum_{k=0}^{\infty} \frac{(T-T_1)^k}{\Gamma(k+1)} \sum_{r=0}^{\infty} \frac{(T_1-T_0)^r}{\Gamma(r+1)} \\
&= \int_{T_0}^{T} \frac{dT_1}{T-T_0} e^{-(T-T_1)} \cdot e^{-(T_1-T_0)} \qquad (3.16) \\
&= \int_{T_0}^{T} \frac{dT_1}{T-T_0} \Psi_D(T,T_1) \cdot \Psi_D(T_1,T_0) \\
&= \int_{T_0}^{T} \frac{dT_1}{T-T_0} \left[\frac{n(T)}{n(T_1)}\right]_D \cdot \left[\frac{n(T_1)}{n(T_0)}\right]_D .
\end{aligned}$$

According to the procedure illustrated in [78], we can embed the *normalization* term $\frac{1}{T-T_0}$ in (3.16) introducing a dummy variable u that ranges in $[0,1]$ as shown below

$$\begin{aligned}
&\frac{d}{dT} \int_{T_0}^{T} dT_1 \int_0^1 du\ \Psi_D(u\ T, u\ T_1) \cdot \Psi_D(u\ T_1, u\ T_0) \\
&= \frac{d}{dT} \int_{T_0}^{T} dT_1 \int_0^1 du\ \left[\frac{n(u\ T)}{n(u\ T_1)}\right]_D \cdot \left[\frac{n(u\ T_1)}{n(u\ T_0)}\right]_D \\
&= \frac{d}{dT} \int_{T_0}^{T} dt_1 \int_0^1 du\ e^{-u(T-T_1)} \cdot e^{-u(T_1-T_0)} \\
&= \frac{d}{dT} \int_{T_0}^{T} dT_1 \int_0^1 du\ e^{-u(T-T_0)} \qquad (3.17) \\
&= e^{-(T-T_0)} \\
&= \left[\frac{n(T)}{n(T_0)}\right]_D \\
&= \Psi_D(T,T_0).
\end{aligned}$$

The strategy to introduce the *dummy* variable u is proven to be very useful in Section 3.3 where we face the problem of the composition of two relaxation syntagms in terms of the one-parameter Mittag-Leffler function.

3.2.2 Composition rule via Reynolds-Leibnitz theorem

In this Subsection, we present another promising and original method based on a kinematic application of the Euler expansion formula (the Reynolds-Leibnitz transport theorem [174]) for the change of an integral of a fluid quantity over an arbitrary fluid volume moving along the fluid path.

The method defines a general integro-differential equation that fulfils the requirement to be a composition rule for anomalous relaxation syntagms and at the same time, it

offers a clear physical interpretation.
Once we establish that the system obeys to the composition rule, we implicitly assume that the relaxation behaves *intensively*. Let us explain what we mean with the concept of intensive behaviour of the relaxation function. The relaxation functions in each time syntagm, $[T_0, T_1]$ and $[T_1, T]$, has the same evolution of the relaxation in the whole time syntagm $[T_0, T]$. For this reason, the relaxation function and the product of its syntagms are considered as an *intensive* property of the system, and therefore we resort to the Reynolds-Leibnitz theorem to track their evolution and their composition. This theorem states that the total rate of the changes of an intensive quantity f in a moving (time-dependent) incompressible volume $\mathcal{V}(T)$ is equal to the generation of this quantity within the volume plus the flux of this property in and out of the volume through the surface $\partial\mathcal{V}(T)$ bounding the volume $\mathcal{V}(T)$ itself.
As the quantity moves and distorts the flowfield, the volume $\mathcal{V}(T)$ and its surface $\partial\mathcal{V}(T)$ move and distort with it.
Mathematically, the Reynolds-Leibnitz theorem reads

$$\frac{d}{dT}\int_{\mathcal{V}(T)} dV\ f = \int_{\mathcal{V}(T)} dV\ \frac{\partial f}{\partial T} + \dot{f}_{\text{net}}, \tag{3.18}$$

where f is an intensive property of the system, $\dot{f}_{\text{net}}$=$\dot{f}_{\text{in}}$-$\dot{f}_{\text{out}}$ denotes the net flux, $\mathcal{V}(T)$ is the control volume or region in the Euclidean space with boundary $\partial\mathcal{V}(T)$.
However, the time syntagms are one-dimensional and therefore, it is possible to reduce the theorem in its one-dimensional case, also known in literature as Leibniz theorem:

$$\frac{d}{dT}\int_{a(T)}^{b(T)} dT_1\ f(T,T_1) = \int_{a(T)}^{b(T)} dT_1\ \frac{\partial f(T,T_1)}{\partial T} + f(b(T),T)\frac{db(T)}{dT} - f(a(T),T)\frac{da(T)}{dT}. \tag{3.19}$$

Now we assume that $a(T) = T_0$, $b(T) = T$ and the intensive function coincides with the product of the relaxation functions in the respective time syntagms

$$\begin{aligned} f(T,T_1) :&= \Psi(T,T_1)\cdot\Psi(T_1,T_0) \\ &= \left[\frac{n(T)}{n(T_1)}\right]\cdot\left[\frac{n(T_1)}{n(T_0)}\right], \end{aligned} \tag{3.20}$$

where T_0 is considered as a constant.

Under these assumptions, we recast (3.19) as follows

$$\begin{aligned} &\frac{d}{dT}\int_{T_0}^{T} dT_1\ \Psi(T,T_1)\cdot\Psi(T_1,T_0) - \int_{T_0}^{T} dT_1\ \frac{d}{dT}\Psi(T,T_1)\cdot\Psi(T_1,T_0) \\ &= \frac{d}{dT}\int_{T_0}^{T} dT_1\ \left[\frac{n(T)}{n(T_1)}\right]\cdot\left[\frac{n(T_1)}{n(T_0)}\right] - \int_{T_0}^{T} dT_1\ \frac{d}{dT}\left[\frac{n(T)}{n(T_1)}\right]\cdot\left[\frac{n(T_1)}{n(T_0)}\right] \\ &= \left[\frac{n(T)}{n(T_0)}\right] \\ &= \Psi(T,T_0). \end{aligned} \tag{3.21}$$

It is possible to compact the notation introducing the commutator operator:

$$\left[\frac{d}{dT}, \int_{T_0}^{T} dT_1\right] f(T,T_1) = \frac{d}{dT}\int_{T_0}^{T} dT_1 f(T,T_1) - \int_{T_0}^{T} dT_1 \frac{d}{dT} f(T,T_1). \tag{3.22}$$

According to the Reynolds-Leibniz theorem, the result of the composition rule represents the *net flow* of the relaxation function in $[T_0, T]$: $\Psi(T, T_0)$. This interpretation based on the commutator operator (3.22) perfectly frames the result since the relaxation function evaluated in the total time range $[T_0, T]$ is made up with its time syntagms, $[T_0, T_1]$ and $[T_1, T]$, and it does not depend on the time instant T_1.

To deeply understand the meaning of the commutator, we introduce the concept of inverse derivative operator. This operator can be also bought on the name of *anti-derivative* (or *negative-derivative*). In fact with this formalism it is possible to evaluate integrals and derivatives on the same footing. In case of real order derivatives, as the present case, the distinction between the derivative and the integral become superfluous and the physical meaning of the evolution equation can emerge.

In [11, 41], the actions of the derivative operator D and its inverse operator ${}_{T_0}D_T^{-1}$ are defined as follows

$$D : f(T) \longmapsto \frac{d}{dT} f(T) \tag{3.23}$$

and

$${}_{T_0}D_T^{-1} : f(T) \longmapsto \int_{T_0}^{T} dT_1 \; f(T_1). \tag{3.24}$$

The inverse operator is a special case of the known formula usually attributed to Cauchy that reduces the calculation of the $n-$primitive of a function to a single integral of convolution type

$${}_{T_0}D_T^{-n} : f(T) \longmapsto \frac{1}{\Gamma(n)} \int_{T_0}^{T} dT_1 \; (T-T_1)^{n-1} f(T_1), \qquad n \in \mathbb{N}. \tag{3.25}$$

In case n is a positive real number, that is $n \in \mathbb{R}^+$, the definition (3.25) is the Riemann-Liouville fractional integral [70, 166].

We extend the definitions of the derivative operator D in (3.23) and its inverse operator ${}_{T_0}D_T^{-1}$ in (3.24) to the function $f(T, T_1)$.

To make the notation we introduced as clear as possible, we add a second subscript to the operators that specifies the variables on which the operators act. Specifically, the subscripts 1 and 2 mean respectively that the operators act on the first or on the second variable in the argument. According to this notation, the operators defined in (3.23) and (3.24) can be generalized as follows:

$$D_1 : f(T,T_1) \longmapsto \frac{d}{dT} f(T,T_1) \tag{3.26}$$

and

$${}_{T_0}D_{T,2}^{-1} : f(T,T_1) \longmapsto \int_{T_0}^{T} dT_1 f(T,T_1). \tag{3.27}$$

The formalism we have just envisaged can be combined with the result (3.22) and we get

$$\begin{aligned}\Big[D_1, {}_{T_0}D^{-1}_{T,2}\Big] f(T,T_1) &= \Big(D_1 \; {}_{T_0}D^{-1}_{T,2} - {}_{T_0}D^{-1}_{T,2} \; D_1\Big) f(T,T_1) \\ &= \frac{d}{dT} \int_{T_0}^{T} dT_1 \; f(T,T_1) - \int_{T_0}^{T} dT_1 \; \frac{d}{dT} f(T,T_1) \\ &= f(T,T).\end{aligned} \tag{3.28}$$

In order to point out the two relaxation syntagms, the result (3.28) can be recast as follows:

$$\begin{aligned}&\Big[D_1, {}_{T_0}D^{-1}_{T,2}\Big] \Psi(T,T_1) \cdot \Psi(T_1,T_0) = \Big(D_1 \; {}_{T_0}D^{-1}_{T,2} - {}_{T_0}D^{-1}_{T,2} \; D_1\Big) \Psi(T,T_1) \cdot \Psi(T_1,T_0) \\ &= \frac{d}{dT} \int_{T_0}^{T} dT_1 \; \Psi(T,T_1) \cdot \Psi(T_1,T_0) - \int_{T_0}^{T} dT_1 \; \frac{d}{dT} \Psi(T,T_1) \cdot \Psi(T_1,T_0) \\ &= \Psi(T,T_0),\end{aligned} \tag{3.29}$$

or equivalently

$$\begin{aligned}&\Big[D_1, {}_{T_0}D^{-1}_{T,2}\Big] \left[\frac{n(T)}{n(T_1)}\right] \cdot \left[\frac{n(T_1)}{n(T_0)}\right] = \Big(D_1 \; {}_{T_0}D^{-1}_{T,2} - {}_{T_0}D^{-1}_{T,2} \; D_1\Big) \left[\frac{n(T)}{n(T_1)}\right] \cdot \left[\frac{n(T_1)}{n(T_0)}\right] \\ &= \frac{d}{dT} \int_{T_0}^{T} dT_1 \; \left[\frac{n(T)}{n(T_1)}\right] \cdot \left[\frac{n(T_1)}{n(T_0)}\right] - \int_{T_0}^{T} dT_1 \; \frac{d}{dT} \left[\frac{n(T)}{n(T_1)}\right] \cdot \left[\frac{n(T_1)}{n(T_0)}\right] \\ &= \left[\frac{n(T)}{n(T_0)}\right].\end{aligned} \tag{3.30}$$

The commutator operator will be always different from zero, since if we compose two non-zero relaxation syntagms, we have a composed relaxation different from zero. Despite its application on the simplest relaxation function, the validity of the approach can be easily generalized to other relaxation functions, as for example in Section 3.4, provided that the relaxation functions are analytical and normalized in zero, i.e. $\Psi(0) = 1$. In case of the Debye relaxation, we have

$$\begin{aligned}&\Big[D_1, {}_{T_0}D^{-1}_{T,2}\Big] \Psi_D(T,T_1) \cdot \Psi_D(T_1,T_0) = \Big(D_1 \; {}_{T_0}D^{-1}_{T,2} - {}_{T_0}D^{-1}_{T,2} \; D_1\Big) \Psi_D(T,T_1) \cdot \Psi_D(T_1,T_0) \\ &= \frac{d}{dT} \int_{T_0}^{T} dT_1 \Psi_D(T,T_1) \cdot \Psi_D(T_1,T_0) - \int_{T_0}^{T} dT_1 \frac{d}{dT} \Psi_D(T,T_1) \cdot \Psi_D(T_1,T_0) \\ &= \frac{d}{dT} \int_{T_0}^{T} dT_1 \; e^{-(T-T_1)} \cdot e^{-(T_1-T_0)} - \int_{T_0}^{T} dT_1 \frac{d}{dT} e^{-(T-T_1)} \cdot e^{-(T_1-T_0)} \\ &= e^{-(T-T_0)} \\ &= \left[\frac{n(T)}{n(T_0)}\right]_D \\ &= \Psi_D(T,T_0).\end{aligned}$$

Hence, if the commutator acts on the relaxation function defined in the whole time interval $[T_0, T]$ we have

$$\begin{aligned}\left[D_{1,\,T_0} D_{T,2}^{-1}\right]\Psi_D(T, T_0) &= \left[D_{1,\,T_0} D_{T,2}^{-1}\right] e^{-(T-T_0)} \\ &= e^{-(T-T_0)} \\ &= \Psi_D(T, T_0).\end{aligned} \tag{3.31}$$

Here the commutator reduces to the identity operator.

3.3 One-Parameter Mittag-Leffler composition rule via Cauchy convolution product

In this Section, the methodology that we set out in Subsection 3.2.1 and in details in [78] has been applied in order to show how it is possible to obtain the composition rule for the one-parameter Mittag-Leffler function whose numerous and various properties have guaranteed it the high-sounding title of Queen function [43, 72, 136, 139]. This special function is defined as follows

$$E_\beta(z) = \sum_{k=0}^{\infty} \frac{z^{\beta k}}{\Gamma(\beta k + 1)}, \tag{3.32}$$

where $z \in \mathbb{C}$ and β is a real positive parameter.
Fixing $z = -\left(\frac{t}{\tau}\right)^\beta$ and assuming $\beta \in (0, 1)$, the one-parameter Mittag-Leffler function acquires a physical and mathematical interest since the the Fourier transform $\mathcal{F}$ on the real positive line (or the Laplace transform $\mathcal{L}$) of its expression

$$\Psi_{ML}(t) = E_\beta\Big(-\left(\frac{t}{\tau}\right)^\beta\Big) \tag{3.33}$$

is the Cole-Cole dispersion model [66]:

$$\hat{\varepsilon}(\omega) = \frac{1}{[1 + (i\omega\tau)^\beta]}, \tag{3.34}$$

where β ranges in $(0, 1]$, τ is the relaxation time, ω denotes the frequency and i is the imaginary unit.

The first step to define the composition rule for the one-parameter Mittag-Leffler relaxation function (3.33) is to fix the notation for the relaxation syntagms in each time interval resorting to the dimensionless time variable $T = \frac{t}{\tau}$:

$$\begin{aligned}\Psi_{ML}(T,T_0) &= E_\beta\Big(-(T-T_0)^\beta\Big) = \Big[\frac{n(T)}{n(T_0)}\Big]_{ML}\\ \Psi_{ML}(T,T_1) &= E_\beta\Big(-(T-T_1)^\beta\Big) = \Big[\frac{n(T)}{n(T_1)}\Big]_{ML}\\ \Psi_{ML}(T_1,T_0) &= E_\beta\Big(-(T_1-T_0)^\beta\Big) = \Big[\frac{n(T_1)}{n(T_0)}\Big]_{ML}.\end{aligned} \tag{3.35}$$

We compose the relaxation syntagms $\Psi(T_1,T_0)$ in $[T_0,T_1]$ and $\Psi(T,T_1)$ in $[T_1,T]$ into the relaxation $\Psi(T,T_0)$ in the whole time interval $[T_0,T]$, as follows

$$\begin{aligned}\Psi_{ML}(T,T_1)\circ\Psi_{ML}(T_1,T_0) &= \Big[\frac{n(T)}{n(T_1)}\Big]_{ML}\circ\Big[\frac{n(T_1)}{n(T_0)}\Big]_{ML}\\ &= E_\beta\Big[-\Big(T-T_1\Big)^\beta\Big]\circ E_\beta\Big[-\Big(T_1-T_0\Big)^\beta\Big]\\ &= E_\beta\Big[-\Big(T-T_0\Big)^\beta\Big]\\ &= \Big[\frac{n(T)}{n(T_0)}\Big]_{ML}\\ &= \Psi_{ML}(T,T_0).\end{aligned} \tag{3.36}$$

As opposed to the Debye model, the simple multiplication cannot replace efficiently the $'\circ'$ operation. We can visualize the onset of the problem that obstacles the composition of the relaxation syntagms (3.36) once we resort to the definition by series of the one-parameter Mittag-Leffler function (3.32) and to the Cauchy identity (3.11), as shown below

$$\begin{aligned}\Psi_{ML}(T,T_1)\circ\Psi_{ML}(T_1,T_0) &= \Big[\frac{n(T)}{n(T_1)}\Big]_{ML}\circ\Big[\frac{n(T_1)}{n(T_0)}\Big]_{ML}\\ &= E_\beta\Big[-\Big(T-T_1\Big)^\beta\Big]\circ E_\beta\Big[-\Big(T_1-T_0\Big)^\beta\Big]\\ &= \sum_{k=0}^{\infty}\frac{(-1)^k(T-T_1)^{\beta k}}{\Gamma(\beta k+1)}\circ\sum_{r=0}^{\infty}\frac{(-1)^r(T_1-T_0)^{\beta r}}{\Gamma(\beta r+1)}\\ &= \sum_{r=0}^{\infty}(-1)^r\sum_{k=0}^{r}\frac{(T-T_1)^{\beta k}\circ(T_1-T_0)^{\beta(r-k)}}{\Gamma(\beta k+1)\Gamma(\beta(r-k)+1)}.\end{aligned} \tag{3.37}$$

At this point we introduced an *ad hoc* definition of the $'\circ'$ operation in order to guarantee that the composition rule (3.36) is satisfied:

$$\Big(T-T_1\Big)^{\beta k}\circ\Big(T_1-T_0\Big)^{\beta(r-k)} = \frac{\Gamma(\beta k+1)\Gamma(\beta(r-k)+1)}{(1+r)\Gamma(\beta r+1)}(T-T_0)^{\beta r}. \tag{3.38}$$

Replacing (3.38) in the last line of (3.37), we get

$$\begin{aligned}
\Psi_{ML}(T,T_1)\circ\Psi_{ML}(T_1,T_0) &= \left[\frac{n(T)}{n(T_1)}\right]_{ML}\circ\left[\frac{n(T_1)}{n(T_0)}\right]_{ML}\\
&= E_\beta\Big[-\Big(T-T_1\Big)^\beta\Big]\circ E_\beta\Big[-\Big(T_1-T_0\Big)^\beta\Big]\\
&= \sum_{k=0}^{\infty}\frac{(-1)^k(T-T_1)^{\beta k}}{\Gamma(\beta k+1)}\circ\sum_{r=0}^{\infty}\frac{(-1)^r(T_1-T_0)^{\beta r}}{\Gamma(\beta r+1)}\\
&= \sum_{r=0}^{\infty}(-1)^r\sum_{k=0}^{r}\frac{(T-T_1)^{\beta k}\circ(T_1-T_0)^{\beta(r-k)}}{\Gamma(\beta k+1)\Gamma(\beta(r-k)+1)}\\
&= \sum_{r=0}^{\infty}(-1)^r\sum_{k=0}^{r}\frac{(T-T_0)^{\beta r}}{(1+r)\Gamma(\beta r+1)}\\
&= E_\beta\Big[-\Big(T-T_0\Big)^\beta\Big]\\
&= \left[\frac{n(T)}{n(T_0)}\right]_{ML}\\
&= \Psi_{ML}(T,T_0).
\end{aligned} \tag{3.39}$$

To validate the result, an important step is to find an integro-differential equation able to embed the $'\circ'$ operation and compose directly the time syntagms. Firstly, we need to re-define the $'\circ'$ operation (3.38) as an integral

$$(T-T_1)^{\beta r}\circ(T_1-T_0)^{\beta(n-r)} := \frac{1+\beta n}{1+n}\frac{1}{T-T_0}\int_{T_0}^{T}dT_1\;(T-T_1)^{\beta r}(T_1-T_0)^{\beta(n-r)} \tag{3.40}$$

and then, we replace the new definition (3.40) in the last line of (3.37) so we obtain:

$$\begin{aligned}
&\Psi_{ML}(T,T_1)\circ\Psi_{ML}(T_1,T_0)\\
&= \left[\frac{n(T)}{n(T_1)}\right]_{ML}\circ\left[\frac{n(T_1)}{n(T_0)}\right]_{ML}\\
&= \int_{T_0}^{T}\frac{dT_1}{T-T_0}\sum_{n=0}^{\infty}\frac{(-1)^n(1+\beta n)}{(1+n)}\sum_{r=0}^{n}\frac{(T-T_1)^{\beta r}(T_1-T_0)^{\beta(n-r)}}{\Gamma(1+\beta r)\Gamma(1+\beta n-\beta r)}.
\end{aligned} \tag{3.41}$$

Following the methodology we illustrated in Subsection 3.2.1 and in details in [78], the composition rule needs to point out the relaxation syntagms.
The relaxation syntagms cannot emerge for the presence not only of the term $\frac{1}{1+n}$, as in the Debye case, but also for the factor $(1+\beta n)$. The first term can be absorbed introducing the dummy variable u ranging in $[0,1]$, therefore $\frac{1}{n+1}$ is replaced by the integral $\int_0^1 du\; u^n$.
Unfortunately, the second obstacle — the presence of the factor $(1+\beta n)$ — is more difficult to fix, and we need more laborious and technical mathematical steps that we collected in the appendix of [78].
Once developed the required procedure, we find the following expression for the com-

position rule, where the two relaxation syntagms in terms of the one-parameter Mittag-Leffler function have been explicitly shown:

$$\frac{d}{dT}\int_{T_0}^{T} dT_1 \int_0^1 du \left[\frac{n(u\,T)}{n(u\,T_1)}\right]_{ML} \cdot \left[\frac{n(u\,T_1)}{n(u\,T_0)}\right]_{ML} = \left[\frac{n(T)}{n(T_0)}\right]_{ML}. \tag{3.42}$$

Here, the symbol $'\ \cdot\ '$ is the usual multiplication. The composition rule rewritten as (3.42) improves its value since it makes evident its nature as an integral-differential evolution equation. As $\beta = 1$, the composition rule (3.42) for the one-parameter Mittag-Leffler function reduces to the Debye composition rule defined in (3.17).

3.4 The general composition rules for anomalous relaxation functions

In this Section, we want to show how the composition rule generated from the Reynolds-Leibnitz theorem can address elegantly the problem of composing anomalous (or non-Debye) relaxation syntagms. The procedure to follow is described in Section 3.2.1 and in [116]. We will consider three examples of application of this method to anomalous relaxation functions: the three-parameter Mittag-Leffler function in Subsection 3.4.1, the one-parameter Mittag-Leffler function in 3.4.2 and the (upper) incomplete Gamma function in Subsection 3.4.3. In this last Subsection and in [116], we will also find out the composition rule for the pulse response function of the (upper) incomplete Gamma function as a derivative of the general composition rule. The result is an important achievement since it shows not only how the general composition rule generates a *daughter* composition rule via differentiation valid for the pulse response function, but also how the theory of semigroup operators is the *natural habitat* for the general composition rule. This fact supports our idea that the composition rule is a *physical* manifestation of the semigroup property.

3.4.1 The case of the relaxation function based on the three-parameter Mittag-Leffler function

As shown in Section 3.3, the composition rule for the one-parameter Mittag-Leffler function has required substantial efforts to be obtained, and the problem is intensifying as the number of the parameters increases. In this Subsection, it is possible to have a direct evidence of the convenience of this method to define the composition of the relaxation syntagms. Among the possible generalizations of the one-parameter Mittag-Leffler function, we consider the three-parameter Mittag-Leffler function known in literature as the Prabhakar function [169]:

$$E^{\alpha}_{\beta,\gamma}(z) := \sum_{k=0}^{\infty} \frac{(\alpha)_k z^k}{k!\Gamma(\beta k+\gamma)}, \quad \alpha,\beta,\gamma \in \mathbb{C}, \quad \Re(\alpha)>0, \quad \Re(\beta)>0, \quad \Re(\gamma)>0, \tag{3.43}$$

where $(\alpha)_n := \frac{\Gamma(\alpha+n)}{\Gamma(n)}$ is the Pochammer symbol [1] and τ is the relaxation time.

Fixing the parameter γ as equal to $\alpha\beta+1$ and assuming $z = -\left(\frac{t}{\tau}\right)^{\beta}$, $\alpha \leq 1$ (or $\alpha\beta \leq 1$ as proposed in [88] and highlighted in [66]) and $\beta > 0$, the three-parameter Mittag-Leffler function reads

$$E^{\alpha}_{\beta,\beta\alpha+1}\Big(-\Big(\frac{t}{\tau}\Big)^{\beta}\Big) = \frac{1}{\Gamma(\alpha)}\sum_{k=0}^{\infty}\frac{(-1)^k\ \Gamma(\alpha+k)t^{\beta k}}{k!\Gamma(\beta k+\alpha\beta)\tau^{\beta k}}. \tag{3.44}$$

The interest in this special function is due to the fact that it is involved in the definition of the following relaxation function

$$\Psi_{3ML}(t) := 1 - \Big(\frac{t}{\tau}\Big)^{\beta\alpha} E^{\alpha}_{\beta,\beta\alpha+1}\Big(-\Big(\frac{t}{\tau}\Big)^{\beta}\Big), \tag{3.45}$$

whose Fourier transform $\mathcal{F}$ on the real positive line (or the Laplace transform $\mathcal{L}$) coincides with the Havriliak-Negami dispersion model [66]:

$$\hat{\varepsilon}(\omega) = \frac{1}{[1+(i\omega\tau)^{\beta}]^{\alpha}}, \tag{3.46}$$

where $\alpha \leq 1$ (or $\alpha\beta \leq 1$), $\beta > 0$, τ is the relaxation time and ω denotes the frequency. Replacing $\frac{t}{\tau}$ with the dimensionless time T in (3.45), we define the relaxation $\Psi_{3ML}(T, T_0)$ in $[T_0, T]$

$$\Psi_{3ML}(T,T_0) = \Big[\frac{n(T)}{n(T_0)}\Big]_{3ML} = 1 - (T-T_0)^{\beta\alpha}\ E^{\alpha}_{\beta,\beta\alpha+1}\Big(-(T-T_0)^{\beta}\Big)$$

and its relaxation syntagms corresponding to the subsets $[T_0, T_1]$ and $[T_1, T]$, respectively labeled as $\Psi(T_1, T_0)$ and $\Psi(T, T_1)$

$$\begin{aligned}\Psi_{3ML}(T,T_1) &= \Big[\frac{n(T)}{n(T_1)}\Big]_{3ML} = 1 - (T-T_1)^{\beta\alpha}\ E^{\alpha}_{\beta,\beta\alpha+1}\Big(-(T-T_1)^{\beta}\Big)\\ \Psi_{3ML}(T_1,T_0) &= \Big[\frac{n(T_1)}{n(T_0)}\Big]_{3ML} = 1 - (T_1-T_0)^{\beta\alpha}\ E^{\alpha}_{\beta,\beta\alpha+1}\Big(-(T-T_1)^{\beta}\Big).\end{aligned}$$

Once introduced the relaxation syntagms and the relaxation function in the whole interval $[T_0, T]$, the general composition rule (3.29) (or (3.30)) reads

$$\begin{aligned}
&\Big[D_1, {}_{T_0}D^{-1}_{T,2}\Big]\Psi_{3ML}(T,T_1)\cdot\Psi_{3ML}(T_1,T_0)\\
&= \Big(D_1\ {}_{T_0}D^{-1}_{T,2} - {}_{T_0}D^{-1}_{T,2}\ D_1\Big)\Psi_{3ML}(T,T_1)\cdot\Psi_{3ML}(T_1,T_0)\\
&= \Big(D_1\ {}_{T_0}D^{-1}_{T,2} - {}_{T_0}D^{-1}_{T,2}\ D_1\Big)\Big[\frac{n(T)}{n(T_1)}\Big]_{3ML}\cdot\Big[\frac{n(T_1)}{n(T_0)}\Big]_{3ML}\\
&= \Big(\frac{d}{dT}\int_{T_0}^{T} dT_1 - \int_{T_0}^{T} dT_1\ \frac{d}{dT}\Big)\Bigg[\Big(1-(T-T_1)^{\beta\alpha}\ E^{\alpha}_{\beta,\beta\alpha+1}\Big(-\Big(T-T_1\Big)^{\beta}\Big)\Big)\\
&\qquad\qquad\Big(1-(T_1-T_0)^{\beta\alpha}\ E^{\alpha}_{\beta,\beta\alpha+1}\Big(-\Big(T_1-T_0\Big)^{\beta}\Big)\Big)\Bigg]\\
&= E^{\alpha}_{\beta,\beta\alpha}\Big[-\Big(T-T_0\Big)^{\beta}\Big]\\
&= \Big[\frac{n(T)}{n(T_0)}\Big]_{3ML}\\
&= \Psi_{3ML}(T,T_0).
\end{aligned}\tag{3.47}$$

3.4.2 The case of the one-parameter Mittag-Leffler function

In this Subsection, we want to point out one of the special cases of the relaxation function $\Psi_{3ML}(T)$ when α is set equal to 1 in (3.45): the one-parameter Mittag-Leffler function. We have therefore a direct comparison with the procedure shown in Section 3.3, and it is possible to have a fair idea of how this method overcomes the difficulties keeping alive a clear physical meaning as explained in Section 3.2.2.
Fixing $\alpha = 1$, the relaxation function $\Psi_{3ML}(T)$ in (3.45) reduces to $\Psi_{ML}(T)$ as shown below

$$\begin{aligned}
\Psi_{3ML}(T)|_{\alpha=1} &= 1 - T^{\beta}E_{\beta,\beta+1}(-T^{\beta})\\
&= E_{\beta}(-T^{\beta})\\
&= \Psi_{ML}(T).
\end{aligned}\tag{3.48}$$

Having got this far, we resort to the relaxation syntagms corresponding to $\Psi_{ML}(T)$ defined in (3.35) so that we can directly apply the general composition rule (3.29) to the product of the relaxation syntagms $\Psi_{ML}(T,T_1)\cdot\Psi_{ML}(T_1,T_0)$ in order to compose them into the total relaxation syntagm $\Psi(T,T_0)$:

$$\begin{aligned}
&\Big[D_1, {}_{T_0}D_{T,2}^{-1}\Big]\Psi_{3ML}(T,T_1)\cdot\Psi_{ML}(T_1,T_0)\\
&=\Big(D_1\ {}_{T_0}D_{T,2}^{-1} - {}_{T_0}D_{T,2}^{-1}\ D_1\Big)\Psi_{ML}(T,T_1)\cdot\Psi_{ML}(T_1,T_0)\\
&=\Big(D_1\ {}_{T_0}D_{T,2}^{-1} - {}_{T_0}D_{T,2}^{-1}\ D_1\Big)\left[\frac{n(T)}{n(T_1)}\right]_{ML}\cdot\left[\frac{n(T_1)}{n(T_0)}\right]_{ML}\\
&=\Big(\frac{d}{dT}\int_{T_0}^{T}dT_1-\int_{T_0}^{T}dT_1\ \frac{d}{dT}\Big)\Big[E_\beta\Big(-\Big(T-T_1\Big)^\beta\Big)\ E_\beta\Big(-\Big(T_1-T_0\Big)^\beta\Big)\Big] \qquad (3.49)\\
&=E_\beta\Big[-\Big(T-T_0\Big)^\beta\Big]\\
&=\left[\frac{n(T)}{n(T_0)}\right]_{ML}\\
&=\Psi_{ML}(T,T_0).
\end{aligned}$$

3.4.3 The case of the (upper) incomplete Gamma function: in the laboratory frame and in the material frame

Without any loss of generality, the issue has been address also for the (upper) incomplete Gamma relaxation function

$$\Psi_G(t)=\frac{\Gamma\Big(\alpha,\frac{t}{\tau}\Big)}{\Gamma(\alpha)}:=\frac{1}{\Gamma(\alpha)}\int_t^\infty d\xi\ e^{-\frac{\xi}{\tau}}\frac{\xi^{\alpha-1}}{\tau^\alpha}, \qquad (3.50)$$

where $\alpha\le 1$ is a real parameter, $\Gamma(\cdot)$ is the well-known Gamma function [1].
This special function describes the relaxation corresponding to the Cole-Davidson dispersion model [66]:

$$\hat{\varepsilon}(\omega)=\frac{1}{(1+i\omega\tau)^\alpha}, \qquad (3.51)$$

where $\alpha\le 1$ and ω denotes the frequency. The calculation of the composition can be simplified introducing the dimensionless time variable $T=\frac{t}{\tau}$. Consequently, the (upper) incomplete Gamma function reads

$$\Psi_G(T)=\frac{\Gamma\Big(\alpha,T\Big)}{\Gamma(\alpha)}:=\frac{1}{\Gamma(\alpha)}\int_T^\infty d\xi\ e^{-\xi}\xi^{\alpha-1}, \qquad (3.52)$$

In order to find the composition rule for the (upper) incomplete Gamma function (3.52), we need to define this relaxation function in the time interval $[T_0,T]$ and in its respective time syntagms $[T_0, T_1]$ and $[T_1, T]$:

$$\begin{aligned}
\Psi_G(T,T_0) &= \left[\frac{n(T)}{n(T_0)}\right]_G = \frac{\Gamma\Big(\alpha, T-T_0\Big)}{\Gamma(\alpha)},\\
\Psi_G(T,T_1) &= \left[\frac{n(T)}{n(T_1)}\right]_G = \frac{\Gamma\Big(\alpha, T-T_1\Big)}{\Gamma(\alpha)},\\
\Psi_G(T_1,T_0) &= \left[\frac{n(T_1)}{n(T_0)}\right]_G = \frac{\Gamma\Big(\alpha, T_1-T_0\Big)}{\Gamma(\alpha)}.
\end{aligned} \tag{3.53}$$

We compose the relaxation syntagms $\Psi(T_1,T_0)$ in $[T_0,T_1]$ and $\Psi(T,T_1)$ in $[T_1,T]$ into the relaxation $\Psi(T,T_0)$ in the whole time interval $[T_0,T]$. According to these time intervals and their corresponding relaxation functions, the composition rule reads

$$\begin{aligned}
\Psi_G(T,T_0)\circ\Psi_G(T_1,T_0) &= \left[\frac{n(T)}{n(T_1)}\right]_G \circ \left[\frac{n(T_1)}{n(T_0)}\right]_G\\
&= \frac{\Gamma\Big(\alpha, T-T_1\Big)}{\Gamma(\alpha)} \circ \frac{\Gamma\Big(\alpha, T_1-T_0\Big)}{\Gamma(\alpha)}\\
&= \left[\frac{n(T)}{n(T_0)}\right]_G = \Psi_G(T,T_0).
\end{aligned} \tag{3.54}$$

As described for the one-parameter Mittag-Leffler function and for the three-parameter Mittag-Leffler function, the multiplication is not the right candidate to be the $'\circ'$ operation good at satisfying the composition rule (3.55). We therefore resort once again to the approach based on the Reynolds-Leibnitz theorem, and we obtain:

$$\begin{aligned}
&\Big[D_1, {}_{T_0}D^{-1}_{T,2}\Big]\Psi_G(T,T_1)\cdot\Psi_G(T_1,T_0)\\
&= \Big(D_1\ {}_{T_0}D^{-1}_{T,2} - {}_{T_0}D^{-1}_{T,2}\ D_1\Big)\Psi_G(T,T_1)\cdot\Psi_G(T_1,T_0)\\
&= \Big(D_1\ {}_{T_0}D^{-1}_{T,2} - {}_{T_0}D^{-1}_{T,2}\ D_1\Big)\left[\frac{n(T)}{n(T_1)}\right]_G\cdot\left[\frac{n(T_1)}{n(T_0)}\right]_G\\
&= \Big(\frac{d}{dT}\int_{T_0}^{T} dT_1 + \int_{T_0}^{T} dT_1\frac{d}{dT}\Big)\frac{\Gamma(\alpha,T-T_1)}{\Gamma(\alpha)}\frac{\Gamma(\alpha,T_1-T_0)}{\Gamma(\alpha)}\\
&= \frac{\Gamma(\alpha,T-T_0)}{\Gamma(\alpha)}\\
&= \left[\frac{n(T)}{n(T_0)}\right]_G\\
&= \Psi_G(T,T_0).
\end{aligned} \tag{3.55}$$

The relaxation function $\Psi_G(T,T_0)$ evaluated on the total time range $[T_0,T]$ is interpreted as the net flux according to the Reynolds-Leibniz theorem.

The semigroup property for the (upper) incomplete Gamma function (3.55) has been verified, and the result receives a preliminary validation, considering that for $\alpha = 1$, the composition rule reduces to the one obtained for the Debye relaxation.

A further validation arises when the composition rule is recast in its integral form as follows

$$\int_T^\infty dx \frac{d}{dT} \int_{T_0}^T dT_1 \frac{e^{-(x-T_1)}(x-T_1)^{\alpha-1}}{\Gamma(\alpha)} \frac{\Gamma(\alpha, T_1-T_0)}{\Gamma(\alpha)} = \frac{\Gamma(\alpha, T-T_0)}{\Gamma(\alpha)}. \tag{3.56}$$

The above expression is a convenient starting point for defining the differential form of the composition rule valid for the pulse response function $\phi_G(T) = -\frac{d\Psi_G(T)}{dT}$. Deriving both sides of (3.56) with respect to T, we obtain

$$\frac{d}{dT} \int_{T_0}^T dT_1 \frac{e^{-(T-T_1)}(T-T_1)^{\alpha-1}}{\Gamma(\alpha)} \frac{\Gamma(\alpha, T_1-T_0)}{\Gamma(\alpha)} = \frac{e^{-(T-T_0)}(T-T_0)^{\alpha}}{\Gamma(\alpha)}. \tag{3.57}$$

The above result (3.57) is exactly the Gamma semigroup with the parameter α. Here, the semigroup operator acts on a function that in this case coincides with the (upper) incomplete Gamma function $\frac{\Gamma[\alpha, T_1-T_0]}{\Gamma(\alpha)}$. It is therefore possible to define the semigroup Gamma operator exploiting the notation used in [102]:

$$W_1(\alpha)\phi_G(T-T_0) = \int_{T_0}^T dT_1 \frac{e^{-(T-T_1)}(T-T_1)^{\alpha-1}}{\Gamma(\alpha)} \phi_G(T_1-T_0). \tag{3.58}$$

At this point, we obtain the differential composition rule for the pulse response function perfectly framed in the context of semigroups theory:

$$\begin{aligned}
&\frac{d}{dT} \int_{T_0}^T dT_1 \frac{e^{-(T-T_1)}(T-T_1)^{\alpha-1}}{\Gamma(\alpha)} \frac{\Gamma(\alpha, T_1-T_0)}{\Gamma(\alpha)} \\
&= \int_{T_0}^T dT_1 \frac{e^{-(T-T_1)}(T-T_1)^{\alpha-1}}{\Gamma(\alpha)} \frac{e^{-(T_1-T_0)}(T_1-T_0)^{\alpha-1}}{\Gamma(\alpha)} \\
&= W_1(\alpha)\phi_G(T-T_0) \\
&= \frac{e^{-(T-T_0)}(T-T_0)^{\alpha-1}}{\Gamma(\alpha)}.
\end{aligned} \tag{3.59}$$

This additional result gives a further validation to the approach, and it brings out its physical meaning not only for the relaxation functions but also for the pulse response function.

As we have shown, the general composition rule is exactly the same for all the relaxation functions considered, and it can be easily extended also to other relaxation functions provided that are analytical and normalized in zero, as for example the Jurlewicz-Weron-Stanislavsky relaxation function. This result is gaining in value if we consider the comment in [66] where the evolution equation of $\Psi_{3ML}(t)$ in terms of the Caputo derivative for $\alpha = 1$ is slightly different from the operator used for defining $\Psi_{ML}(t)$. In other words, the evolution equation of the most general case does not coincide with the one found for its special case when we fix $\alpha = 1$.

Mathematically, the issue can be figure out comparing

$$ {}_0^C D_t^{\beta} \Psi_{ML}(t) = -\frac{1}{\tau^{\beta}} \Psi_{ML}(t), \tag{3.60}$$

with

$$ {}^C\Big({}_0D_t^{\beta} + \frac{1}{\tau^{\beta}}\Big) \Psi_{ML}(t) = -\frac{1}{\tau^{\beta}} \tag{3.61}$$

that is the special case of the following evolution equation when $\alpha = 1$:

$$\begin{aligned} {}^C\Big({}_0D_t^{\beta} + \frac{1}{\tau^{\beta}}\Big)^{\alpha} \Psi_{3ML}(t) &= \int_0^t du\ (t-\xi)^{-\alpha\beta} E^{-\alpha}_{\beta,1-\alpha\beta}\Bigg(-\frac{(t-\xi)^{\beta}}{\tau^{\beta}}\Bigg) \Psi'_{3ML}(\xi) \\ &= -\frac{1}{\tau^{\alpha\beta}}, \end{aligned} \tag{3.62}$$

where the action of the operator ${}^C\Big({}_0D_t^{\beta} + \frac{1}{\tau^{\beta}}\Big)^{\alpha}$ is defined in formula (B.23) in [66]. Here below, we remind the definition of the Caputo fractional derivative:

$$ {}^C D_T^{\beta} f(T) = \frac{1}{\Gamma(1-\beta)} \int_0^T dY\ \frac{1}{(T-Y)^{\beta}} \frac{d}{dY} f(Y).$$

As explained in the appendix of [66], the two operators (3.61) and (3.60) are different, but it is possible to consider the first evolution equation as a special case of (3.60) assuming a Caputo regularization that affects only the fractional derivative and not the identity operator as well.

3.5 Material time: the counterpart of material frequency in anomalous dispersion models

The idea to consider the relaxation function as an intensive quantity and the formulation of a general composition rule in terms of a commutator (3.29) (or (3.30)) suggests once again that the anomalous behaviours are disturbing effects linked to the choice of the frame. In other words, the anomalies that we observe are due to a sort of a *lens* that distorts, compresses, and stretches the laboratory frame. The presence of the anomalies causes the system to be too complicated to be clearly understood. It is therefore vital to figure out how this lens works so that the dynamics can emerge.

Our strategy is to recognize that there are two sources of anomalous behaviours. The first source is rooted in the material time and in its frequency counterpart. We have encountered this first type in Chapter 2 and in [123]. We found that the KWW relaxation function stands out when we move from the material frame to the laboratory frame if their clocks do not mark the time in the same way. The clock set in the material frame can accelerate or decelerate, and it is a distinctive feature of the material medium under relaxation. In this case the dynamics of the anomalous behaviour has been encoded in the material medium as a damped harmonic oscillator and its effects are modelled by the material time that stretches and compresses the laboratory frame. In the ideal Debye case, the clocks of the two frames mark the time in the same way and the relaxation function is a *pure* exponential function.

The other source emerges for the presence of a *compensating force*, an internal force that has been generated when the external field or the external force acts on the system. In that event, the material frame has been distorted.

In this Section, we focus our attention on the first type of source that is linked to the material time, since we need to define its frequency counterpart: the *material frequency*. This step is an important achievement since it *restores the symmetry* between the frequency and the time domain, both of them described by nonlinear variables. Let us explain what we mean with restoring the symmetry and its importance in the description of anomalous behaviours. All anomalous (dispersion and relaxation) models have the Debye model as a limit case, therefore we want to gather the result obtained up to now in order to show how the correct calibration of the frame allows not only to restore the Debye model from an anomalous point of view, but it also explains the experimental recurrences of the KWW function and the Havrialiak-Negami models.

As highlighted in Chapter 1, Havriliak and Negami empirically introduced a nonlinear frequency in order to generalize the Cole-Davidson dispersion model that is known in literature as the Havriliak-Negami dispersion model [66]. In Chapter 2 and in [123], we introduced the material time $t^* = t^\beta$ (or the dimensionless material time $T^* = \frac{t^\beta}{\tau^\beta}$) that is a nonlinear time variable, pointing out its key role in the physical interpretation of experimental data in photoluminescent relaxation processes. Accordingly, we replace the time variable with the material time into the (upper) incomplete Gamma relaxation (3.54) as it corresponds to the Cole-Davidson (CD) dispersion model whose expression is

$$\hat{\varepsilon}_{CD}(\omega) = \frac{\varepsilon_r(\omega) - \varepsilon_\infty}{\Delta\varepsilon} = \frac{1}{[1 + (i\omega\tau)]^\alpha},$$

and we get a sort of modified (upper) incomplete Gamma function:

$$\Psi_G(T^*) = \frac{\Gamma\Big[\alpha, T^*\Big]}{\Gamma(\alpha)}. \tag{3.63}$$

What makes this modified version of the (upper) incomplete Gamma function interesting, is the fact that for $\alpha = 1$, we can recover the KWW function! By keeping the α parameter equals to 1 also in the Havriliak-Negami (HN) dispersion model whose expression is

$$\hat{\varepsilon}_{HN}(\omega) = \frac{\varepsilon_r(\omega) - \varepsilon_\infty}{\Delta\varepsilon} = \frac{1}{[1 + (i\omega\tau)^\beta]^\alpha},$$

we obtain the Cole-Cole (CC) dispersion model:

$$\hat{\varepsilon}_{CC}(\omega) = \frac{\varepsilon_r(\omega) - \varepsilon_\infty}{\Delta\varepsilon} = \frac{1}{1 + (i\omega\tau)^\beta}.$$

Gathering all these considerations, it is licit to assume that there should be a link between the Havriliak-Negami dispersion model and the KWW relaxation function. Last but not least, as for the other relaxation functions presented in Section 3.4, the modified (upper) incomplete Gamma function (3.63) obviously fulfils the general composition rule. Consequently even the KWW function obeys to the general composition rule since it is a special case of the former.

However, despite we followed what Havriliak and Negami did in the frequency regime, the relaxation function obtained (i.e. the generalized (upper) incomplete Gamma function) is not the Fourier-Laplace counterpart of the Havriliak-Negami dispersion model. *The symmetry is broken.* However, a broken symmetry is always a fundamental source of information, and therefore it is essential to understand how to fix it. During the dispersion or the relaxation, the system in the laboratory is below our lens and consequently, it manifests the observed anomalous behaviours. By introducing nonlinear variables it is possible to extract the anomalies due to the stretching or the compressing of the frame favouring the emergence of the physical meaning and fixing the value of the parameter α is possible to control the compensating force.

For this reason, it is essential to introduce a transform that keeps in consideration the presence of the *lens* and therefore, it is possible to *calibrate* correctly the problem.

In this Section, we consequently want to close the circle: the material time should have a counterpart in the frequency regime that it is called from now on *material frequency* $\omega = \omega^\beta$ (or the dimensionless material frequency $\Omega^* = \omega^\beta \tau^\beta$).

The idea is to introduce a novel transform that modifies the Fourier transform in order to relate the material frequency space to the material time space. According to this point of view, it is possible to justify the empirical modification introduced by Cole-Cole and then by Havriliak and Negami as a natural consequence of the material frame. Together with the results illustrated in Chapter 2 we formalize the material frame and its role in the analysis of relaxation processes.

This novel transform named *material Λ transform* explains experimental evidences of the recurrence of the KWW function in the time domain and the Cole-Cole dispersion (or the Havriliak-Negami dispersion) in the frequency regime.

In this way we finish restoring the symmetry between the dynamics in the frequency and in the time domain, as it will be highlighted at the end of this Chapter.

The material Λ transform can be defined starting from the Fourier transform and replacing the time and frequency variables with the non-linear variables called material frequency and material time. Moreover, we need to introduce an operator that describes how the frame has been twisted. In fact the anomalous behaviour that we observe experimentally is not only related to the compression or stretching of the timescale but also to the rotation of the frame itself.

This second requirement can be realized resorting to the exponential operator method. We introduce a similarity transformation described by an operator named complex-scaling operator $\hat{S}_{T,\theta}$:

$$\hat{S}_{T,\theta} := e^{i\theta} e^{i\theta T \frac{\partial}{\partial T}}, \tag{3.64}$$

where the rotation angle θ is a real parameter and the variable of integration in the material Λ transform integral is $T \in \mathbb{R}$ —in our case its domain is restricted to the real positive line, i.e. $\mathbb{R}^+$ since T denotes the normalized time variable.

The factor $e^{i\theta}$ can be considered as a unit vector which describes a *rotated* line by an angle θ with respect to the real line ($\theta = 0$). In other words, the axis of the measurement is rotated through the angle θ.

The action of the operator $\hat{S}_{T,\theta}$ on the function $f(T)$ is shown here:

$$\hat{S}_{T,\theta} f(T) = e^{i\theta} f(Te^{i\theta}) = f_\theta(T). \tag{3.65}$$

Once defined the dimensionless material variables

$$\Omega^* = \omega^* \tau^* = \omega^\beta \tau^\beta$$

and

$$T^* = \frac{t^*}{\tau^*} = \frac{t^\beta}{\tau^\beta}$$

and using the definition of the complex-scaling operator $\hat{S}_{T^*,\theta}$, we can introduce the material Λ transform

$$\Lambda_{T^*,\theta}[f(T^*)](\Omega^*) = \int_0^\infty dT^* \; e^{-iT^*\Omega^*} f_\theta(T^*). \tag{3.66}$$

This transform acts on the system that not only experienced a compression or stretching of its scale because of the presence of the material variables, but also it has been twisted as a direct result of the action of the complex-scaling operator on the integrand function. The definition of the material transform (3.66) leads to the following property:

$$\begin{aligned}
\Lambda_{T^*,\theta}[f_\theta(T^*)](\Omega^*) &= \int_0^\infty dT^* \; e^{-iT^*\Omega^*} f_\theta(T^*) \\
&= \int_0^\infty dT^* \; e^{-iT^*\Omega^*} e^{i\theta} f(e^{i\theta} T^*) \\
&= e^{i\theta} \hat{S}_{\Omega^*,-\theta} \int_0^\infty dT^* \; e^{-iT^*\Omega^*} f(T^*) \\
&= \hat{F}(e^{-i\theta}\Omega^*).
\end{aligned} \tag{3.67}$$

A formal equivalence with the scaling property of the Fourier transform clearly emerges. In Fig. 3.1, the action of the complex scaling operator on the functions involved in the transforms has been schematically shown. To better understand the role of the complex-scaling operator, it is possible to consider Fig. 3.2 where the angle of the Cole-Cole dispersion model has been shown with respect to the Debye one.

3.5.1 The material Λ transform and the hidden relationship between KWW and HN

The aim of this Subsection is to show explicitly the link between the KWW relaxation function and the Havriliak-Negami dispersion model by using the material Λ transform (3.66). As explained in Section 3.5, the operator $\hat{S}_{T,\theta}$ acts on the integrand function of the material transform and the imaginary unit i gains an exponent that depends on the value of the θ angle. In other words, the power of the imaginary unit i is related to how twisted is the reference frame. Firstly, we need to define the pulse response

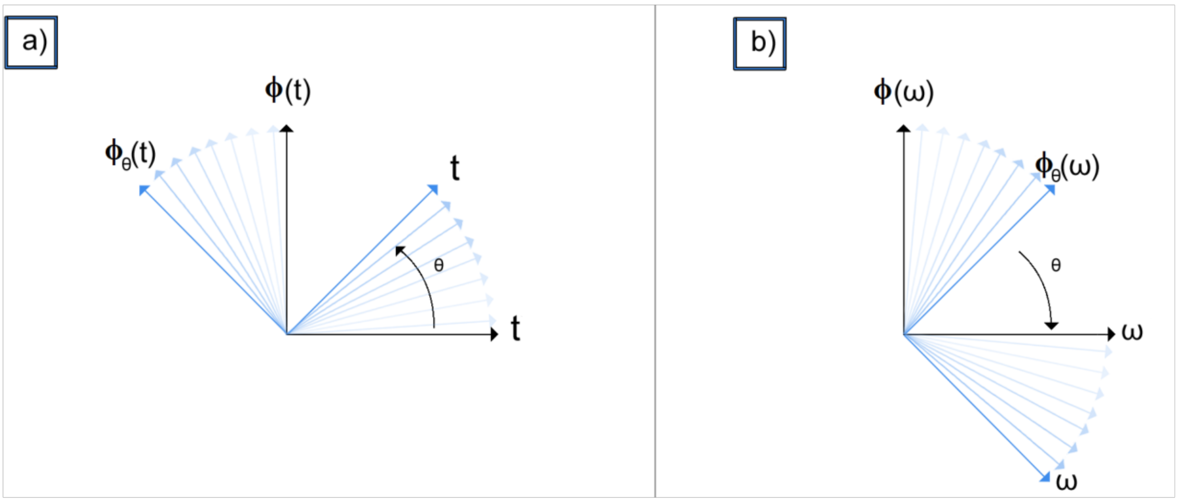

Figure 3.1: A graphical representation of the action of the complex-scaling operator in the Λ transform. As expected, the complex-scaling property shows a behaviour similar to the known scaling property of the Laplace-Fourier transform: a complex-scaling rotation in the time domain implies another one in the opposite direction in the frequency domain.

function ϕ_G that will be transformed in the material frequency space, that is

$$\begin{aligned} \phi_G(T^*) &= -\frac{d}{dT^*}\Psi(T^*) \\ &= -\frac{d}{dT^*}\frac{\Gamma[\alpha, T^*]}{\Gamma(\alpha)} \\ &= e^{-\frac{t^*}{\tau^*}}\frac{t^{*(\alpha-1)}}{\Gamma(\alpha)\tau^*} \end{aligned} \tag{3.68}$$

and then, the action of the material Λ transform on this pulse response function ϕ_G gives the corresponding normalized dielectric permittivity $\hat{\varepsilon}(\Omega^*)$ as shown here below

$$\begin{aligned} \Lambda\Big[\phi_{G,\theta}(T^*)\Big](\Omega^*) &= \int_0^\infty dT^*\ e^{-iT^*\Omega^*}\phi_{G,\theta}(T^*) \\ &= \int_0^\infty dT^*\ e^{-iT^*\Omega^*}\hat{S}_{T^*,\theta}\ \phi_G(T^*) \\ &= \int_0^\infty dT^*\ \frac{e^{i\theta}(e^{i\theta}T^*)^{\alpha-1}e^{-T^*e^{i\theta}}}{\Gamma(\alpha)}e^{-iT^*\Omega^*}dT^* \\ &= \frac{1}{[1+ie^{-i\theta}\Omega^*)]^\alpha}. \end{aligned} \tag{3.69}$$

The above novel dispersion-relaxation pair introduced by applying the material Λ transform is the seed for the generation of a very useful dispersion-relaxation pair: the Havriliak-Negami dispersion model and the modified (upper) incomplete Gamma relaxation. Looking at the left-hand side of (3.69), the relaxation function obtained by the material transform is equal to the Havriliak-Negami by a proper selection of the θ

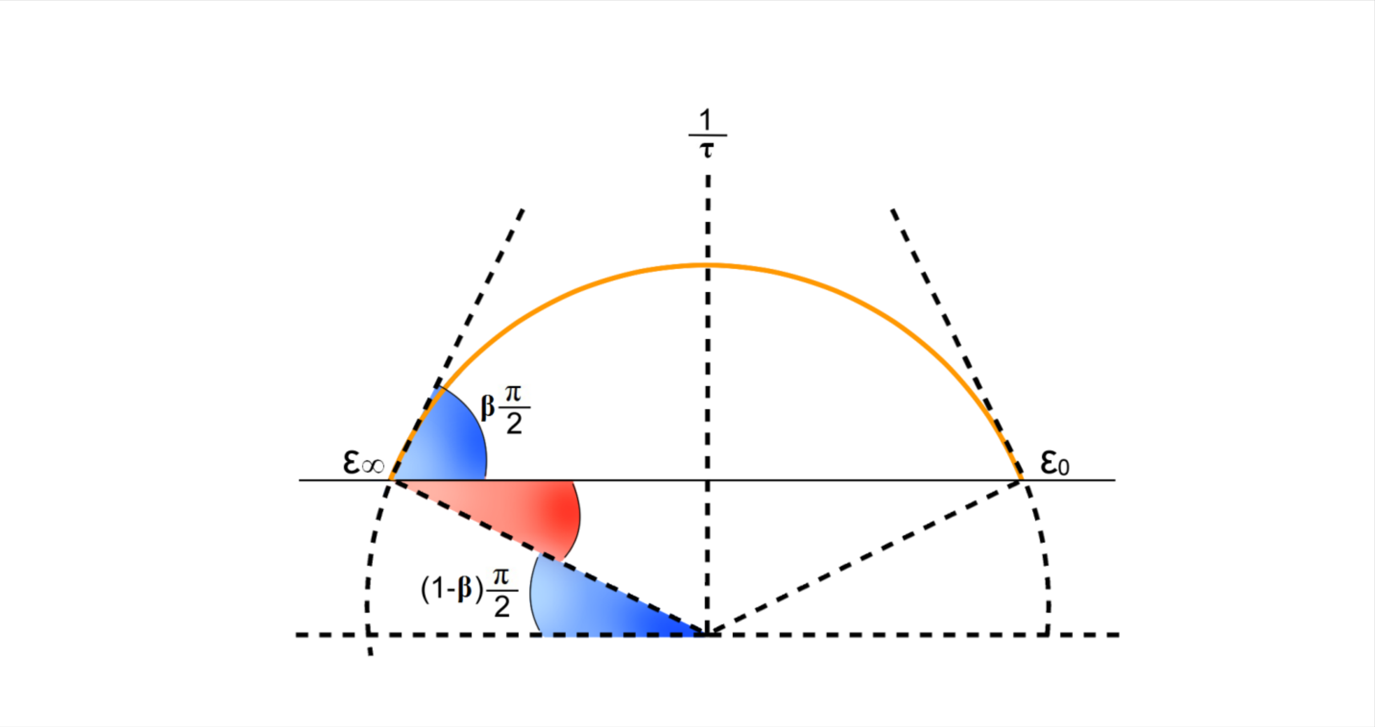

Figure 3.2: Cole-Cole plot for the Cole-Cole dispersion model where the angles with respect to the Debye diagrams have been shown.

parameter.
Fixing the value of the angle θ equals to $\frac{\pi}{2}(1-\beta)$ and restoring the linear dimensionless time variable $\frac{t^*}{\tau^*}=\left(\frac{t}{\tau}\right)^\beta$, the material transform pair (3.69) writes

$$\begin{aligned}\frac{1}{[1+(i\omega\tau)^\beta]^\alpha} &= \int_0^\infty dt^\beta\ e^{-it^\beta\omega^\beta}\,\hat{S}_{t^\beta,\frac{\pi}{2}(1-\beta)}\Big(\frac{(\frac{t^\beta}{\tau^\beta})^{\alpha-1}e^{-\frac{t^\beta}{\tau^\beta}}}{\Gamma(\alpha)\tau^\beta}\Big)\\ &= \int_0^\infty dt^\beta\ e^{-it^\beta\omega^\beta}\,i^{1-\beta}\frac{(i^{1-\beta}\frac{t^\beta}{\tau^\beta})^{\alpha-1}e^{-i^{1-\beta}\frac{t^\beta}{\tau^\beta}}}{\Gamma(\alpha)\tau^\beta}.\end{aligned} \tag{3.70}$$

The integrand of (3.70) is clearly related to the KWW function. The coefficient in front of the exponential $e^{-\frac{t^\beta}{\tau^\beta}}$ can be interpreted in the framework of the diffusive trap model [54, 109, 163]. Assuming that the material is filled with randomly distributed traps, excited molecules diffuse through the material and then fill the traps. The term which multiplies the exponential describes the difficulty of an excited molecule to find a trap when the traps are going to be almost all filled.

The integrand of (3.70) represents the well-known probability density function of the Gamma distribution. It nests both the power and the exponential function generalizing the structure of the power law. It is possible to consider separately the behaviour of the pulse response function in its limiting ranges. Near zero the trend is ruled by a power law, whereas in the long-times region the power law is dampened by the exponential function in agreement with the Jonsher's Universal law [97, 99] that has

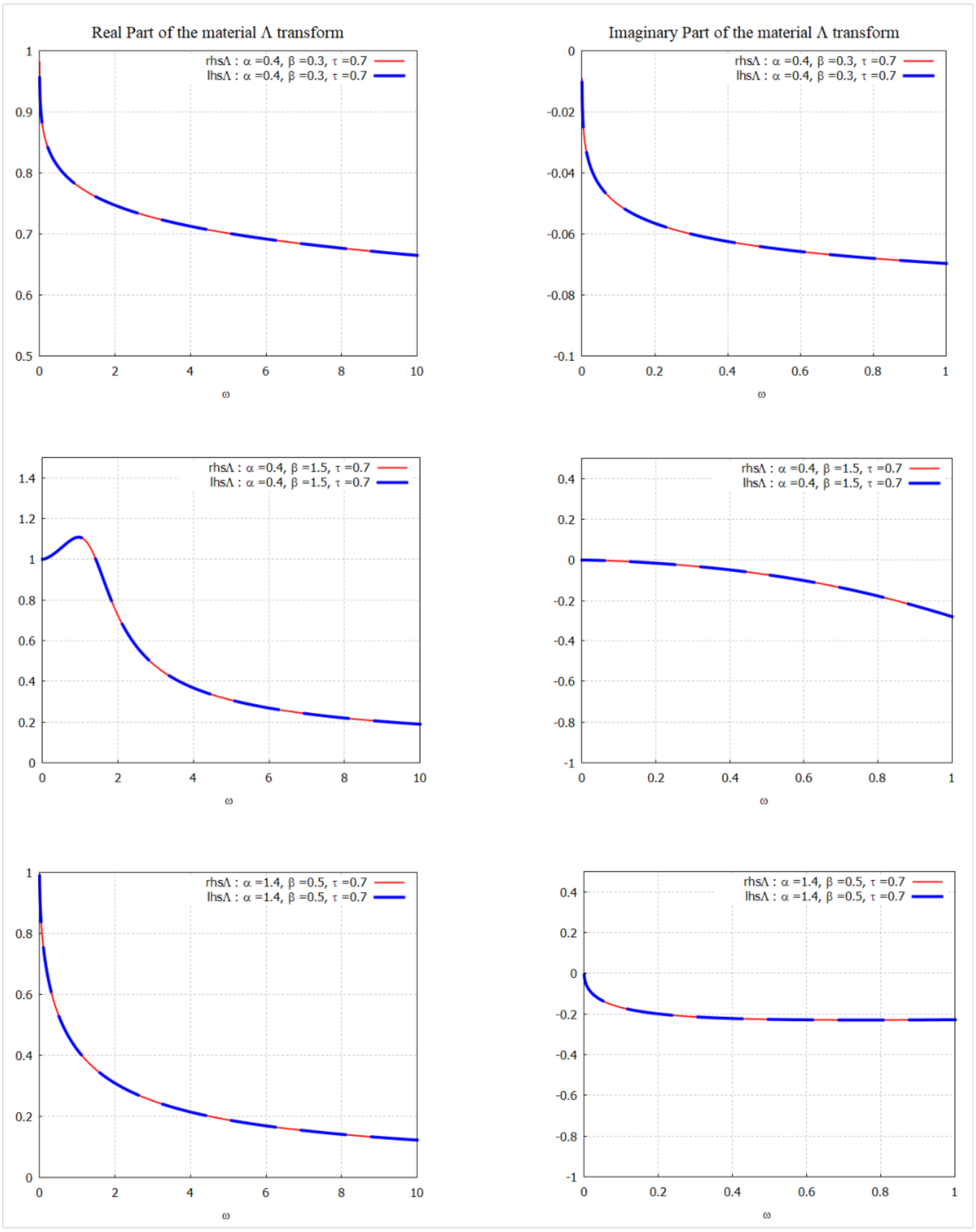

Figure 3.3: Comparison between the real and the imaginary parts of (3.70) for different values of the parameters α and β. In the left-hand side (lhs) we have the Havriliak-Negami function (dashed blue line) and in the right-hand side (rhs) we have the Λ transformed function after the action of the complex-scaling operator (solid red line).

been introduced in Chapter 1.
In Fig. 3.3, the right and the left-hand sides of (3.70) are plotted for different values of the parameters. Fixing the parameters α and β, the pair (3.70) can be reduced to the following special cases.

1. For $\beta > 0$ and $\alpha = 1$, we obtain that the material counterpart of the Cole-Cole dispersion relation is exactly the KWW function

$$\frac{1}{[1+(i\omega\tau)^{\beta}]} = \int_0^{\infty} dt^{\beta}\ e^{-it^{\beta}\omega^{\beta}}\hat{S}_{t^{\beta},(1-\beta)\frac{\pi}{2}}\Big(\frac{e^{-\frac{t^{\beta}}{\tau^{\beta}}}}{\tau^{\beta}}\Big). \tag{3.71}$$

   Among the special cases, the material Λ transform pair that links the KWW function and the Cole-Cole dispersion model is the most relevant one since it gives another novel useful pair able to restore the symmetry with respect to the Debye relaxation and dispersion models [196];

2. for $\beta = 1$ and $\alpha \leq 1$, the material clock and the laboratory clock mark the time in the same way. Consequently, the distortion effect does not stretch or compress the material medium as it results considering the complex-scaling operator that in this case is equal to 1. Here, the general pulse response function (3.68) reduces to the (upper) incomplete Gamma function and then, its material Λ transform results to be the Cole-Davidson dispersion model:

$$\frac{1}{[1+i\omega\tau]^{\alpha}} = \int_0^{\infty} dt\ e^{-it\omega}\Big(\frac{t^{\alpha-1}}{\tau^{\alpha}\Gamma(\alpha)}\Big)e^{-\frac{t}{\tau}}. \tag{3.72}$$

3. Finally for $\beta = 1, \alpha = 1$, the Debye dispersion and relaxation have been recovered again;

$$\frac{1}{[1+i\omega\tau]} = \int_0^{\infty} dt\ \frac{e^{-\frac{t}{\tau}}}{\tau}e^{-it\omega}. \tag{3.73}$$

The introduction of the material transform along with the similarity transformation operator $\hat{S}_{\theta,t}$ gives another evidence in favour of the model proposed: the experimental recurrences of the dispersion models as the Havriliak-Negami and the Cole-Cole are linked to the KWW function.

3.6 Evolution equations for relaxation processes in dynamical systems

The aim of this Section is to collect and frame the results in the context of evolution equations so that it is possible to have a further validation of their correctness.

3.6.1 Evolution equation for the one-parameter Mittag-Leffler relaxation

As we highlighted in [66, 78, 166], the integro-differential equation based on the composition rule for the one-parameter Mittag-Leffler function $E_{\beta}(-T^{\beta})$ is equivalent to the following fractional differential equation:

$${}^{C}D_{T}^{\beta}\Big[\frac{n(T)}{n(T_0)}\Big]_{ML} = -\Big[\frac{n(T)}{n(T_0)}\Big]_{ML}, \tag{3.74}$$

where $\left[\frac{n(T)}{n(T_0)}\right]_{ML} = E_\beta(-(T-T_0)^\beta)$, the fractional derivative is in the Caputo sense [166],

$$ {}^{C}D_T^\beta f(T) = \frac{1}{\Gamma(n-\beta)} \int_0^T dY \; \frac{f^{(n)}(Y)}{(T-Y)^{\beta+1-n}}, \tag{3.75}$$

and $n-1<\beta<n$. In this case, the parameter β runs in $(0,1)$ and therefore $n=1$ and the above definition of the fractional Caputo derivative is

$$ {}^{C}D_T^\beta f(T) = \frac{1}{\Gamma(1-\beta)} \int_0^T dY \; \frac{1}{(T-Y)^\beta} \frac{d}{dY} f(Y). \tag{3.76}$$

In other words, the Mittag-Leffler function is eigenfunction for the fractional Caputo derivative operator.
By replacing the Caputo derivative (3.76) with the Riemann-Liouville derivative [166]

$$ {}^{RL}D_T^\beta f(T) = \frac{1}{\Gamma(1-\beta)} \frac{d}{dT} \int_0^T dY \;\; (T-Y)^{\beta-1} f(Y), \tag{3.77}$$

we end up to

$$ {}^{RL}D_T^\beta \Big[\frac{n(T)}{n(T_0)}\Big]_{ML} = -\Big[\frac{n(T)}{n(T_0)}\Big]_{ML} + \frac{T^{-\beta}}{\Gamma(1-\beta)}. \tag{3.78}$$

Although the relaxation and diffusion processes describe very different physical situations and the functions depend respectively on one or two variables, the above equation (3.78) is similar to the well-known fractional Fokker-Planck equation

$$ {}^{RL}D_T^\beta F_\beta(x,t) = \hat{L}_{FP} F_\beta(x,t) + \frac{t^{-\beta}}{\Gamma(1-\beta)} F_\beta(x,0). \tag{3.79}$$

This resemblance is more evident if the Fokker-Planck operator $\hat{L}_{FP}$ is set equal to -1 and the initial condition is $F_\beta(x,0)=1$ [75, 78]. However, we should point out that the two equations describe two different physical processes (i.e. anomalous relaxation and anomalous diffusion respectively) and therefore the consideration about the similarity is concerning the mathematical tools and methodologies that allows us to solve the equations. The solution of the fractional Fokker-Planck equation can be obtained in more than one way [19, 75, 77]. The most common procedure is to apply the Fourier-Laplace transform as shown in [107, 166], so we end up to the following general expression:

$$ F_\beta(x,t) = \int_{-\infty}^{+\infty} dk \; e^{ikx} E_\beta(t^\beta \hat{L}_{FP}^{(F)}) \tilde{F}(k,0), \qquad 0<\beta<1. \tag{3.80}$$

The result (3.80) can be also interpreted in the light of the evolution operator method. We often resort to this method not only for solving the Fokker-Planck equation, but also for other evolutionary problems as we have shown in [117, 118, 120, 122, 193, 194]. The formal solution in terms of the evolution operator $\hat{U}_\beta = E_\beta(t^\beta \hat{L}_{FP})$ reads

$$ F_\beta(x,t) = \hat{U}_\beta F_\beta(x,0). \tag{3.81}$$

Another possibility is to use the umbral method we illustrated in [77], once the Mittag-Leffler function has been represented as an umbral function [11]. The aforementioned methods allow to find the solution for a wide class of Fokker-Planck operator but if the $\hat{L}_{FP}$ operator is simply a constant as in our case, the solution can be determined in terms of Lévy stable distribution [167]:

$$\left[\frac{n(T)}{n(0)}\right]_{ML} = \int_0^\infty ds\; e^{-s}\kappa_\beta(s,T). \tag{3.82}$$

Here, $\kappa_\beta(s,T)$ is equal to $\frac{T s^{-(1+\frac{1}{\beta})} g_\beta(T, s^{-\frac{1}{\beta}})}{\beta}$ where g_β is a one-side Lévy stable distribution. On that subject it is of paramount importance the results collecting in [73] and [74] where the Lévy stable distribution is defined in a closed analytical form and in terms of hypergeometric function.

3.6.2 Evolution equation for the modified (upper) incomplete Gamma function and its sub-classes

As observed in [123] and in Chapter 2, the Kohlarusch-Williams-Watts function is the solution of the second order differential equation:

$$\begin{aligned} &\frac{d^2 n(t^*)}{dt^{*2}} + \frac{2}{\tau^*}\frac{dn(t^*)}{dt^*} + \frac{n(t^*)}{\tau^{*2}} = 0 \\ &n(0) = n_0 \\ &\frac{dn(t^*)}{dt}|_{t^*=0} = -\frac{n_0}{\tau^*}. \end{aligned} \tag{3.83}$$

The physical meaning of (3.83) is explained in Chapter 2 as a result of the restoring and frictional forces acting on the system. In particular, we analysed the physical meaning in both the material frame $t^* = t^\beta$ and in the laboratory, where time flows linearly. In order to give a further validation to the correctness of the model, we want to unravel the semigroup property hidden in its evolution (3.83). This issue allows to understand the connection between the semigroups operators governing the differential equation (3.83) and the commutator operator that describes in a complementary way the evolution starting from the physical manifestation of the semigroups, i.e. the composition rule. In particular, as it will be shown, the analysis framed in the context of semigroups allows to find a generalization and the corresponding solution for the second order differential equation (3.83).

The first step is to reduce the second order differential equation (3.83) to a system of two first order differential equations as follows

$$\frac{d}{dt^*}\begin{pmatrix} u_1(t^*) \\ u_2(t^*) \end{pmatrix} = \begin{pmatrix} 0 & 1 \\ -\frac{1}{\tau^{*2}} & -\frac{2}{\tau^*} \end{pmatrix}\begin{pmatrix} u_1(t^*) \\ u_2(t^*) \end{pmatrix} \tag{3.84}$$

with the initial conditions

$$\Phi(0) = \begin{pmatrix} u_1(0) \\ u_2(0) \end{pmatrix}. \tag{3.85}$$

The system of differential equation (3.84) can be written in a matrix form as follows

$$\frac{dn(t^*)}{dt^*} = \begin{pmatrix} 0 & 1 \\ -\frac{1}{\tau^{*2}} & -\frac{2}{\tau^*} \end{pmatrix} n(t^*), \tag{3.86}$$

where

$$n(t^*) = \begin{pmatrix} u_1(t^*) \\ u_2(t^*) \end{pmatrix}. \tag{3.87}$$

Now we can introduce the concept of semigroups [37, 56, 57, 82, 160]. Among the applications of semigroups, we will focus our attention on the translation semigroups.

> **Definition 3.6.1.** Let $(\mathfrak{X}\,, \|\cdot\|)$ denote a given Banach space on $\mathbb{W}$ (i.e. $\mathbb{W} = \mathbb{R}$ or $\mathbb{W} = \mathbb{C}$) equipped with a norm $\|\cdot\|$ and let $\hat{T} : [0, \infty) \to \mathcal{L}_{\mathbb{W}}(\mathfrak{X})$ be a linear and bounded operator[1] on $\mathfrak{X}$, i.e. $\hat{T} \in \mathcal{L}_{\mathbb{W}}(\mathfrak{X})$ where the symbol $\mathcal{L}_{\mathbb{W}}(\mathfrak{X})$ indicates the space of bounded linear operators in $\mathfrak{X}$.
> The family of bounded linear operators $\mathfrak{A} \equiv \{\hat{T}(t) : t \geq 0\} \subset \mathcal{L}_{\mathbb{W}}(\mathfrak{X})$ forms a semigroup if the following functional equation is satisfied
>
> $$\hat{T}(t+s) = \hat{T}(t) \cdot \hat{T}(s), \quad t \geq 0, \quad s \geq 0. \tag{3.88}$$
>
> If additionally, $\hat{T}(0) = I$ and the map $\hat{T}(\cdot)x : [0, \infty) \to \mathfrak{X}$ is continuous for each $x \in \mathfrak{X}$, then $\mathfrak{A}$ is called strongly continuous operator semigroup or shortly C_0-semigroup.

C_0-semigroup serves to describe the time evolution of linear systems and for this reason, it is crucial to frame the differential equation in this context.
It gives a further validation to the key role of the material frame in modelling anomalous relaxation processes and to the general composition rule in (3.29) (or (3.30)) as a manifestation of the semigroup property.

> **Definition 3.6.2.** Given a C_0-semigroup $\mathfrak{A}$, one defines the infinitesimal generator, or shortly, the generator $\hat{A}$ of the semigroup $\hat{T}$ as a linear and closed (not necessarily bounded) operator on $\mathfrak{X}$ by
>
> $$\hat{A}x = \lim_{t \to 0^+} \frac{\hat{T}(t)x - x}{t} \tag{3.89}$$
>
> with domain
>
> $$D(\hat{A}) := \left\{ x \in X : \lim_{t \to 0^+} \frac{\hat{T}(t)x - x}{h} \ \text{exists} \right\}. \tag{3.90}$$
>
> Then, $D(\hat{A})$ is dense in $\mathfrak{X}$ and it is the subspace where the (right) derivative $\hat{A}x$ exists.

As a conclusion, the functional equation (3.88) is satisfied by the C_0-semigroup given by:

$$\hat{T}(t) := e^{t\hat{A}}. \tag{3.91}$$

---

[1] We will say that the linear operator $\hat{T}$ is bounded if there exists $M \geq 0$ such that $\forall x \in \mathfrak{X}$ one has $\left\|\hat{T}(x)\right\| \leq M \|x\|$.

The requirement for the generator $\hat{A}$ to be bounded is essential since it assures that $e^{t\hat{A}}$ converges. This semigroup corresponds to the solution semigroup of the differential equation (3.84) with its initial conditions (3.85). Considering the semigroup relation in (3.88) with $\hat{T}(0) = 1$, it is evident that this functional equation can be regarded as an analogue of the well-known Cauchy functional equation that is formally equivalent to (3.88):

$$\begin{aligned} u(t+s) &= u(t) \cdot u(s),\ t \geq 0,\ s \geq 0 \\ u(0) &= 1. \end{aligned} \tag{3.92}$$

The solution of the system of differential equations (3.86) is given by

$$u(t^*) = e^{t^*\hat{A}}\Phi(0), \tag{3.93}$$

where

$$\hat{A} := \begin{pmatrix} 0 & 1 \\ -\frac{1}{\tau^{*2}} & -\frac{2}{\tau^*} \end{pmatrix}. \tag{3.94}$$

The matrices $e^{t^*\hat{A}}$ may be thought of as *solution operators* mapping the initial value $\Phi(\tau^*)$ to the solution $e^{t^*\hat{A}}\Phi(\tau^*)$ at time t^*.

Using the theory of exponential operators framed in the context of semigroups, the above result can be generalized in order to define a differential evolution equation also for the modified (upper) incomplete Gamma function.

As we stated for the material Λ transform, we should follow the symmetry and then, the generalization does not have to change the structure of the second order differential equation. The second-order differential equation (3.83) (and the corresponding differential equation in the (linear) time domain) are built up from physical considerations on the forces acting on the system. However, considering Fig. 1.5 in Chapter 1, we immediately note that the Cole-Davidson dispersion model has been represented as a flattened semicircle with respect to the Debye and the Cole-Cole dispersion models. This observation lead us to introduce a non-homogeneous term for the second-order differential equation that carries out another source for the anomalous behaviour responsible for the asymmetry.

The primary source of anomalous behaviour is collected in the material variables that stretches and compresses the timescale explaining for example rejuvenation or ageing effect in materials. This source of anomalous behaviour is intrinsic to the dynamical system. On the other hand, the second source should be originated *externally* to the system as for example when an external field is acting on the system and then when the external force has been switched off, the system naturally *compensate*. This *compensation force* drives the damping of the harmonic oscillator. Adding the non-homogeneous term, $g(t^*, \tau^*)$, in the differential equation (3.83) and we get

$$\frac{d^2 n(t^*)}{dt^{*2}} + \frac{2}{\tau^*}\frac{dn(t^*)}{dt^*} + \frac{n(t^*)}{\tau^{*2}} = g(t^*). \tag{3.95}$$

Once the second order differential equation (3.95) has been decoupled into two of first order equations, its solution is

$$n(t^*) = e^{t^*\hat{A}}\Phi(0) + \int_0^{t^*} ds^*\ e^{(t^*-s^*)\hat{A}}\Xi(s^*), \tag{3.96}$$

for every $t > 0$. Here the only symbol not previously explained is the non-homogeneous term that in the system takes the following form:

$$\Xi(t^*) = \begin{pmatrix} 0 \\ g(t^*) \end{pmatrix}. \tag{3.97}$$

In case

$$g(t^*) = \frac{(\alpha-1)}{\Gamma(\alpha)\tau^{*2}}\left(\Gamma\left[\alpha-1, \frac{t^*}{\tau^*}\right] + e^{-\frac{t^*}{\tau^*}}\left(\frac{t^*}{\tau^*}\right)^{\alpha-2}\right),$$

the solution is exactly the modified (upper) incomplete Gamma function:

$$n(t^*) = \frac{\Gamma[\alpha, \frac{t^*}{\tau^*}]}{\Gamma(\alpha)}. \tag{3.98}$$

As expected when $\alpha = 1$, this general case reduced to the one described in Chapter 2. To conclude this Chapter, it is fascinating to remark once again that the differential equation (3.95) describes a driven damped harmonic oscillator, whereas (3.83) depicts a damped one, since the external source has been set equal to zero and the system is unable to generate a compensation. These initial value problems for anomalous relaxation functions, as the KWW function and the modified (upper) incomplete Gamma function, in terms of harmonic oscillators establish a parallelism with the Lorentz model outlined in Chapter 1.

By introducing the material variables, the material Λ transform and an external source, we restore the symmetry in the dynamics between the relaxation and dispersion models.

3.7 Conclusions to Chapter 3

Fractional calculus, operator methods and exponential operators' theory [23, 24] framed in the context of semigroups are the mathematical tools used to model the evolution of anomalous relaxation processes in dynamical systems.

The essential foundations of the evolution are rooted in a natural property named composition rule that is the *physical* manifestation of the semigroup property.

The term composition rule was introduced in [78, 79] and it was applied to the one-parameter Mittag-Leffler function, the counterpart of the Cole-Cole relaxation via Laplace transform [66]. However, the concept of the material frame inspired the research to consider the relaxation function as an *intensive* property. This paves the way to the use of the Reynolds-Leibnitz theorem that gives a general composition rule for the relaxation functions that are normalized and analytical in zero.

This original result concerning the composition rule is defined in terms of a commutator involving a derivative and its inverse operator that can be bought under the name of anti-derivative [116]. The crucial value of the result is not only in its mathematical form in terms of a commutator, in fact all fundamental physics is based on the operators that do not commute, but also in its generality and in its physical meaning. The commutator is equal to the net flux of the product between the relaxation functions in their respective time syntagms: $[T_0, T_1]$ and $[T_1, T]$ and at the end, it coincides with the relaxation function in the whole time syntagm $[T_0, T]$. In other words, the commutator can be regarded as an integro-differential equation describing the evolution of the system under consideration.

We considered here four examples of its application: the composition of two Debye relaxations, the composition of two Prabhakar (or three-parameter Mittag-Leffler) relaxation functions, the composition of two one-parameter Mittag-Leffler and the composition of two (upper) incomplete Gamma relaxation functions. In particular, we focus our attention on the latter case, it was possible not only to define the composition rule for the relaxation function but also for its pulse response. The composition rule for pulse response function coincides with the semigroup operator of the Gamma function known in literature [102] and it gives a further validation of the result.

The idea to consider the relaxation functions as an intensive quantity and the formulation of a general composition rule in terms of a commutator suggests once again that the anomalous behaviours are only disturbing effects linked to the choice of the frame. For this reason, we introduce a novel transform, the material Λ transform, that keeps in consideration the disturbing effects. Such a transform is a modified Fourier transform, where we consider the action of a complex-scaling operator in the material frame that has made clear the connection between the Havriliak-Negami dispersion model and the KWW function. Moreover, we observe that we have two sources of anomalous behaviours: one is mathematically embeded in the material variables that stretch, compress and twist the frame, whereas the other one is rooted in the (upper) incomplete Gamma function and in the external source (or compensating source internal to the system) in its second-order differential equation.

This result intrigues us, and for this reason we framed the second-order differential equation in the context of exponential operators and semigroups. It was therefore possible to bring out a concrete connection between the semigroup operator of the differential equation and the composition rule valid for its solutions. As known, the operators methods simplifies the approach, and we can easily generalize the result for a non-homogeneous second-order differential equation, that is a driven damped harmonic oscillator. Fixing an opportune function for the non-homogeneous term, we can obtain as a solution the modified (incomplete) Gamma relaxation function. This confirms our suspect that there are two origins for anomalous behaviours: one intrinsic to the frame and it is the cause of rejuvenation and ageing effect, whereas the other one is due to the presence of an external influence and its effects once the force has been switched off are described by a compensating force. A visual effect of the subtle external influence can be appreciated considering the Cole-Cole plot in Fig. 1.5 in Chapter 1 where the Cole-Davidson and the Havriliak-Negami dispersion models show a clear flattened asymmetric semicircle with respect to the Cole-Cole and the Debye ones. A last but not least comment concerns the initial value problems. The differential equation for the KWW function has been presented for the first time in Chapter 2 and thanks to the exponential operators and semigroups theory we generalize the result to describe the evolution of a more general relaxation function in terms of a driven damped harmonic oscillator. Both these evolution equations allow to restore the symmetry in the description of the dynamics between the relaxation and the dispersion models. The latter are described by the Lorentz model as outlined in Chapter 1 that is basically a driven damped harmonic oscillator.

Chapter 4

Complete monotonicity and special functions in relaxation processes

4.1 Special functions: an overview.

As Richard Askey states in the preface of his book [9]: "*Certain functions appear so often that it is convenient to give them names. These are collectively called special functions. There are many examples and no single way of looking at them can illuminate all examples or even all the important properties of a single example of a special function*".

Special functions form a remarkable area of mathematics which is particularly interesting for applied sciences. Such functions, characterized by specific notations, established names and a fair amount of properties, have proved to be indispensable and precious tools in the current scientific scenario.

Among all the special functions, we focus our attention on the Mittag-Leffler function and on the Meijer G-function that we encountered in Chapter 3 as relaxation functions.

4.1.1 The Mittag-Leffler function

At the end of the 19th century, the Swedish mathematician Gösta Magnus Mittag-Leffler introduced a new special function, the so-called Mittag-Leffler function $E_\alpha(z)$, in order to solve the problem of the analytic continuation of power series outside the disc of their convergence [85, 176].

Definition 4.1.1. The Mittag-Leffler function is defined as follows:

$$E_\alpha(z) := \sum_{n=0}^{\infty} \frac{z^n}{\Gamma(\alpha n + 1)}, \quad \alpha \in \mathbb{C} \quad \Re(\alpha) > 0 \quad z \in \mathbb{C}, \tag{4.1}$$

and it is treated in [58, 69, 86, 166–168, 199]. The series (4.1) converges in the whole complex plane if $\Re(\alpha) > 0$. On the other hand, for $\Re(\alpha) < 0$ the series diverges everywhere on $\mathbb{C}$ (except in $z = 0$). In the watershed case $\Re(\alpha) = 0$, the series (4.1) has a radius of convergence $R = e^{\frac{\pi}{2}|\Im z|}$.

This function caught the attention of the mathematicians since the very beginning, in fact several generalizations have been formulated and their classification is on the number of parameters involved. For this reason the definition (4.1) has known in literature as one-parameter Mittag-Leffler function.

The first generalization of $E_\alpha(z)$ is the Wiman function (1905) [199] and it is also known as two-parameter Mittag-Leffler function. This special function is a complex function defined by the following power series

$$E_{\alpha,\beta}(z) := \sum_{n=0}^{\infty} \frac{z^n}{\Gamma(\alpha n + \beta)}, \quad \alpha, \beta \in \mathbb{C}, \quad \Re(\alpha) > 0, \quad \Re(\beta) > 0 \quad z \in \mathbb{C}. \tag{4.2}$$

The two-parameter Mittag-Leffler function (4.2) coincides with the Mittag-Leffler function $E_\alpha(z)$ (4.1) as $\beta = 1$. On the other hand, the convergence conditions closely follows the one above defined. Last but not least, most of the properties are intensively studied in [86].

Another generalization of the Mittag-Leffler function based on the Wiman function was introduced by Prabhakar in 1971 [169]:

$$E^{\gamma}_{\alpha,\beta}(z) := \sum_{n=0}^{\infty} \frac{(\gamma)_n \; z^n}{n!\Gamma(\alpha n + \beta)}, \; \alpha, \beta, \gamma \in \mathbb{C}, \quad \Re(\alpha) > 0, \quad \Re(\beta) > 0, \quad \Re(\gamma) > 0, \quad z \in \mathbb{C}, \tag{4.3}$$

where $(\gamma)_n := \frac{\Gamma(\gamma+n)}{\Gamma(n)}$ is the Pochammer symbol [1].

Moreover, there are another two possible generalizations of the Mittag-Leffler function that involve four parameters.

In 2007, Shukla and Parakapati introduced a four-parameters generalization of the Mittag-Leffler function [185]:

$$\begin{aligned} E^{\gamma,q}_{\alpha,\beta}(z) := \sum_{n=0}^{\infty} \frac{(\gamma)_{nq} \; z^n}{n!\Gamma(\alpha n + \beta)}, \quad & \alpha, \beta, \gamma \in \mathbb{C}, \quad \Re(\alpha) > 0, \quad \Re(\beta) > 0, \quad \Re(\gamma) > 0, \\ & q \in (0,1) \cup \mathbb{N}, \quad z \in \mathbb{C}, \end{aligned} \tag{4.4}$$

where $(\gamma)_{nq} = \frac{\Gamma(\gamma+qn)}{\Gamma(\gamma)}$ is the generalized Pochammer symbol.

Another generalization of the three-parameter Mittag-Leffler function (4.3) was presented by Srivastava and Tomovski in 2009 [188] where the parameter q has been replaced by k with $\Re(k) > 0$. This last four-parameter Mittag-Leffler embeds also the generalization (4.4) as a special case if we set $k = q$ and $\min\{\Re(\beta), \Re(\gamma)\} > 0$.

The blooming of Mittag-Leffler functions highlighted the considerable interest of mathematicians. However, only in the last decades, the Mittag-Leffler function evolves from *Cinderella* to *Queen* [45, 137] for its numerous applications in fractional calculus [16, 17, 34, 48, 53, 71, 86, 91, 107, 127, 135, 154, 166, 176, 178, 179, 195, 197]. Among the possible applications, we remind here the role of the Mittag-Leffler function as solution of the Fokker-Planck equation, as shown in Chapter 3 and in more details in [77].

4.1.2 The Meijer G-function

The Meijer G-function, introduced by Cornelis Simon Meijer in 1936, represents a wide range of mathematical relations from basic elementary functions to the majority of the special functions such as the generalized hypergeometric function and the MacRobert's E-function.

> **Definition 4.1.2.** The Meijer G-function is given by the following contour integral in the complex plane: [4, 108, 131, 147]:
>
> $$G_{p,q}^{m,n}\left[z\left|\begin{matrix}a_1\dots a_p\\ b_1\dots b_q\end{matrix}\right.\right]=\frac{1}{2\pi i}\int_\ell ds\,\frac{\prod_{j=1}^{m}\Gamma(b_j+s)\prod_{j=1}^{n}\Gamma(1-a_j-s)}{\prod_{j=n+1}^{p}\Gamma(a_j+s)\prod_{j=m+1}^{q}\Gamma(1-b_j-s)}z^{-s}, \tag{4.5}$$
>
> where the upper and lower indices (m,n,p,q) are non-negative integers such that $0\le m\le q$ and $0\le n\le p$, the parameters a_i $(i=1,\dots,p)$ and b_j $(j=1,\dots,q)$ may be real or complex numbers, and Γ denotes the Gamma function. Here the empty product is equal to unity, i.e.
>
> $$\prod_{j=1}^{0}\Gamma(b_j+s)=1;\quad\prod_{j=1}^{0}\Gamma(1-a_j-s)=1;\quad\prod_{j=n+1}^{n}\Gamma(a_j+s)=1;\prod_{j=m+1}^{m}\Gamma(1-b_j-s)=1. \tag{4.6}$$

It is worth noting that the Meijer G-function (4.5) can be viewed as a Mellin-Barnes integral [21], i.e. an inverse Mellin transform where the integrand is a ratio of Gamma functions with linear arguments.

In (4.5) the contour ℓ is an integration path in the complex s-plane from $\infty-i\tau$ to $\infty+i\tau$ where τ is a positive number. As shown in Definition 4.1.2, the argument of the Meijer G-function does not depend on τ. The convergence of the integral does not depend on the chosen integration path.

The aforementioned contour ℓ, also known as Bromwich path, is one of the three possible choices, as was noticed by Erdelyi [58, pp. 206-222].

If it is possible to choose more than one path, the result of the integral will be the same, as follows from the Cauchy's residue theorem.

Throughout this Chapter, the parameters a_i $\quad(i=1,\dots,p)$ and b_j $\quad(j=1,\dots,q)$ have to fulfil the following condition

$$a_i-b_j\neq\text{a positive integer},\quad(i=1,\dots,n;\quad j=1,\dots,m). \tag{4.7}$$

This last assumption (4.7) implies that the contour ℓ is always chosen to separate the poles in $\Gamma[b_j-s]$ from any pole of $\Gamma[1-a_i+s]$, otherwise the Meijer G-function is not defined.

Although the Meijer G-function is rather general, there are a few special functions that could not be presented in its terms if we consider the more general case involving irrational weights for the s variable, as for example the Mittag-Leffler [150] and the Wright generalized hypergeometric function [200]. This is why the Fox H-function [91, 143], a generalization of the Meijer G-function, has been introduced.

Definition 4.1.3. The Fox H-function is defined by the following complex contour integral

$$H^{m,n}_{p,q}\left[z\left|\begin{matrix}(a_1,A_1) & (a_2,A_2) & \dots & (a_p,A_p)\\ (b_1,B_1) & (b_2,B_2) & \dots & (b_q,B_q)\end{matrix}\right.\right] = \frac{1}{2\pi i}\int_\ell ds\,\frac{\prod_{j=1}^{m}\Gamma(b_j+B_js)\prod_{j=1}^{n}\Gamma(1-a_j-A_js)}{\prod_{j=n+1}^{p}\Gamma(a_j+A_js)\prod_{j=m+1}^{q}\Gamma(1-b_j-B_js)}z^{-s}, \quad (4.8)$$

where A_j and B_j, called weights, are assumed to be positive numbers and all the parameters a_j and b_j may be real or complex. The components of the orders follow the same restrictions imposed on the Meijer G-function.

Comparing the definition between the Fox H-function and the Meijer G-function, we obtain a formal correlation between the two functions. Mathematically, the Fox H-function reduces to the Meijer G-function when $A_1 = \cdots = A_p = B_1, \cdots = B_q = C$, where C is a positive number [187, p. 50].
In this case,

$$H^{m,n}_{p,q}\left[z\left|\begin{matrix}(a_1,A_1) & (a_2,A_2) & \dots & (a_p,A_p)\\ (b_1,B_1) & (b_2,B_2) & \dots & (b_q,B_q)\end{matrix}\right.\right] = \frac{1}{C}G^{m,n}_{p,q}\left[z^{\frac{1}{C}}\left|\begin{matrix}a_1\cdots a_p\\ b_1\cdots b_q\end{matrix}\right.\right]. \quad (4.9)$$

Moreover, if $C = 1$ in (4.9) the Fox H-function is exactly the Meijer G-function.
This identity (4.9) is quite interesting, since it simply allows us to realize how it is possible to extend the result also to the Fox H-function. Moreover, this identity shows clearly the importance of the Meijer G-function among all the special functions[1].
In addition to its ability to represent most of the well-known special functions, the Meijer G-function has also fascinating closure properties under several operations such as integration, differentiation, the Laplace transform, the Euler transform and even the multiplicative convolution [22, 81, 170]. Therefore, some results that could be evaluated only numerically can now instead be expressed in closed form in terms of the Meijer G-function. For this reason, modern computer algebra software programs such as Maple, Mathematica and Maxima contain an implementation for the Meijer G-function.
In light of these properties, the Meijer G-function is nowadays considered an effective and handy tool and its growing importance emerges from various applications in different areas from applied mathematics to physics [40, 104–106, 164, 165].

4.1.3 The motivations behind the investigations on the complete monotonicity

Among the properties fulfilled by these two special functions, there is the complete monotonicity once we impose adequate restrictions on the parameters involved. In

---

[1] Other interesting and useful relations between the Meijer G-function and the Fox H-function can be found in [170]

Chapter 2 and in [123], we observed that this mathematical property has a clear physical meaning since its presence (or absence) reveals the nature of the dynamics behind relaxation processes. The complete monotonicity is associated to a *single dynamics*, i.e. the system experienced only damping mechanism and therefore, it follows only decay pathways. On the other hand, the relaxation described by monotone function is heterogeneous, and we have the so-called *dual dynamics*: there is not only a dumping mechanism but also a pumping mechanism.

As proven in Chapter 2 and in [123], the two types of dynamics, validated by experimental data, explain the observed anomalous behaviour and the improvement of the system performances when the relaxation is described by complete monotone functions. In other words, the mathematical modelling of relaxation processes by complete monotone functions implies that the system has a higher-ordered organization of its parts, with consequent improvement of the performances (as for example the intensity of the luminescent emission).

To sum up, finding the constraints on the parameters involved in these special functions allows to determine the nature of the dynamics in physical systems affected by anomalous relaxation processes. The issue has also a mathematical interest.

As remarked in [80], the proof of the complete monotonicity of the three-parameter Mittag-Leffler function as an *independent* mathematical object has not been investigated.

Therefore, we want to broaden the already rich literature on the complete monotonicity of the three-parameter Mittag-Leffler function (see for example [45, 138, 192]) summarizing the result we obtained in [80].

The theorem on complete monotonicity of the three-parameter Mittag-Leffler function in [80] is the natural extension of the result obtained by Pollard [168] for the Mittag-Leffler (4.1) and by Schneider [182] for the Wiman function (4.2).

On the other hand, even the Meijer G-function is gaining a key role in the description of relaxation processes. This special function embraces the modified (upper) incomplete Gamma function defined in Chapter 3 as its special case, and the use of the material Λ transform allows to extend the physical meaning also to the frequency regime. In the light of the results obtained in Chapter 2 and in [123] concerning the dynamics of complex systems, it is fascinating to find the mathematical requirements to have a complete monotone relaxation function in terms of the Meijer G-function.

Even in this case, the complete monotonicity has been previously investigated as for example in [104, 106] but, the crucial plus points of this original result, presented in Section 4.3, are both in its simplicity able to directly highlight the relationship between the parameters and coefficients, and in its strategic methodology that paves the way to generalizations of the result for more convoluted Meijer G-functions. A last but not least asset concerns the set of values where the parameters range: now, the parameters can assume also negative values! *Standing on the shoulders of giants* of literature devoted to the Meijer G-function [2, 3, 83, 104–106, 142], it was possible to go beyond what is known and conjecture the idea from which the result stands out.

For our purposes, it will be useful to remind here below the definition of complete monotone function [149] introduced in Chapter 2 and the statement of the Bernstein theorem:

Definition 4.1.4. A real valued function f, defined on an interval $I \subset \mathbb{R}$, is called complete monotone on I, if the function f has derivatives of all orders and satisfies the condition

$$(-1)^r f^{(n)}(x) \geq 0, \quad n \in \mathbb{N}_0, \quad x \in I \subset \mathbb{R}, \tag{4.10}$$

where $f^{(n)}$ represents the n-th derivative with respect to x.

From this definition a complete monotone function is non-negative as it is immediate to conclude considering the case $n = 0$ in (4.10).

Theorem 4.1.1 (**Bernstein theorem**)**.** A real function f is a completely monotone function if and only if there exists a positive measure μ on $[0, \infty)$ such that $t \mapsto e^{-xt}$ is integrable with respect to μ for all $x > 0$ and

$$f(x) = \int_0^\infty d\mu(t)\; e^{-xt}. \tag{4.11}$$

Further details can be found in [27, 114].

4.2 Complete monotonicity for the three-parameter Mittag-Leffler function

As hinted in Section 4.1.1, our proof of complete monotonicity for the three-parameter Mittag-Leffler function is outlined proceeding as Pollard did for the one-parameter Mittag-Leffler function [167, 168].
The main result is the formulation of the following theorem published in [80].

Theorem 4.2.1. The three-parameter generalized Mittag-Leffler function $E^{\gamma}_{\alpha,\beta}(-z)$ is completely monotone for $0 < \alpha \leq 1$, $\gamma > 0$, and $\beta \geq \alpha\gamma$.

Proof. The cornerstone of the proof is to write the three-parameter Mittag-Leffler function as a Laplace transform of a positive function so we can use the Bernstein theorem 4.1.1 to complete the proof.
Our starting point is to consider the inverse Laplace transform of the Prabhakar function

$$E^{\gamma}_{\alpha,\beta}(-xt^{\alpha}) = \frac{t^{1-\beta}}{2\pi} \int_{\ell_s} ds\; e^{st} \frac{s^{\alpha\gamma-\beta}}{(s^{\alpha}+x)^{\gamma}}\,, \tag{4.12}$$

where ℓ_s is the Bromwich contour with $\Re(s) > 0$. Now, we can replace the argument of the transform with the following Gamma identity formula

$$(\xi + xt^{\alpha})^{-\gamma} = \frac{1}{\Gamma(\gamma)} \int_0^\infty du\; e^{-(\xi+xt^{\alpha})u} u^{\gamma-1}\,, \tag{4.13}$$

and we obtain

$$E^{\gamma}_{\alpha,\beta}(-xt^{\alpha}) = \frac{1}{2\pi i\alpha} \int_{\ell_\xi} d\xi\; e^{\xi^{1/\alpha}} \xi^{\frac{\alpha\gamma-\beta+1}{\alpha}-1} \left[\frac{1}{\Gamma(\gamma)} \int_0^\infty du\; e^{-(\xi+xt^{\alpha})u} u^{\gamma-1}\right]. \tag{4.14}$$

We should remark that the integral contour ℓ_s was changed in ℓ_ξ by the replacement $\xi = (st)^\alpha$ and consequently $\Re(s) = |s^\alpha| t^\alpha \cos(\alpha y(s)) > 0$. The absolute convergence of the integrals allows us to swap their order, so we get

$$E^{\gamma}_{\alpha,\beta}(-xt^\alpha) = \frac{1}{2\pi i \alpha \Gamma(\gamma)} \int_0^\infty du\; e^{-xt^\alpha u} u^{\gamma-1} \left[\int_{\ell_\xi} d\xi\; e^{\xi^{1/\alpha} - u\xi} \xi^{\frac{\alpha\gamma-\beta+1}{\alpha}-1} \right]. \tag{4.15}$$

After performing another change of variable $\xi = u^{-1} z^\alpha$ and introducing the function $g^{\gamma}_{\alpha,\beta}$, defined as follows

$$\begin{aligned} g^{\gamma}_{\alpha,\beta}(y) &= \frac{\alpha}{\Gamma(\gamma)} \frac{y^{-\beta}}{2\pi i} \int_\ell dz\; e^{yz} z^{\alpha\gamma-\beta} e^{-z^\alpha} \\ &= \frac{\alpha}{\Gamma(\gamma)\, y^\beta} f^{\gamma}_{\alpha,\beta}(y), \end{aligned} \tag{4.16}$$

the three-parameter Mittag-Leffler function now reads

$$\begin{aligned} E^{\gamma}_{\alpha,\beta}(-xt^\alpha) &= \frac{1}{\alpha} \int_0^\infty du\; e^{-xt^\alpha u} u^{-1-\frac{1}{\alpha}} g^{\gamma}_{\alpha,\beta}(u^{-\frac{1}{\alpha}}) \\ &= \frac{1}{\Gamma(\gamma)} \int_0^\infty du\; e^{-xt^\alpha u} u^{-1-\frac{1}{\alpha}+\frac{\beta}{\alpha}} f^{\gamma}_{\alpha,\beta}(u^{-\frac{1}{\alpha}}). \end{aligned} \tag{4.17}$$

To conclude the proof we need to demonstrate the non-negativity of $f^{\gamma}_{\alpha,\beta}$ on $\mathbb{R}_+$. In fact, the strategy consists in the application of the Bernstein theorem 4.1.1 as a serial and logical interlocking implication between the non-negativity and the complete monotonicity in Laplace pairs. It is therefore of vital importance to identify the first ring of the chain: the function $f^{\gamma}_{\alpha,\beta}$. By straightforward comparison between the two lines in (4.16), the function $f^{\gamma}_{\alpha,\beta}$ can be defined as the inverse Laplace transform of the function $\tilde{f}(z) := z^{\alpha\gamma-\beta} e^{-z^\alpha}$, that is completely monotone for

$$0 < \alpha \leq 1, \gamma > 0, \text{ and } \beta \geq \alpha\gamma,$$

since it is the product of complete monotone functions (see theorem 1 in [149, p. 390]): a power function and the KWW stretched exponential function [168]. At this point, we can apply once again the Bernstein theorem 4.1.1 to (4.17) and then, we conclude the proof. □

4.3 Complete monotonicity for the Meijer G-function

In this Section, we present an original result concerning the mathematical requirements that the Meijer G-function $G^{q,0}_{p,q}$ should fulfil to be a non-negative and complete monotone function. Since this function is a less well-known with respect to the Mittag-Leffler function, we need to remind the definition of logarithmically complete monotone function and some useful theorems and lemmas that will be used in the proof.

Definition 4.3.1. A positive function $f(x)$ is said to be logarithmically completely monotone function on an interval $I \subset \mathbb{R}$ if it has derivatives of all orders on I and its logarithm $\log(x)$ satisfies

$$(-1)^n \,[\log f(x)]^{(n)} \geq 0, \; n \in \mathbb{N}_0, \; x \in I \subset \mathbb{R}, \tag{4.18}$$

where $[\log f(x)]^{(n)}$ is the n-th derivative with respect to x [10, 35, 202].
Moreover, the function f is said to be strictly logarithmically completely monotone function if inequality (4.18) is strict.
It has been proved that any logarithmically completely monotone function on I is also completely monotonic on I, but not conversely.

Lemma 4.3.1. Let φ a complete monotone function and let ψ a positive function with a complete monotonic derivatives, then $\varphi(\psi)$ is completely monotone.

Lemma 4.3.2. If the first derivative of the function h, h', is completely monotonic on $(0, \infty)$, then e^{-h} is also completely monotonic on $(0, \infty)$.
A proof of the previous two Lemmas 4.3.1 and 4.3.2 can be found in [28, p. 83] and in [59, p. 441].

This last lemma is equivalent to the following theorem:

Theorem 4.3.1. If $\varphi(x)$ is a complete monotone function, then $e^{\varphi(x)}$ is a complete monotone function. The proof can be found in [149, p. 391-392].

Lemma 4.3.3. Let a_i $(i = 1, \ldots, k)$ and b_i $(i = 1, \ldots, k)$ be real numbers such that: $a_k \geq \cdots \geq a_1$; $b_k \geq \cdots \geq b_1$ and $\sum_{i=1}^{k} a_i \geq \sum_{i=1}^{k} b_i$ for $i = 1, \ldots, k$. If the function f is decreasing and convex in $\mathbb{R}$, then

$$\sum_{i=1}^{k} f(b_i) \geq \sum_{i=1}^{k} f(a_i). \tag{4.19}$$

In 1949 Tomić demonstrated this lemma and its proof can be found in [140, p. 157].

Theorem 4.3.2. Let $K(s, t)$ be completely monotone function in s for all the $t \in (0, \infty)$ and let a non-negative locally integrable function $f(t)$ such that the integral

$$F(s) = \int_0^\infty dt \; K(s, t) \; f(t) \tag{4.20}$$

converges uniformly in a neighborhood of any point $s \in (0, \infty)$. Then $F(s)$ is completely monotone function. This theorem can be found in [149, p.392].

At this point, we can formulate the statement concerning the mathematical requirements for the non-negativity and the complete monotonicity of the Meijer G-function.

Theorem 4.3.3 (the Meijer G-*conjectured* theorem). Let a_i $(i = 1, \dots, p)$ and b_j $(j = 1, \dots, q)$ be real numbers such as

$$\begin{aligned} a_p &\geq \cdots \geq a_1 \\ b_q &\geq \cdots \geq b_1 \end{aligned} \tag{4.21}$$

where $q \geq p$, $a_1 > b_1$ and moreover the following inequality has been satisfied

$$\sum_{i=1}^{p} a_i \geq \sum_{i=1}^{p} b_i, \tag{4.22}$$

then for any real x, the Meijer G-function

$$G_{p,q}^{q,0}\left[x \,\middle|\, \begin{matrix} a_1 \cdots a_p \\ b_1 \cdots b_q \end{matrix}\right] \tag{4.23}$$

is non-negative in x on $(0, \infty)$ when $q \geq p$.
Introducing as additional conditions the non-positiveness of the smallest b parameter, i.e. $b_1 \leq 0$, and $a_1 > b_2$, and

$$\sum_{i=1}^{p} a_i \geq \sum_{i=2}^{p+1} b_i, \tag{4.24}$$

the Meijer G-function in (4.23) for $q > p$ results to be complete monotonic in x on $(0, \infty)$.
It should be also remarked that it is possible to define a *family* of complete monotonic Meijer G-function using the closure properties under the convolution of two Meijer G-functions extending the validity of the result.
Just one caveat: not all the software programs use the same definition of the Meijer G-function. Here, we assume the Definition 4.1.2 that is adopted by Mathematica but not by Maple. So, before making any numerical check please be sure that the definition of the Meijer G-function used by the software programs and in this thesis coincide.

Proof. Highlights of the proof:

- ◇ Firstly we prove the complete monotonicity of the Gamma functions ratio for $s \in (-b_1, 1 - b_1)$ when $p = q$ according to the following steps:
  (a) we introduce a real-valued function $h(s)$ and we investigate its non-negativity;
  (b) we prove the complete monotonicity of $h(s)$ evaluating its derivatives and their signs under the conditions established in the statement;
  (c) we show the (logarithmically) complete monotonicity of the ratio of Gamma functions resorting to theorem 4.3.1 (or see theorem 3 in [149, p. 391-392] for further details).

- ◇ Secondly, we demonstrate the non-negativity of the Meijer G-function $G_{p,p}^{p,0}$ on $(0,\infty)$ as listed below:
  - (d) we resort to the definition of the Meijer G-function (4.5) as an inverse Mellin transform;
  - (e) once observed that the path chosen does not contain any pole, we can reduce the limit of integration ;
  - (f) after performing a change of variable, we resort to the Bernstein theorem to prove the non-negativity of the Meijer G-function in the integrand.
- ◇ And number three, we show the complete monotonicity of the Meijer G-function $G_{p,q}^{q,0}$ on $(0,\infty)$ as follows:
  - (g) we define the Meijer G-function $G_{p,q}^{q,0}$ as an integral transform with a complete monotone kernel acting on the non-negative locally integrable Meijer G-function $G_{p,p}^{p,0}$;
  - (h) the theorem 4.3.2 (or theorem 4 [149, p. 392]) guarantees the complete monotonicity of the Meijer G-function $G_{p,q}^{q,0}$ on $(0,\infty)$.
    This completes the proof.

Firstly, we focus on the requirements for the non-negativity of the Meijer G-function $G_{p,p}^{p,0}$ and the key element is the formula here below:

$$\frac{\prod_{i=1}^{p}\Gamma(b_i+s)}{\prod_{i=1}^{p}\Gamma(a_i+s)} = \int_0^{\infty} dt\; t^{s-1} G_{p,p}^{p,0}\left[t\left|\begin{matrix}a_1\cdots a_p\\ b_1\cdots b_q\end{matrix}\right.\right]. \tag{4.25}$$

As hinted in the highlights of the proof (and as it will be explained in details in the following), the complete monotonicity of the Gamma functions ratio implies the non-negativity of the Meijer G-function, therefore it is vital to demonstrate independently of the right-hand side of (4.25) the complete monotonicity of the Gamma functions ratio. To pursue our aim, we introduce the following real function.
Let

$$h(s) = \sum_{i=1}^{p} \ln\Gamma(s+b_i) - \sum_{i=1}^{p} \ln\Gamma(s+a_i) + c, \tag{4.26}$$

where $s \in (-b_1, 1-b_1)$ and c is a positive constant that guarantees the non-negativity of the function $h(s)$. We should note that the function $h(s)$ is the logarithm of the ratio of Gamma function, consequently the conditions for the complete monotonicity that we found in the following are logarithmically complete monotonic conditions according to the definition 4.3.1.
The strategy to find the value of the c constant is based on the analysis of the higher order derivatives of the function $h(s)$. In fact as we will see here below, the second order derivative is positive under the conditions imposed in the statement 4.3.3. The non-negativity of the second order differential equation implies that the function is convex in $(-b_1, 1-b_1)$. Here below there are the explicit mathematical steps that allows us not only to define the convexity of the function

but also to observe how the derivatives at all the orders of the function $h(s)$ are alternating their signs.
The first derivative of $h(s)$ with respect to s, denoted with $h'(s)$, reads

$$h'(s) = \sum_{i=1}^{p} \frac{\Gamma'(s+b_i)}{\Gamma(s+b_i)} - \sum_{i=1}^{p} \frac{\Gamma'(s+a_i)}{\Gamma(s+a_i)}, \tag{4.27}$$

where the symbol Γ' means the first derivative of the Gamma function with respect to s.
For convenience we rewrite (4.27) in terms of the Digamma function $\psi(x) = \frac{\Gamma'(x)}{\Gamma(x)}$ [58, p. 15-20] [1, p. 258-259]:

$$h'(s) = \sum_{i=1}^{p} \psi(s+b_i) - \sum_{i=1}^{p} \psi(s+a_i). \tag{4.28}$$

For higher order derivative ($n \in \mathbb{N}_0$ or $n \geq 0$), Eq. (4.28) can be written as

$$[h(s)]^{(n+1)} = \sum_{i=1}^{p} \psi^{(n)}(s+b_i) - \sum_{i=1}^{p} \psi^{(n)}(s+a_i). \tag{4.29}$$

Here $[h(s)]^{(n+1)}$ represents the $n+1$ derivative of (4.28) and $\psi^{(n)}(s) = \frac{d^n}{ds^n}\psi(s) = \frac{d^{n+1}}{ds^{n+1}}\log\Gamma(s)$ is n-th derivative of the Digamma function also well known as Polygamma function [1, p. 260]. As follows from the notation just explained, the symbol $\psi^{(0)}$ corresponds to ψ.
Exploiting the integral transform tabulated in [133, p. 16]

$$\psi(x) = -\gamma + \int_0^\infty dt\ \frac{e^{-t} - e^{-tx}}{1 - e^{-t}} \quad (\Re(x) > 0), \tag{4.30}$$

where γ is the Euler-Mascheroni constant, the Polygamma function reads

$$\psi^{(n)}(x) = (-1)^{(n+1)} \int_0^\infty dx\ \frac{e^{-tx}t^n}{1 - e^{-t}} \quad (\Re(x) > 0,\ \text{and } n \in \mathbb{N}_0, \dots), \tag{4.31}$$

and we finally obtain for $n \in \mathbb{N}_0$

$$[h(s)]^{(n+1)} = (-1)^{n+1} \int_0^\infty dt\ \frac{e^{-ts}t^n}{1 - e^{-t}} \Big(\sum_{i=1}^{p} e^{-tb_i} - \sum_{i=1}^{p} e^{-ta_i} \Big). \tag{4.32}$$

Lemma 4.3.3 guarantees the non-negativeness of the function in round brackets and then the non-negativity of the integral (4.32) since the function $s \mapsto e^{-ts}$ is decreasing and convex. This result also implies that

$$(-1)^{n+1}[h(s)]^{(n+1)} \geq 0 \tag{4.33}$$

for $n \in \mathbb{N}_0$. In particular, fixing $n = 1$, we obtain that the second order derivative of $h(s)$ is non-negative, i.e. $h''(s) \geq 0$ and consequently, we demonstrated that

the function $h(s)$ is convex.
Now we have all the necessary elements to fix the value of the constant c in order to guarantee that the function $h(s)$ is non-negative in $(-b_1, 1-b_1)$. We calculate the limits at the endpoints of the interval $(-b_1, 1-b_1)$:

$$\begin{aligned} c_1 &:= \lim_{s\to -b_1^+} \sum_{i=1}^{p} \ln\Gamma(b_i+s) - \sum_{i=1}^{p} \ln\Gamma(a_i+s) \qquad (4.34a)\\ &= \sum_{i=1}^{p} \ln\Gamma(b_i-b_1) - \sum_{i=1}^{p} \ln\Gamma(a_i-b_1) = +\infty \\ c_2 &:= \lim_{s\to (1-b_1)^-} \sum_{i=1}^{p} \ln\Gamma(b_i+s) - \sum_{i=1}^{p} \ln\Gamma(a_i+s) \qquad (4.34b)\\ &= \sum_{i=1}^{p} \ln\Gamma(b_i+1-b_1) - \sum_{i=1}^{p} \ln\Gamma(a_i+1-b_1). \end{aligned}$$

At this point we understand the importance of the condition $a_1 > b_1$ in the statement: it avoids the indeterminate form in the limit (4.34a). Once evaluated the limits, we consider the presence of the local minimum c_3 in $(-b_1, 1-b_1)$ and then, we can compare the result with the ones found previously calculating the limits (4.34). At this point, we find the value of the constant c as the modulus of the minimum value between c_1, c_2 and c_3:

$$c \geq \left|\min\{c_1, c_2, c_3\}\right| . \qquad (4.35)$$

The constant c allows us to shift the function $h(s)$ in the first quadrant and then, the function $h(s)$ is non-negative. The non-negativity of $h(s)$ with the result concerning the alternating signs of its derivatives in (4.33) allow us to conclude that $h(s)$ is (logarithmically) completely monotone on $(-b_1, 1-b_1)$. As it will be shown below, this constant c is a *dummy* constant for our final purposes, and it can be easily dropped. Applying Lemma 4.3.1 we obtain that

$$e^{h(s)} = e^c \frac{\prod_{j=1}^{p} \Gamma(b_i+s)}{\prod_{i=1}^{p} \Gamma(a_i+s)} \qquad (4.36)$$

is also completely monotonic on $(-b_1, 1-b_1)$. Under such conditions, the left-hand side of (4.36) can be represented in terms of Meijer's G-function exploiting the following Mellin transform

$$e^c \frac{\prod_{i=1}^{p} \Gamma(b_i+s)}{\prod_{i=1}^{p} \Gamma(a_i+s)} = \int_0^\infty dt\; e^c\, t^{s-1} G^{p,0}_{p,p}\left[t \left| \begin{matrix} a_1 \cdots a_p \\ b_1 \cdots b_p \end{matrix} \right.\right] . \qquad (4.37)$$

It is now clear that the non-negative constant c plays the role of a multiplicative constant and therefore, without loss of generality, can be dropped out and we get

$$\frac{\prod_{i=1}^{p} \Gamma(b_i+s)}{\prod_{i=1}^{p} \Gamma(a_i+s)} = \int_0^\infty dt\; t^{s-1} G^{p,0}_{p,p}\left[t \left| \begin{matrix} a_1 \cdots a_p \\ b_1 \cdots b_p \end{matrix} \right.\right] . \qquad (4.38)$$

The integral representation (4.38) arises from the Mellin-Barnes integral (4.5) used for the definition of the Meijer G-function in Section 4.1.2. We should remark that we will reduce the limits of integration in (4.38) from $[0,\infty)$ to $[0,1]$ because the Meijer G-function $G^{p,0}_{p,p}$ is zero for $|t|>1$ as it is evident considering the definition of the Meijer G-function (4.5) for the case $n=0$. In fact, when the upper index n is zero, the integration path ℓ in (4.5), chosen among all the possible paths established by Erdelyi (see [58, pp. 206-222]), is a loop beginning and ending at $+\infty$ that does not encircle any pole, i.e. $\prod_{i=1}^{n=0}\Gamma(1-a_i-s)=1$, gives an empty product, and since we excluded by construction all the poles from the b parameters, the Meijer G-function vanishes for $|t|>1$. On these considerations, the integral on the right-hand side of (4.38) now reads

$$\frac{\prod_{i=1}^{p}\Gamma(b_i+s)}{\prod_{i=1}^{p}\Gamma(a_i+s)}=\int_0^1 dt\ t^{s-1}G^{p,0}_{p,p}\left[t\,\middle|\,\begin{matrix}a_1\cdots a_p\\ b_1\cdots b_p\end{matrix}\right] \tag{4.39}$$

and performing the change of variable $t\to e^{-y}$, we obtain the following expression

$$\frac{\prod_{i=1}^{p}\Gamma(b_i+s)}{\prod_{i=1}^{p}\Gamma(a_i+s)}=\int_0^\infty dy\ e^{-ys}G^{p,0}_{p,p}\left[e^{-y}\,\middle|\,\begin{matrix}a_1\cdots a_p\\ b_1\cdots b_p\end{matrix}\right]. \tag{4.40}$$

Now we apply the Bernstein theorem 4.1.1 that gives a sufficient and necessary condition to the non-negativity of the Meijer G-function in (4.40). We therefore declare that the Meijer G-function in (4.40) has domain $[0,\infty)$ and ranges included in $[0,\infty)$. Observing that this Meijer G-function is a composite function of the type $g(f(y))$ where g is the Meijer G-function and f is the exponential function, we gain information also on the co-domain of the Meijer G-function with t as argument since its co-domain has to be the same co-domain of the composite function according to the composite function rule, so we can write:

$$G^{p,0}_{p,p}:[0,\infty)\mapsto[0,\infty). \tag{4.41}$$

Once we demonstrate the non-negativity of the Meijer G-function (4.41), the complete monotonicity and (then) the non-negativity of the Meijer G-function follow considering the closure properties under the convolution of the Meijer G-functions (formula 2.24.1.1 in [170]): the product of two arbitrary Meijer's G-functions integrated over the positive real axis can be represented by just another Meijer's G-function.

For our purposes, we define the convolution below

$$\begin{aligned}\int_0^\infty dt\frac{1}{t}G^{1,0}_{0,1}\left[\frac{x}{t}\,\middle|\,\begin{matrix}-\\ k\end{matrix}\right]G^{p,0}_{p,p}\left[t\,\middle|\,\begin{matrix}a_1\cdots a_p\\ b_1\cdots b_q\end{matrix}\right]&=G^{p+1,0}_{p,p+1}\left[x\,\middle|\,\begin{matrix}a_1,\cdots,a_p\\ k,b_1,\cdots,b_{p+1}\end{matrix}\right]\\&=G^{p+1,0}_{p,p+1}\left[x\,\middle|\,\begin{matrix}a_1,\cdots,a_p\\ b_1',\cdots,b_{p+1}'\end{matrix}\right],\end{aligned} \tag{4.42}$$

where k is a real number.

The first Meijer G-function in (4.42), $G^{1,0}_{0,1}\left[\frac{x}{t}\,\middle|\,\begin{matrix}-\\ k\end{matrix}\right]$ multiplied by $\frac{1}{t}$, plays the role of the kernel of the integral transform and it is simply $e^{-\frac{x}{t}}\left(\frac{x}{t}\right)^k$. As it is evident the kernel is non-negative in x for all $t \in (0,\infty)$, and as previously demonstrated, the second Meijer G-function $G^{p,0}_{p,p}\left[t\left|\begin{matrix}a_1\cdots a_p\\ b_1\cdots b_p\end{matrix}\right.\right]$ is a non-negative function.

Now let us focus our attention on the value of the k parameter.

For $k \leq 0$ the kernel introduced in (4.42) is complete monotonic in x for all $t \in (0,\infty)$. However, the action of this kernel influences both the indices and the parameters, so we should keep in mind that the k parameter will be enrolled among the b parameters and the order could change. In case b_1 is positive, the k parameter can assume any non-positive real value, i.e. $k \leq 0$ without perturbing the order, otherwise if $b_1 \leq 0$, we should choose the k parameter as a negative number such that

$$\sum_{i=1}^{p} a_i - \sum_{i=2}^{p} b_i + k \geq 0. \tag{4.43}$$

This inequality assure us that the introduction of the k parameter among the b parameters do not invalidate the non-negativity condition (4.22) even in case of exchange between b_1 and k. So in the end, after evaluating the transform we obtain that the new b'_1 is the smallest negative b parameter as required in the statement and two inequalities

$$\sum_{i=1}^{p} a_i - \sum_{i=1}^{p} b'_i \geq 0, \tag{4.44}$$

and

$$\sum_{i=1}^{p} a_i - \sum_{i=2}^{p+2} b'_i \geq 0. \tag{4.45}$$

Both (4.44) and (4.45) are always satisfied once the Meijer G-function in the integrand of (4.42) is defined as a non-negative function. In fact, assuming for example that the smallest and negative b' parameter is the k parameter, i.e. $k = b'_1$, the inequality (4.44) is verified since it built from the inequality for the non-negativity condition when we replaced b_1 with k, and we have that $k < 0$ and $k < b_1$. It goes without saying that $a_1 > b'_1 = k$. Quite simply, the negative b'_1 helps the inequality to be satisfied since it increases the sum of positive terms. On the other hand the second inequality in (4.45) is also satisfied. In (4.45) we assume $b'_1 = k$, so now we have $b'_2 = b_1$ and therefore the parameters involved in (4.45) are the same parameters of the non-negative Meijer G-function in (4.42). Consequently, the inequality (4.45) is the inequality that proven the non-negativity condition for the Meijer G-function, and it explains the condition $a_1 > b_2$ in the statement, that here reads $a_1 > b'_2$.

According to these considerations and once the inequalities (4.44) and (4.45) are satisfied, the Meijer G-function in the right-hand side of (4.42) is a complete monotone function as follows from theorem 1 in 4.3.2.

In case the parameter k is positive (i.e. $k > 0$), the integral of the product of two non-negative functions is again a non-negative function without any further

restriction. In fact, for any choice of $k > 0$, the inequality statement (4.22) is always verified: for $k > b_p$, the k is outside the range of the series and if $0 < k < b_p$, the k parameter takes the place of one of the b parameter, and it helps verify the inequality since it contributes with a term smaller than that carried by the parameter b replaced.
Each time we apply the integral transform the number of b parameters increases by one and so do the q indices and therefore we can generate a family of non-negative or complete monotone function whose parameters q and p differ for more than one unit:

$$\begin{aligned}\int_0^\infty dt \frac{1}{t} G^{1,0}_{0,1}\left[\frac{x}{t}\middle|\begin{matrix}-\\ k'\end{matrix}\right] G^{q,0}_{p,q}\left[t\middle|\begin{matrix}a_1\cdots a_p\\ b'_1\cdots b'_q\end{matrix}\right] &= G^{q+1,0}_{p,q+1}\left[x\middle|\begin{matrix}a_1,\cdots,a_p\\ k',b'_1,\cdots,b'_q\end{matrix}\right]\\ &= G^{q+1,0}_{p,q+1}\left[x\middle|\begin{matrix}a_1,\cdots,a_p\\ b''_1,\cdots,b''_{q+1}\end{matrix}\right],\end{aligned} \tag{4.46}$$

where $k' \in \mathbb{R}$ and it follows the same considerations discussed for k.
This completes the proof. □

The family of the Meijer G-functions (4.42) generated by the convolution embeds among its special cases the (upper) incomplete Gamma function, the modified Bessel function of the second kind and the Wittaker function as shown in Subsection 4.3.1.
The fascinating problem to define a complete monotone kernel in terms of Meijer's G-functions able to define the non-negativity and complete monotonicity requirements not only for the kernel itself but also for the corresponding Gamma functions ratio has been addressed in Subsection 4.3.2 providing an intriguing example of application of the *conjectured* theorem 4.3.3 to a more general and complex situation.

4.3.1 Special functions and the *conjectured* theorem

Let us consider some examples of well-known special functions in order to probe the validity of the Meijer G-*conjectured* theorem 4.3.3 as a useful tool for determining the conditions of their non-negativity and complete monotonicity.

◇ Among the special functions, the (upper) incomplete Gamma function [1, p. 260] has an honourable mention among the examples of application of the *conjectured* theorem. Firstly, the (upper) incomplete Gamma function equipped with a non-linear argument t^β is the relaxation function introduced to be the counterpart in the material frame approach delineated in Chapter 3 to the Havriliak-Negami model. When the parameter β is set equal to 1, the (upper) incomplete Gamma function is the relaxation function corresponding to the Cole-Davidson dispersion model.
Secondly, the importance of this special function springs from its applications in statistics as a remarkable tool for evaluating the χ^2-distribution functions, the cumulative Poisson or Erlang distributions, exponential integrals and even the Error functions.

Here below, a representation of the incomplete Gamma function in terms of Meijer's G-function follows:

$$\Gamma(\delta, x) = G^{2,0}_{1,2}\left[x \left| \begin{matrix} 1 \\ \delta, 0 \end{matrix} \right.\right] . \tag{4.47}$$

Considering the assumptions in the statement 4.3.3, this function is non-negative for any value of $\delta \in \mathbb{R}$. This conclusion arises from the fact that for any choice of δ there is always at least one of the two values of the parameters b is less than a_1. In addition, the (upper) incomplete Gamma function (4.47) results to be also a complete monotone function since the requirements $b_1 \leq 0$ and (4.24) are always satisfied provided that $\delta \leq 1$.

- ◇ Another class of functions that we encountered in practical applications of mathematical physics, as for example in the analysis of the Salpeter equation and the Pearcey equation in quantum mechanics [118, 120, 122, 193, 194], is the modified Bessel function of the second kind (also known as Mcdonald function) $K_\nu(x)$ [179] which in terms of Meijer's G-function reads:

$$K_\nu(x) = \frac{1}{2} G^{2,0}_{0,2}\left[\frac{x^2}{4} \left| \begin{matrix} - \\ -\frac{\nu}{2}, \frac{\nu}{2} \end{matrix} \right.\right] . \tag{4.48}$$

Since p is equal to zero, there are no parameters indicated by the letter "a", therefore the inequality (4.22) in the statement 4.3.3 is always verified for $\nu \in \mathbb{R}$:

$$\sum_{i=1}^{2} b_i = \frac{\nu}{2} - \frac{\nu}{2} = 0, \tag{4.49}$$

and the modified Bessel function of the second kind (4.48) results to be a non-negative function. In addition, observing that one of the b parameters is always negative for any choice of $\nu \in \mathbb{R}$, the modified Bessel function of the second kind (4.48) is also a complete monotone function.

- ◇ Our analysis ends with a more engaging example: the Whittaker function. This function written in terms of Meijer's G-function is represented as follows [1, pp. 503-515]:

$$W_{\nu,\mu}(x) = e^{x/2} G^{2,0}_{1,2}\left[x \left| \begin{matrix} 1-\nu \\ \mu+\frac{1}{2}, \frac{1}{2}-\mu \end{matrix} \right.\right] . \tag{4.50}$$

According to the requirements in the statement of the *conjectured* theorem 4.3.3 this function will be non-negative when $a_1 \geq b_1$. The parameter a_1 is equal to $1-\nu$ whereas b_1 is the smallest value among all the b-values. The range of parameters that guarantees the non-negativity of the Meijer G function is governed by one of the two following inequality depending on the value of μ:

$$\nu \leq \frac{1}{2} + |\mu|, \quad \mu \in \mathbb{R}. \tag{4.51}$$

Imposing the additional requirement that $b_1 \leq 0$, i.e. $\mu \geq \frac{1}{2}$ or $\mu \leq -\frac{1}{2}$ (here, the inequalities (4.22) and (4.24) are the same and for this it has been satisfied for the non-negativity condition), the Meijer G-function involved in the definition of the Whittaker function is a complete monotone function.

4.3.2 A corollary: the complete monotone Meijer G kernel

In this Subsection, we show how the Meijer G-*conjectured* theorem 4.3.3 can be used to build a complete monotone kernel in terms of Meijer's G-functions and then, determine its complete monotonicity providing an intriguing example of application of the previous results in a more complex situation.
The ratio of Gamma functions in (4.25) can be generalized as follows

$$\frac{\prod_{j=1}^{q}\Gamma(b_j+s)}{\prod_{j=1}^{p}\Gamma(a_j+s)}=\int_0^\infty dt\; t^{s-1}G_{p,q}^{q,0}\left[t\,\middle|\begin{matrix}a_1\cdots a_p\\ b_1\cdots b_q\end{matrix}\right], \tag{4.52}$$

where this more general Gamma functions ratio is related to a Meijer G-function of the type $G_{p,q}^{q,0}$.
We can define the requirement concerning the complete monotonicity of the left-hand side of (4.52) proceeding as shown in the proof in a total independent way from the other side. In fact once we fixed the requirements for the parameters as required in the statement 4.3.3, the complete monotonicity of the Gamma functions ratio follows immediately since the crucial inequality

$$\left(\sum_{i=1}^{q}e^{-tb_i}-\sum_{i=1}^{p}e^{-ta_i}\right)\geq 0 \tag{4.53}$$

is evidently satisfied. The extra b parameters help verify the inequality (4.53). However, the right-hand side of (4.52) should be rewritten in order to clearly bring out the complete monotonicity of the kernel in s for all t in the range of integration and the non-negativity locally integrable function in order to generate a complete monotone Gamma functions ratio as stated in theorem 4.3.2.
Firstly we use a basic functional relation of the Meijer G-function that allows us to move the s variable into the parameters of the Meijer G-function. This functional relation that can be found in formula 9.31.5 in [81, p. 1034] is reported here below

$$t^zG_{p,q}^{q,0}\left[t\,\middle|\begin{matrix}a_1\cdots a_p\\ b_1\cdots b_q\end{matrix}\right]=G_{p,q}^{q,0}\left[t\,\middle|\begin{matrix}a_1+z\cdots a_p+z\\ b_1+z\cdots b_q+z\end{matrix}\right]. \tag{4.54}$$

Applying (4.54) to the integrand of (4.55), we obtain

$$\frac{\prod_{j=1}^{q}\Gamma(b_j+s)}{\prod_{j=1}^{p}\Gamma(a_j+s)}=\int_0^\infty dt\;G_{p,q}^{q,0}\left[t\,\middle|\begin{matrix}a_1+s-1\cdots a_p+s-1\\ b_1+s-1\cdots b_q+s-1\end{matrix}\right]. \tag{4.55}$$

The use of this functional relation allows us to identify the non-negative locally integrable function with the constant function $f(t)=1$ whereas the Meijer G-function plays the role of the kernel $K(s,t)$ of the integral transform. In order to use the theorem 4.3.2, we need to bring out the complete monotonicity of the kernel $K(s,t)$.
At this point we focus on the limits of integration so that we can split the integral into

two contributions:

$$
\begin{aligned}
&\int_0^\infty dt\; G^{q,0}_{p,q}\left[t \left| \begin{matrix} a_1+s-1 & \cdots & a_p+s-1 \\ b_1+s-1 & \cdots & b_q+s-1 \end{matrix}\right.\right] = \\
&= \int_0^1 dt\; G^{q,0}_{p,q}\left[t \left| \begin{matrix} a_1+s-1 & \cdots & a_p+s-1 \\ b_1+s-1 & \cdots & b_q+s-1 \end{matrix}\right.\right] + \int_1^\infty dt\; G^{q,0}_{p,q}\left[t \left| \begin{matrix} a_1+s-1 & \cdots & a_p+s-1 \\ b_1+s-1 & \cdots & b_+ s-1 \end{matrix}\right.\right] \\
&= \int_0^1 dt\; G^{q,0}_{p,q}\left[t \left| \begin{matrix} a_1+s-1 & \cdots & a_p+s-1 \\ b_1+s-1 & \cdots & b_q+s-1 \end{matrix}\right.\right] + \int_0^1 dy\; G^{q,0}_{p,q}\left[\frac{1}{y} \left| \begin{matrix} a_1+s-1 & \cdots & a_p+s-1 \\ b_1+s-1 & \cdots & b_q+s-1 \end{matrix}\right.\right] \\
&= \int_0^1 dt\; \left(G^{q,0}_{p,q}\left[t \left| \begin{matrix} a_1+s-1 & \cdots & a_p+s-1 \\ b_1+s-1 & \cdots & b_q+s-1 \end{matrix}\right.\right] + G^{q,0}_{p,q}\left[\frac{1}{t} \left| \begin{matrix} a_1+s-1 & \cdots & a_p+s-1 \\ b_1+s-1 & \cdots & b_q+s-1 \end{matrix}\right.\right] \right).
\end{aligned}
\tag{4.56}
$$

In the second integral of the third line of (4.56), we performed a change of variable, i.e. $t \mapsto \frac{1}{y}$, and then, since the new variable y is a *dummy* variable we restored the letter t. The first Meijer G-function in (4.56) is completely monotone (and so it is positive) according to the requirements in the statement 4.3.3 and for $-b_1 < s < 1 - b_1$. On the other side, what we know about the second Meijer G-function is that the function is positive since it is a composite function of two positive functions, one is the constant function $f(t) = 1$ and the other one is the Meijer G-function whose non-negativity is proven by applying the requirements in 4.3.3 provided that $-b_1 < s < 1 - b_1$. It is therefore possible to conclude that the function between the round brackets in (4.56) is non-negative.

At this point we derive the above integral with respect to s in order to check if the signs of the derivatives are alternating as required by the property of the complete monotonicity. Let us evaluate the first derivative of the integral in (4.56):

$$
\begin{aligned}
&\frac{d}{ds}\int_0^\infty dt\; G^{q,0}_{p,q}\left[t \left| \begin{matrix} a_1+s-1 & \cdots & a_p+s-1 \\ b_1+s-1 & \cdots & b_q+s-1 \end{matrix}\right.\right] = \\
&= \int_0^\infty dt\; \frac{d}{ds}\, G^{q,0}_{p,q}\left[t \left| \begin{matrix} a_1+s-1 & \cdots & a_p+s-1 \\ b_1+s-1 & \cdots & b_q+s-1 \end{matrix}\right.\right] \\
&= \int_0^1 dt\; \log(t) \left(G^{q,0}_{p,q}\left[t \left| \begin{matrix} a_1+s-1 & \cdots & a_p+s-1 \\ b_1+s-1 & \cdots & b_q+s-1 \end{matrix}\right.\right] - G^{q,0}_{p,q}\left[\frac{1}{t} \left| \begin{matrix} a_1+s-1 & \cdots & a_p+s-1 \\ b_1+s-1 & \cdots & b_q+s-1 \end{matrix}\right.\right] \right).
\end{aligned}
\tag{4.57}
$$

Even in this case, the first Meijer G-function is completely monotone provided that the assumptions in 4.3.3 are satisfied, and in particular, we want to point out that this function is not only positive but also decreasing as observed in the "domino-effect" algorithm illustrated in Chapter 2 (see Section 2.2.3). Conversely, the second Meijer G-function is an increasing function. This behaviour is predictable, considering once again that the second Meijer G-function is a composite function where both the functions are decreasing. The difference between the two Meijer G-function in (4.57) is positive as it can be easily verified evaluating the difference between their Mellin-Barnes integral representations: t^{-s} is always greater the t^s for any $s \in (b_1, 1 - b_1)$ when $t \in (0, 1)$. The presence of the natural logarithm as a factor provides the minus sign to the overall function that assures the negative sign of the first derivative. We can continue to perform higher order derivatives, and we observe that for a general n-derivative we have

$$\begin{aligned} &\frac{d^n}{ds^n}\int_0^\infty dt\; G^{q,0}_{p,q}\left[t\left|\begin{matrix} a_1+s-1 & \cdots & a_p+s-1 \\ b_1+s-1 & \cdots & b_q+s-1\end{matrix}\right.\right] = \\ &= \int_0^\infty dt\; \frac{d^n}{ds^n}\; G^{q,0}_{p,q}\left[t\left|\begin{matrix} a_1+s-1 & \cdots & a_p+s-1 \\ b_1+s-1 & \cdots & b_q+s-1\end{matrix}\right.\right] \\ &= \int_0^1 dt\; (\log(t))^n\; \left(G^{q,0}_{p,q}\left[t\left|\begin{matrix} a_1+s-1 & \cdots & a_p+s-1 \\ b_1+s-1 & \cdots & b_q+s-1\end{matrix}\right.\right]\right. \\ &\qquad\qquad \left. + (-1)^n\; G^{q,0}_{p,q}\left[\frac{1}{t}\left|\begin{matrix} a_1+s-1 & \cdots & a_p+s-1 \\ b_1+s-1 & \cdots & b_q+s-1\end{matrix}\right.\right]\right). \end{aligned} \tag{4.58}$$

The function in the round brackets results to be a completely monotone kernel acting on a constant function equals to 1. The ratio of Gamma function in (4.52) turns out to be a complete monotone function according to theorem 4.3.2. In order to check the correctness of the result, we can reproduce the same steps illustrated in the proof in order to demonstrate the complete monotonicity independently of the right-hand side. Such complete monotonicity arises provided that $-b_1 < s < 1 - b_1$ and if the requirements established by 4.3.3 are fulfilled.

4.4 Conclusions to Chapter 4

Among the properties enjoyed by the special functions, the complete monotonicity is one of the most fashionable mathematical property and until now its meaning in the modelling dynamical systems was also quite elusive. The complete monotonicity not only gives information on the special function that fulfils the requirements, but also the behaviour of its derivatives without any calculation. As observed in Chapter 2 and in [123], we introduced a "domino-effect" algorithm where starting on basic assumption on the function, it is possible to establish a chain of properties that leads us to verify the complete monotonicity of the relaxation function. Last but not least, as observed in Chapter 2 and in [123], it was possible to associate a physical meaning to the complete monotonicity in modelling relaxation processes. The complete monotonicity emerges when the dynamics of the system is ruled by purely damping mechanisms. Therefore, it is crucial to investigate what are the minimum requirements to impose on the parameters involved to guarantee the complete monotonicity from a different perspective of what we presented with the "domino-effect" algorithm in Chapter 2 and in [123].
Our attention has been focused on two special functions: the Mittag-Leffler function and the Meijer G-function that are officially presented at the beginning of the Chapter. The choice to consider these two special functions is due to the fact that they are involved in the modeling of relaxation processes. In particular, the Mittag-Leffler function is the relaxation function corresponding to the Cole-Cole relaxation [66]. On the other hand, the Meijer G-function generalizes the relaxation function in the material frame defined in terms of incomplete Gamma function. Once ended the presentation

of the special functions, we presented a theorem for establishing the complete monotonicity of the three-parameter Mittag-Leffler function. The result has been published in [80] and its proof has been inspired by Pollard [168] and by Schneider [182]. This is the peculiar mark of the result: it establishes a formal connection with these works enriching the demonstrations on the three-parameter Mittag-Leffler function known in literature [45, 138, 192].

Concerning the Meijer G-function, a novel and original result has been conjectured and proven in Section 4.3. This result allows us to approach to the complete monotonicity of the Meijer G-function simplifying the determination of the constraints on the parameters. The proof is based on the work of Alzer [2, 3] and it offers a different perspective from the results known in literature [104–106] and it provides a methodology that can extend the strategy and the validity of the results to more general cases. In both the proofs presented in this Chapter, the Bernstein theorem has a key role.

Chapter 5

Conclusions

This thesis aimed to extricate the complexity that affects the anomalous relaxation processes proposing novel methodologies and approaches able to enlarge the landscape of the possible mathematical methods and deepen the understanding of their physical interpretations.

After briefly reviewing the fundamentals of the classical electromagnetic theory and presenting the main anomalous relaxation and dispersion models developed from the Debye model in Chapter 1, we focus our attention on two of these well-known and successful models: the Kohlrausch-Williams-Watts function used for describing relaxation in the time domain, and the Havriliak-Negami dispersion model (and its special cases) applied to the analysis in the frequency domain.

In Chapter 2 and in [123], we have faced the problem of the physical origin of the Kohlrausch-Williams-Watts function introducing a phenomenological model able to unveil the origin of this relaxation function and the nature of its singularity resorting to a comprehensive approach in agreement with the experimental data and able to define the role of the monotonicity in the mathematical modelling of relaxation processes. This important achievement paves the way to a novel approach in the analysis of the time-resolved photoluminescence, and it was acknowledged in the book written by Prof. Giuseppe Baldacchini titled "Organometallic Luminescence: A Case Study on Alq3, an OLED Reference Material" published by Elsevier in 2020. This point of view allowed the understanding of the issues linked to the function itself (in its stretched and compressed versions) but also to the realization of a general model where the role of the restoring and frictional forces have been related to a physical quantity as the time-dependent reduced mass. To understand the crucial value of the model and the approach, we should bear in mind the difficulties in the interpretation of the nonlinear friction mentioned in [132] where the approximation to a first order differential equation elegantly avoids the mathematical obstacle to solve a second-order differential equation with time-dependent coefficients, in this case the downside is the difficulty in understanding the nature of the nonlinear forces. Our model preserves the second order differential equation and introduces the nonlinear time variable, named material time or material clock, as a change in the coordinates. Part of these results were presented at the conference "33rd M. Smoluchowski Symposium" held in Kraków on the 3th and 4th of December 2020.

The essential role of the material time in the description of anomalous relaxation pro-

cesses has been unveiled in Chapter 3. In this Chapter there are three main outcomes that have been carried out using our papers [23, 24, 77–79] as starting point for the research. Firstly, we introduced a general composition rule in terms of a commutator to describe the evolution of anomalous relaxation processes that can generalize and simplify the approach we presented in [78] and in [79]. This formula roots its physical interpretation in the Reynold-Leibnitz theorem and it is based on the assumption that the relaxation function should be considered as a *intensive function* [116]. Secondly, we linked the material time to the material frequency introducing a material transform based on the Fourier transform reinterpreted in the light of a frame that twists and rotates. This transform bridges a time-weighted Kohlrausch-Williams-Watts relaxation function with the Havriliak-Negami dispersion model. This is a significant achievement since not only the material transform explains the success of these two models in their respective domains as two faces of the same coin, but also it paves the way to interesting theoretical and experimental applications in the field of frustrated magnetism as pyrochlore systems. The third result concerns the generalization of the model proposed in Chapter 2: the harmonic oscillator results to be also driven by an external force. This outcome shows that there are two different origins of anomalous behaviours, one that is nested in the material medium and described by the material time, the other one emerges when an external force has been applied. This result explains respectively the distortion and the damping observed in the semicircles illustrated in the Cole-Cole plot in Chapter 1. Part of the results have been presented at the conference "XXXVII International Symposium on Dynamical Properties of Solids" held in Ferrara (IT) from the 8th to 12th of September 2019 [121], and in other two occasions where I was invited lecturer: at the conference "International Conference of Physics and Related Science Education" held in Subotica from the 17th to the 19th of October 2019 [119] and at the seminary at the Physics Department of the University of Ferrara held on the 13th of Febraury 2020.
Last but absolutely not least, Chapter 4 collects the theorem (published in [80]) about the minimum requirements that the three-parameter Mittag-Leffler function should fulfill to be a complete monotone function. In second place, an original result on the non-negativity and complete monotonicity of the Meijer G-function has been presented in Chapter 4. The result extends the set where the parameters range: now it is possible to consider also negative values for the parameters! The choice of this function is due to the fact that it plays a key role in our framework of anomalous relaxation processes since its material-frequency counterpart is the Havriliak-Negami dispersion model.

There are a number of additional areas for further research that have been highlighted by the studies undertaken for this thesis. These include the further investigations of other photoluminescent materials in addition to the Alq3 molecule in order to extend the validity of the model and its predictions to other experimental situations. However, it seems to be equally interesting to use this model *in order to reverse the course* and try to anticipate the experimental observations introducing novel relaxation functions as we presented in [124]. In this paper we introduced a stretched hyperbolic decay generalizing the Becquerel decay law via fractional calculus. The result presented is significant since not only it enlarges the landscape of the functions that model photoluminescence but it is an example of how the model presented in this thesis allows

to proceed in modelling non-exponential or anomalous behaviour, merging the physical meaning and the mathematical requirement. In particular, it is worth to mention that the results can be extended to the description of non-exponential current decay in superconductors as we show in [124]. The interplay between different fields of condensed matter physics favours a clearer physical interpretation for these anomalous behaviours. As reminded previously, it could be very interesting to extend the research in the direction of frustrated magnetism in order to use the transform and the mathematical tools introduced in this thesis to analyse complex systems as pyrochlores.
Regarding the analysis of the complete monotonicity requirement for special functions, an extension for the near future is to promote this *conjectured theorem* as a *theorem* and then, generalize the methodology set out in this thesis in order to define the minimum set of conditions for convoluted special functions as the Meijer G-function with all different indices and the Fox H-function.

Bibliography

[1] M. Abramowitz and I. A. Stegun. *Handbook of mathematical functions with formulas, graphs, and mathematical tables*, volume 55. US Government printing office, 1970.

[2] H. Alzer. Some gamma function inequalities. *Mathematics of Computation of the American Mathematical Society*, 60(201):337–346, 1993.

[3] H. Alzer. On some inequalities for the gamma and psi functions. *Mathematics of Computation of the American Mathematical Society*, 66(217):373–389, 1997.

[4] L. Andrews. *Special functions for engineers and applied mathematicians.* McGraw-Hill, New York, 1992.

[5] W. Arendt, A. Grabosch, G. Greiner, U. Moustakas, R. Nagel, U. Schlotterbeck, U. Groh, H. P. Lotz, and F. Neubrander. *One-parameter semigroups of positive operators*, volume 1184. Springer, Berlin, 1986.

[6] J. R. Argand. *Essai sur une manière de représenter les quantités imaginaires dans les constructions géométriques.* [Anonymous publ.], Paris (summarised in [7]), 1806.

[7] J. R. Argand. Essai sur une manière de représenter les quantités imaginaires dans les constructions géométriques. *Annales de Mathématiques*, 4:133–147, 1876.

[8] N. W. Ashcroft and N. D. Mermin. *Solid state physics.* Saunders College Publishing, Harcourt College Publishing, New York, 1976.

[9] R. A. Askey, T. H. Koornwinder, and W. J. Schempp. *Special functions: group theoretical aspects and applications.* D. Reindel Publishing Co., Dordrecht, 1984.

[10] R. Atanassov and U. Tsoukrovski. Some properties of a class of logarithmically completely monotonic functions. *Dokladi na Bolgarskata Akademiya na Naukite*, 41(2):21–23, 1988.

[11] D. Babusci, G. Dattoli, S. Licciardi, and E. Sabia. *Mathematical methods for physicists.* World Scientific Publishing Co. Pte. Ltd., Singapore, 2020.

[12] G. Baldacchini. *Organometallic Luminescence. A Case Study on Alq$_3$, an OLED Reference Material.* Woodhead Publishing (Elsevier), Sawston (UK), 2020.

[13] G. Baldacchini, T. Baldacchini, P. Chiacchiaretta, R. Pode, and Q.-M. Wang. Morphological phase transitions in Alq3 films. *Journal of Luminescence*, 129 (12):1831–1834, 2009.

[14] G. Baldacchini, P. Chiacchiaretta, R. Reisfeld, and E. Zigansky. The origin of luminescence blueshifts in Alq3 composites. *Journal of Luminescence*, 129(12): 1849–1852, 2009.

[15] G. Baldacchini, P. Chiacchiaretta, R. Montereali, R. Pode, and M. Vincenti. Singular photoluminescence behavior of Alq3 films at very long decay time. *Journal of Luminescence*, 193:106–113, 2018.

[16] D. Baleanu, Z. B. Güvenç, and J. T. Machado. *New Trends in Nanotechnology and Fractional Calculus Applications*. Springer, Dordrecht, 2010.

[17] D. Baleanu, K. Diethelm, E. Scalas, and J. J. Trujillo. *Fractional calculus: models and numerical methods*, volume 3. World Scientific Publishing Publishing (Elsevier), Sawston, 2012.

[18] C. Baleizão and M. N. Berberan-Santos. Thermally activated delayed fluorescence as a cycling process between excited singlet and triplet states: Application to the fullerenes. *The Journal of Chemical Physics*, 126(20):204510, 2007.

[19] E. Barkai. Fractional Fokker-Planck equation, solution, and application. *Physical Review E*, 63(4):046118, 2001.

[20] D. Barnes. Lcd or oled: Who wins? In *SID Symposium Digest of Technical Papers*, volume 44, pages 26–27. Wiley Online Library, 2013.

[21] E. W. Barnes. A new development of the theory of the hypergeometric functions. *Proceedings of the London Mathematical Society*, 2(1):141–177, 1908.

[22] R. Beals and J. Szmigielski. Meijer G-functions: A Gentle Introduction. *Notices of the American Mathematical Society*, 60(06):866, 2013.

[23] N. Behr, G. Dattoli, and A. Lattanzi. Operator ordering and solution of pseudo-evolutionary equations. *Axioms*, 8(1):35, 2019.

[24] N. Behr, G. Dattoli, A. Lattanzi, and S. Licciardi. Dual numbers and operational umbral methods. *Axioms*, 8(3):77, 2019.

[25] C. M. Bender and S. A. Orszag. *Advanced mathematical methods for scientists and engineers I: Asymptotic methods and perturbation theory.* Springer, New York, 2013.

[26] H. Bergström. On some expansions of stable distribution functions. *Arkiv för Matematik*, 2(4):375–378, 1952.

[27] S. Bernstein et al. Sur les fonctions absolument monotones. *Acta Mathematica*, 52:1–66, 1929.

[28] S. Bochner. *Harmonic analysis and the theory of probability.* University of California Press, Berkeley, 2020.

[29] E. Bodunov, Y. A. Antonov, and A. L. Simões Gamboa. On the origin of stretched exponential (Kohlrausch) relaxation kinetics in the room temperature luminescence decay of colloidal quantum dots. *The Journal of Chemical Physics*, 146 (11):114102, 2017.

[30] C. J. F. Böttcher, O. C. van Belle, P. Bordewijk, and A. Rip. *Theory of electric polarization*, volume 1. Elsevier, Amsterdam, 1973.

[31] C. J. F. Böttcher, O. C. van Belle, P. Bordewijk, and A. Rip. *Theory of electric polarization*, volume 2. Elsevier, Amsterdam, 1978.

[32] A. Buckley. *Organic light-emitting diodes (OLEDs): materials, devices and applications.* Woodhead Publishing, Cambridge, 2013.

[33] P. Caldirola. Forze non conservative nella meccanica quantistica. *Il Nuovo Cimento (1924-1942)*, 18(9):393–400, 1941.

[34] R. Caponetto. *Fractional order systems: modeling and control applications*, volume 72. World Scientific Publishing Co. Pte. Ltd., Singapore, 2010.

[35] C.-P. Chen and F. Qi. Logarithmically completely monotonic functions relating to the gamma function. *Journal of Mathematical Analysis and Applications*, 321 (1):405–411, 2006.

[36] R. Chen. Apparent stretched-exponential luminescence decay in crystalline solids. *Journal of Luminescence*, 102:510–518, 2003.

[37] A. H. Clifford and G. B. Preston. *The algebraic theory of semigroups, Volume II.* American Mathematical Society, Providence (Rhode Island), 1967.

[38] K. S. Cole and R. H. Cole. Dispersion and absorption in dielectrics i. alternating current characteristics. *The Journal of Chemical Physics*, 9(4):341–351, 1941.

[39] E. Condon. A theory of intensity distribution in band systems. *Physical Review*, 28(6):1182, 1926.

[40] M. Daoud. Photon-added coherent states for exactly solvable hamiltonians. *Physics Letters A*, 305(3-4):135–143, 2002.

[41] G. Dattoli, A. Arena, and P. E. Ricci. Laguerrian eigenvalue problems and Wright functions. *Mathematical and Computer Modelling*, 40(7-8):877–881, 2004.

[42] G. Dattoli, K. Górska, A. Horzela, and K. Penson. Photoluminescence decay of silicon nanocrystals and lévy stable distributions. *Physics Letters A*, 378(30-31): 2201–2205, 2014.

[43] G. Dattoli, K. Górska, A. Horzela, S. Licciardi, and R. M. Pidatella. Comments on the properties of Mittag-Leffler function. *The European Physical Journal Special Topics*, 226(16-18):3427–3443, 2017.

[44] D. W. Davidson and R. H. Cole. Dielectric relaxation in glycerol, propylene glycol, and n-propanol. *The Journal of Chemical Physics*, 19(12):1484–1490, 1951.

[45] E. C. De Oliveira, F. Mainardi, and J. Vaz. Models based on Mittag-Leffler functions for anomalous relaxation in dielectrics. *The European Physical Journal Special Topics*, 193(1):161–171, 2011.

[46] P. Debye. Zur theorie der spezifischen wärmen. *Annalen der Physik*, 344(14): 789–839, 1912.

[47] P. Debye. Polar molecules. *Chemical Catalog Company, Inc., New York*, pages 77–108, 1929.

[48] K. Diethelm. The analysis of differential equations of fractional order: An application-oriented exposition using differential operators of caputo type. *Lecture Notes in Mathematics*, 2004, 2004.

[49] K. Doss, C. J. Wilkinson, Y. Yang, K.-H. Lee, L. Huang, and J. C. Mauro. Maxwell relaxation time for non-exponential α-relaxation phenomena in glassy systems. *Journal of the American Ceramic Society*.

[50] A. Drapella. The complementary Weibull distribution: unknown or just forgotten? *Quality and Reliability Engineering International*, 9(4):383–385, 1993.

[51] P. Drude. Zur elektronentheorie der metalle. *Annalen der physik*, 306(3):566–613, 1900.

[52] B. Dybiec and E. Gudowska-Nowak. Subordinated diffusion and continuous time random walk asymptotics. *Chaos: An Interdisciplinary Journal of Nonlinear Science*, 20(4):043129, 2010.

[53] M. Dzhrbashyan. Integral transforms and representations of functions in the complex domain. *Nauka*.

[54] O. Edholm and C. Blomberg. Stretched exponentials and barrier distributions. *Chemical Physics*, 252(1-2):221–225, 2000.

[55] M. D. Ediger, C. A. Angell, and S. R. Nagel. Supercooled liquids and glasses. *The Journal of Physical Chemistry*, 100(31):13200–13212, 1996.

[56] K.-J. Engel and R. Nagel. One-parameter semigroups for linear evolution equations. In *Semigroup forum*, volume 63, pages 278–280. Springer, 2001.

[57] T. Engel. *Physical chemistry.* Pearson Education, India, 2006.

[58] A. Erdélyi. *Higher Transcendental Functions*, volume 1,2,3. McGraw-Hill, New York, 1953-1955.

[59] W. Feller. An introduction to probability theory and its applications.

[60] W. N. Findley and F. A. Davis. *Creep and relaxation of nonlinear viscoelastic materials*. North Holland, New York, 2013.

[61] B. R. Fisher, H.-J. Eisler, N. E. Stott, and M. G. Bawendi. Emission intensity dependence and single-exponential behavior in single colloidal quantum dot fluorescence lifetimes. *The Journal of Physical Chemistry B*, 108(1):143–148, 2004.

[62] J. Franck and E. Dymond. Elementary processes of photochemical reactions. *Transactions of the Faraday Society*, 21(February):536–542, 1926.

[63] K. A. Franz, W. G. Kehr, A. Siggel, J. Wieczoreck, and W. Adam. Luminescent materials. *Ullmann's Encyclopedia of Industrial Chemistry*, 2000.

[64] H. Fukumura, K. Kikuchi, K. Koike, and H. Kokubun. Temperature effect on inverse intersystem crossing of anthracenes. *Journal of Photochemistry and Photobiology A: Chemistry*, 42(2-3):283–291, 1988.

[65] P. Gallo, M. Rovere, M. Ricci, C. Hartnig, and E. Spohr. Non-exponential kinetic behaviour of confined water. *EPL (Europhysics Letters)*, 49(2):183, 2000.

[66] R. Garrappa, F. Mainardi and G. Maione. Models of dielectric relaxation based on completely monotone functions. *Fractional Calculus and Applied Analysis*, 19 (5):1105–1160, 2016.

[67] B. Geffroy, P. Le Roy, and C. Prat. Organic light-emitting diode (oled) technology: materials, devices and display technologies. *Polymer International*, 55(6): 572–582, 2006.

[68] J. A. Goldstein. *Semigroups of linear operators and applications*. Courier Dover Publications, New York, 2017.

[69] R. Gorenflo and F. Mainardi. Fractional calculus. In *Fractals and fractional calculus in continuum mechanics*, pages 223–276. Springer,Vienna, 1997.

[70] R. Gorenflo and F. Mainardi. Fractional calculus: Integral and differential equations of fractional order. *arXiv:0805.3823*, 2008.

[71] R. Gorenflo and S. Vessella. *Abel integral equations*, volume 1461. Springer-Verlag Berlin Heidelberg, 1991.

[72] R. Gorenflo, F. Mainardi, and S. Rogosin. Mittag-Leffler function: properties and applications. *Handbook of Fractional Calculus with Applications*, 1:269–296, 2019.

[73] K. Górska and K. Penson. Lévy stable two-sided distributions: Exact and explicit densities for asymmetric case. *Physical Review E*, 83(6):061125, 2011.

[74] K. Górska and K. Penson. Lévy stable distributions via associated integral transform. *Journal of Mathematical Physics*, 53(5):053302, 2012.

[75] K. Górska, K. Penson, D. Babusci, G. Dattoli, and G. Duchamp. Operator solutions for fractional Fokker-Planck equations. *Physical Review E*, 85(3):031138, 2012.

[76] K. Górska, A. Horzela, G. Dattoli, and K. Penson. The Havriliak-Negami relaxation and its relatives: the response, relaxation and probability density functions. *Journal of Physics A*, 51(13):135202, 2018.

[77] K. Górska, A. Lattanzi, and G. Dattoli. Mittag-Leffler function and fractional differential equations. *Fractional Calculus and Applied Analysis*, 21(1):220–236, 2018.

[78] K. Górska, A. Horzela, and A. Lattanzi. Composition law for the Cole-Cole relaxation and ensuing evolution equations. *Physics Letters A*, 383(15):1716–1721, 2019.

[79] K. Górska, A. Horzela, A. Lattanzi, and P. Bochnacki. The causality-composition law for the non-Debye relaxations. In *Journal of Physics: IOP Conference Series*, volume 1194:012038, 2019.

[80] K. Górska, A. Horzela, A. Lattanzi, and T. K. Pogány. On complete monotonicity of three parameter Mittag-Leffler function. *Applicable Analysis and Discrete Mathematics*, (15):118–128, 2021.

[81] I. Gradshteyn, I. Ryzhik, and R. H. Romer. Tables of integrals, series, and products: 7eds., 2007.

[82] P. A. Grillet. *Semigroups: an introduction to the structure theory.* Routledge, London, 2017.

[83] A. Grinshpan and M. Ismail. Completely monotonic functions involving the gamma and q-gamma functions. *Proceedings of the American Mathematical Society*, 134(4):1153–1160, 2006.

[84] P. Hamm, J. Helbing, and J. Bredenbeck. Stretched versus compressed exponential kinetics in α-helix folding. *Chemical Physics*, 323(1):54–65, 2006.

[85] G. H. Hardy. Gösta Mittag-Leffler. *Proceeding Royal Society of London (A)*, 119: 1846–1927, 1928.

[86] H. J. Haubold, A. M. Mathai, and R. K. Saxena. Mittag-Leffler functions and their applications. *Journal of Applied Mathematics*, Volume 2011, 2011.

[87] S. Havriliak and S. Negami. A complex plane representation of dielectric and mechanical relaxation processes in some polymers. *Polymer*, 8:161–210, 1967.

[88] S. Havriliak Jr and S. Havriliak. Results from an unbiased analysis of nearly 1000 sets of relaxation data. *Journal of Non-Crystalline Solids*, 172-174:297–310, 1994.

[89] O. Heaviside. On the forces, stresses, and fluxes of energy in the electromagnetic field. *Philosophical Transactions of the Royal Society of London A*, IX(183): 423–480, 1892.

[90] T. Hecksher, N. B. Olsen, K. Niss, and J. C. Dyre. Physical aging of molecular glasses studied by a device allowing for rapid thermal equilibration. *The Journal of Chemical Physics*, 133(17):174514, 2010.

[91] R. Hilfer. *Applications of fractional calculus in physics.* World Scientific Publishing, 2000.

[92] R. Hilfer. Analytical representations for relaxation functions of glasses. *Journal of Non-Crystalline Solids*, 305(1-3):122–126, 2002.

[93] R. Hilfer. Experimental evidence for fractional time evolution in glass forming materials. *Chemical Physics*, 284(1-2):399–408, 2002.

[94] N. E. Hill. *Dielectric properties and molecular behaviour.* Van Nostrand Reinhold, London, New York, 1969.

[95] M. Humi and W. Miller. *Second course in ordinary differential equations for scientists and engineers.* Springer-Verlag, New York, 2012.

[96] A. K. Jonscher. Dielectric relaxation in solids. 1983.

[97] A. K. Jonscher. The universal dielectric response and its physical significance. *IEEE Transactions on Electrical Insulation*, 27(3):407–423, 1992.

[98] A. K. Jonscher. *Universal relaxation law: a sequel to dielectric relaxation in solids.* Chelsea Dielectrics Press, London, 1996.

[99] A. K. Jonscher. Dielectric relaxation in solids. *Journal of Physics D: Applied Physics*, 32(14):R57, 1999.

[100] A. Jurlewicz, J. Trzmiel, and K. Weron. Two-power-law relaxation processes in complex materials. *Acta Physica Polonica B*, 41(5):1001, 2010.

[101] E. Kanai. On the quantization of the dissipative systems. *Progress of Theoretical Physics*, 3(4):440–442, 1948.

[102] S. Kantorovitz. Characterization of the gamma semigroup. 95(2):251–258, 2017.

[103] I. G. Kaplan. *The Pauli Exclusion Principle: Origin, Verifications, and Applications.* John Wiley & Sons, Chichester, 2017.

[104] D. Karp and J. López. A class of Meijer's G functions and further representations of the generalized hypergeometric functions. *arXiv:1801.08670*, 2018.

[105] D. Karp and J. López. On a particular class of Meijer's G functions appearing in fractional calculus. *International Journal of Applied Mathematics*, 31(5):521–543, 2018.

[106] D. Karp and E. Prilepkina. Completely monotonic gamma ratio and infinitely divisible H-function of Fox. *Computational Methods and Function Theory*, 16(1): 135–153, 2016.

[107] A. Kilbas, H. Srivastava, and J. Trujillo. *Theory and applications of fractional differential equations*, volume 204. Elsevier Science Inc. New York, 2006.

[108] V. S. Kiryakova. *Generalized fractional calculus and applications.* Longman Scientific & Technical, John Wiley & Sons Inc., New York, 1993.

[109] J. Klafter and M. F. Shlesinger. On the relationship among three theories of relaxation in disordered systems. *Proceedings of the National Academy of Sciences*, 83(4):848–851, 1986.

[110] W. Kob. Computer simulations of supercooled liquids and glasses. *Journal of Physics: Condensed Matter*, 11(10):R85, 1999.

[111] W. Kob and H. C. Andersen. Testing mode-coupling theory for a supercooled binary lennard-jones mixture. ii. intermediate scattering function and dynamic susceptibility. *Physical Review E*, 52(4):4134, 1995.

[112] R. Kohlrausch. Theorie des elektrischen rückstandes in der leidener flasche. *Annalen der Physik und Chemie (Poggendorff)*, 167(2):56–82,179–214, 1854.

[113] M. Köpf, C. Corinth, O. Haferkamp, and T. Nonnenmacher. Anomalous diffusion of water in biological tissues. *Biophysical Journal*, 70(6):2950–2958, 1996.

[114] S. Koumandos and H. L. Pedersen. On the Laplace transform of absolutely monotonic functions. *arXiv:1612.02257*, 2016.

[115] G. Kristensson. *Second order differential equations: special functions and their classification.* Springer-Verlag, New York, 2010.

[116] A. Lattanzi. Commutator and composition rule for relaxation functions. *In preparation*, .

[117] A. Lattanzi. The Pearcey equation: from the Salpeter relativistic equation to quasiparticles. *Accepted to be published as a chapter of the book series SEMA-SIMAI SPRINGER SERES (2020-2021)*, .

[118] A. Lattanzi. Evolution equations in a nutshell. *Conference Proceedings CSPM 2018*, 2019.

[119] A. Lattanzi. Debye or non-Debye. This is the question. *Published in Conference Proceedings ICPRSE*, 2020.

[120] A. Lattanzi. How to deal with nonlocality and pseudodifferential operators. an example: The Salpeter equation. In *Quantum Theory and Symmetries: Proceedings of the 11th International Symposium, Montréal, Canada*, page 101. Springer Nature, 2021.

[121] A. Lattanzi, K. Górska, and A. Horzela. Non-Debye vs. Debye dielectric relaxation: How does memory effect arise? *Multidisciplinary Digital Publishing Institute Proceedings*, 26(1):43, 2019.

[122] A. Lattanzi, D. Levi, and A. Torre. The missing piece: a new relativistic wave equation, the Pearcey equation. In *Journal of Physics: Conference Series*, volume 1194, page 012065. IOP Publishing, 2019.

[123] A. Lattanzi, G. Dattoli, and G. Baldacchini. Physics and mathematics of the photoluminescence of complex systems. *arXiv:2012.04645*, 2020.

[124] A. Lattanzi, G. Casasanta, and R. Garra. On the application of Mittag-Leffler functions to hyperbolic-type decay of luminescence. *arXiv:2103.05979*, 2021.

[125] K. B. Lee, J. Siegel, S. Webb, S. Leveque-Fort, M. Cole, R. Jones, K. Dowling, M. Lever, and P. French. Application of the stretched exponential function to fluorescence lifetime imaging. *Biophysical Journal*, 81(3):1265–1274, 2001.

[126] M. Lee, J. Kim, J. Tang, and R. M. Hochstrasser. Fluorescence quenching and lifetime distributions of single molecules on glass surfaces. *Chemical Physics Letters*, 359(5-6):412–419, 2002.

[127] A. Letnikov and V. Chernykh. The foundations of fractional calculus (with applications to the theory of oil and gas production, underground hydrodynamics and dynamics of biological systems). 2011.

[128] Q. Li, X. Peng, and G. B. McKenna. Physical aging and compressed exponential behaviors in a model soft colloidal system. *Soft Matter*, 15(11):2336–2347, 2019.

[129] J. C. Lindon, G. E. Tranter, and D. Koppenaal. *Encyclopedia of spectroscopy and spectrometry*. Academic Press, 2016.

[130] J.-M. Liu. *Principles of Photonics*. Cambridge University Press, Sheridans Books Inc., New York, 2016.

[131] Y. L. Luke. *Special functions and their approximations*, volume 1. Academic press, New York, 1969.

[132] A. Lukichev. Physical meaning of the stretched exponential kohlrausch function. *Physics Letters A*, 383(24):2983–2987, 2019.

[133] W. Magnus, F. Oberhettinger, and R. P. Soni. *Formulas and theorems for the special functions of mathematical physics*, volume 52. Springer-Verlag, Berlin Heidelberg, 2013.

[134] S. A. Maier. *Plasmonics: fundamentals and applications.* Springer-Verlag, New York, 2007.

[135] F. Mainardi. *Fractional calculus and waves in linear viscoelasticity: an introduction to mathematical models.* Imperial College Press, London, World Scientific Publishing, Singapore, 2010.

[136] F. Mainardi. On some properties of the Mittag-Leffler function e_α (-t^α), completely monotone for $t > 0$ with $0 < \alpha < 1$. *arXiv:1305.0161*, 2013.

[137] F. Mainardi. Why the Mittag-Leffler function can be considered the queen function of the fractional calculus? *Entropy*, 22(12):1359, 2020.

[138] F. Mainardi and R. Garrappa. On complete monotonicity of the Prabhakar function and non-Debye relaxation in dielectrics. *Journal of Computational Physics*, 293:70–80, 2015.

[139] F. Mainardi and R. Gorenflo. Time-fractional derivatives in relaxation processes: a tutorial survey. *Fractional Calculus and Applied Analysis, 10:269–308, 2007 (or also in arXiv:0801.4914, 2008).*

[140] A. W. Marshall, I. Olkin, and B. C. Arnold. *Inequalities: Theory of Majorization and Its Applications.* Springer, New York, 2011.

[141] R. Martin. *Ageing of composites.* Woodhead Publishing (Elsevier), Cambridge, 2008.

[142] A. M. Mathai and R. K. Saxena. *Generalized hypergeometric functions with applications in statistics and physical sciences*, volume 348. Springer, Berlin, Heidelberg, 2006.

[143] A. M. Mathai, R. K. Saxena, and H. J. Haubold. *The H-function: theory and applications.* Springer-Verlag, New York, 2009.

[144] J. C. Maxwell. *A treatise on electricity and magnetism*, volume 1. Clarendon press, Macmillan & Co, Cambridge, 1881.

[145] J. C. Maxwell. *A dynamical theory of the electromagnetic field.* Wipf and Stock Publishers, Eugene, Oregon, 1996.

[146] A. D. McNaught, A. Wilkinson, et al. *Compendium of chemical terminology*, volume 1669. Blackwell Science, Oxford, 1997.

[147] C. Meijer. On the G-function. In *Proceedings of the Koninklijke Nederlandse Akademie van Wetenschappen Series A.* North-Holland, Amsterdam, 1946.

[148] J. Merodio and R. Ogden. *Constitutive Modelling of Solid Continua.* Number 262. Springer, 2020.

[149] K. Miller and S. Samko. Completely monotonic functions. *Integral Transforms and Special Functions*, 12(4):389–402, dec 2001. doi: 10.1080/10652460108819360. URL `https://doi.org/10.1080\%2F10652460108819360`.

[150] G. Mittag-Leffler. Sur la nouvelle fonction $e_\alpha(x)$. *Comptes Rendus de l'Académie des Sciences,(Ser. II)*, 137:554–558, 1903.

[151] T. Morishita. Compressed exponential relaxation in liquid silicon: Universal feature of the crossover from ballistic to diffusive behavior in single-particle dynamics. *The Journal of Chemical Physics*, 137(2):024510, 2012.

[152] G. S. Mudholkar and G. D. Kollia. Generalized Weibull family: a structural analysis. *Communications in Statistics-Theory and Methods*, 23(4):1149–1171, 1994.

[153] D. P. Murthy, M. Xie, and R. Jiang. *Weibull models*, volume 505. John Wiley & Sons Inc., Hoboken, New Jersey, 2004.

[154] A. Nakhushev. Fractional calculus and its applications. *Moscow: Fizmatlit*, page 272, 2003.

[155] O. Narayanaswamy. A model of structural relaxation in glass. *Journal of the American Ceramic Society*, 54(10):491–498, 1971.

[156] K. Ngai. Non-Debye relaxation in condensed matter. *Ed. T.V. Ramakrishnan and M. Raj Lakshimi.*

[157] K. Ngai. *Relaxation and diffusion in complex systems.* Springer-Verlag, New York, 2011.

[158] M. A. Omary and H. H. Patterson. Luminescence, theory. 2017.

[159] W. Pauli. Über den zusammenhang des abschlusses der elektronengruppen im atom mit der komplexstruktur der spektren. *Zeitschrift für Physik*, 31(1):765–783, 1925.

[160] A. Pazy. *Semigroups of linear operators and applications to partial differential equations*, volume 44. Springer-Verlag, New York, 2012.

[161] K. Penson and K. Górska. Exact and explicit probability densities for one-sided lévy stable distributions. *Physical Review Letters*, 105(21):210604, 2010.

[162] J. Phillips. Kohlrausch relaxation and glass transitions in experiment and in molecular dynamics simulations. *Journal of Non Crystalline Solids*, 182(1):155–161, 1995.

[163] J. Phillips. Stretched exponential relaxation in molecular and electronic glasses. *Reports on Progress in Physics*, 59(9):1133, 1996.

[164] A. Pishkoo. A G-function form of radial states in carbon and hydrogen atoms: absorption or emission of radiation. *Advanced Studies in Theoretical Physics*, 9 (3):145–154, 2015.

[165] A. Pishkoo and M. Darus. On Meijer's G-functions and its applications. *Reviews in Theoretical Science*, 3(2):216–223, 2015.

[166] I. Podlubny. *Fractional differential equations: an introduction to fractional derivatives, fractional differential equations, to methods of their solution and some of their applications.* Academic Press (Elsevier), San Diego, 1998.

[167] H. Pollard. The representation of $e^{-x^{\lambda}}$ as a laplace integral. *Bulletin of the American Mathematical Society*, 52(10):908–910, 1946.

[168] H. Pollard. The completely monotonic character of the Mittag-Leffler function $\mathrm{E}_{\alpha}(-x)$. *Bulletin of the American Mathematical Society*, 54(12):1115–1116, 1948.

[169] T. R. Prabhakar et al. A singular integral equation with a generalized Mittag-Leffler function in the kernel. *Yokohama Mathematical Journal*, 19:7–15, 1971.

[170] A. P. Prudnikov, Y. A. Brychkov, and O. I. Marichev. *Integrals and series: More Special Function*, volume 3. FizMatLit, 2003 (Russian edition).

[171] E. Rainville. *Elementary differential equations 8th eds.* Pearson, 2013.

[172] G. Raju. *Dielectrics in electric fields.* Marcel Dekker Inc., New York, Basel, 2003.

[173] R. M. Redheffer and D. Port. *Differential equations: theory and applications.* Jones & Bartlett Learning, Boston, 1991.

[174] O. Reynolds. *The sub-mechanics of the universe*, volume 3. University Press, Cambridge, 1903.

[175] R. T. Rockafellar. *Convex analysis.* Number 28. Princeton University press, 1970.

[176] S. Rogosin. The role of the Mittag-Leffler function in fractional modeling. *Mathematics*, 3(2):368–381, 2015.

[177] C. B. Roth. *Polymer glasses.* CRC Press, Boca Raton, 2016.

[178] J. Sabatier, O. P. Agrawal, and J. T. Machado. *Advances in fractional calculus*, volume 4. Springer, 2007.

[179] S. Samko, A. Kilbas, and O. Marichev. *Fractional Integrals and Derivatives: Theory and Applications.* Gordon and Breach, Yverdon, Switzerland, 1993.

[180] B. K. P. Scaife. Principles of dielectrics. 1989.

[181] G. Schlegel, J. Bohnenberger, I. Potapova, and A. Mews. Fluorescence decay time of single semiconductor nanocrystals. *Physical Review Letters*, 88(13):137401, 2002.

[182] W. Schneider. Completely monotone generalized Mittag-Leffler functions. *Expositiones Mathematicae*, 14:3–24, 1996.

[183] S. Schols. *Device Architecture and Materials for Organic Light-Emitting Devices: Targeting High Current Densities and Control of the Triplet Concentration.* Springer, Netherlands, 2011.

[184] J.-A. Seo, H.-J. Kwon, K. Kataoka, K.-i. Ohshima, D.-M. Shin, H.-K. Kim, and Y.-H. Hwang. Compressed-exponential relaxations in supercooled liquid trehalose. *Current Applied Physics*, 12(6):1548–1552, 2012.

[185] A. Shukla and J. Prajapati. On a generalization of Mittag-Leffler function and its properties. *Journal of Mathematical Analysis and Applications*, 336(2):797–811, 2007.

[186] I. M. Sokolov and J. Klafter. From diffusion to anomalous diffusion: a century after einstein's brownian motion. *Chaos: An Interdisciplinary Journal of Nonlinear Science*, 15(2):026103, 2005.

[187] H. M. Srivastava and H. L. Manocha. *A Treatise on Generating Functions.* Ellis Horwood, Wiley, New York, 1984.

[188] H. M. Srivastava and Ž. Tomovski. Fractional calculus with an integral operator containing a generalized Mittag-Leffler function in the kernel. *Applied Mathematics and Computation*, 211(1):198–210, 2009.

[189] G. G. Stokes. On the change of refrangibility of light. In *Abstracts of the Papers Communicated to the Royal Society of London*, number 6, pages 195–200. The Royal Society London, 1854.

[190] F. Tanaka, M. Okamoto, and S. Hirayama. Pressure and temperature dependences of the rate constant for s1-t2 intersystem crossing of anthracene compounds in solution. *The Journal of Physical Chemistry*, 99(2):525–530, 1995.

[191] C. W. Tang and S. A. VanSlyke. Organic electroluminescent diodes. *Applied Physics Letters*, 51(12):913–915, 1987.

[192] Ž. Tomovski, T. K. Pogány, and H. M. Srivastava. Laplace type integral expressions for a certain three-parameter family of generalized Mittag-Leffler functions with applications involving complete monotonicity. *Journal of The Franklin Institute*, 351(12):5437–5454, 2014.

[193] A. Torre, A. Lattanzi, and D. Levi. Time-dependent free-particle Salpeter equation: Numerical and asymptotic analysis in the light of the fundamental solution. *Annalen der Physik*, 529(9):1600231, 2017.

[194] A. Torre, A. Lattanzi, and D. Levi. Time-dependent free-particle Salpeter equation: Features of the solutions. In *Quantum Theory And Symmetries*, pages 297–307. Springer, Singapore, 2017.

[195] V. V. Uchaikin. *Fractional derivatives for physicists and engineers*, volume 2. Springer-Verlag Berlin Heidelberg, 2013.

[196] K. Weron and M. Kotulski. On the cole-cole relaxation function and related mittag-leffler distribution. *Physica A: Statistical Mechanics and its Applications*, 232(1-2):180–188, 1996.

[197] B. West, M. Bologna, and P. Grigolini. *Physics of fractal operators*. Springer-Verlag New York, 2012.

[198] G. Williams and D. C. Watts. Non-symmetrical dielectric relaxation behaviour arising from a simple empirical decay function. *Transactions of the Faraday Society*, 66:80–85, 1970.

[199] A. Wiman et al. Über die nullstellen der funktionen $\mathrm{E}_\alpha(\mathrm{x})$. *Acta Mathematica*, 29:217–234, 1905.

[200] E. M. Wright. The asymptotic expansion of the generalized hypergeometric function. *Journal of the London Mathematical Society*, 1(4):286–293, 1935.

[201] X. Xia and P. G. Wolynes. Microscopic theory of heterogeneity and nonexponential relaxations in supercooled liquids. *Physical Review Letters*, 86(24):5526, 2001.

[202] T.-H. Zhao and Y.-M. Chu. A class of logarithmically completely monotonic functions associated with a gamma function. *Journal of Inequalities and Applications*, 2010:1–11, 2010.

[203] Z. Zheng, J. C. Mauro, and D. C. Allan. Modeling of delayed elasticity in glass. *Journal of Non-Crystalline Solids*, 500:432–442, 2018.